 ©2026 Uspekhi Fizicheskikh Nauk, Russian Academy of Sciences

CONFERENCES AND SYMPOSIA

PACS numbers: 87.19.xj, **87.55. – x, 87.56. – v**

History, current status, and prospects for the development of boron neutron capture therapy *

I.N. Zavestovskaya, S.M. Deyev, S.Yu. Taskaev, D.S. Petrunya

DOI: https://doi.org/10.3367/UFNe.2025.05.040137

Contents

1. Introduction **681**
2. Historical background and fundamental physical principles of neutron capture therapy **685**
3. Modern neutron sources for boron neutron capture therapy **690**
3.1 Major neutron-generating nuclear reactions; 3.2 Epithermal neutron beam shaping assembly; 3.3 Operational accelerator-based neutron sources for boron neutron capture therapy
4. Development of boron delivery agents for targeted transport to tumor cells **696**
4.1 Low-molecular-weight boron-containing compounds; 4.2 Targeted boron-containing bioconjugates; 4.3 Nanoscaled boron-containing delivery systems
5. Absorbed dose monitoring techniques **704**
5.1 Neutron energy spectrum measurement; 5.2 Measurement of individual absorbed dose components; 5.3 Real-time *in vivo* dosimetry methods; 5.4. Treatment planning systems
6. Conclusion. Prospects for the development of boron neutron capture therapy **710**
References **710**

Abstract. This review outlines the history, developmental trajectory, and prospects of neutron capture therapy, one of the most potent nuclear physics-based modalities in modern medicine, representing a variant of binary hadron therapy. The method is based on the nuclear reaction of thermal neutron capture by nuclei of elements characterized by a high cross section for this process (> 500 barn). Such nuclei include isotopes of boron-10, lithium-6, gadolinium-157, uranium-235, and several others; however, only a few (n, α) and (n, f) reactions can ensure energy deposition localized to within one to two cells. Owing to the absence of radioactivity and the low toxicity of boron, boron neutron capture therapy has found clinical application, while recent years have seen active investigations into lithium neutron capture therapy. The review focuses on the development of accelerator neutron sources that meet IAEA requirements, novel boron delivery drugs, and dosimetry tools and methods.

Keywords: boron neutron capture therapy, epithermal neutron sources, boron delivery agents, dosimetry methods, nanoparticles

I.N. Zavestovskaya [1, 2, a], **S.M. Deyev** [1, 2, 3, b], **S.Yu. Taskaev** [2, 4, 5, c], **D.S. Petrunya** [1, 2, d]
[1] National Research Center 'Kurchatov Institute', pl. Akademika Kurchatova 1, 123182 Moscow, Russian Federation
[2] Lebedev Physical Institute, Russian Academy of Sciences, Leninskii prosp. 53, 119991 Moscow, Russian Federation
[3] Shemyakin-Ovchinnikov Institute of Bioorganic Chemistry of the Russian Academy of Sciences, ul. Miklukho-Maklaya 16/10, 117997 Moscow, Russian Federation
[4] Budker Institute of Nuclear Physics, Siberian Branch of the Russian Academy of Sciences, prosp. Akademika Lavrenteva 11, 630090 Novosibirsk, Russian Federation
[5] Novosibirsk State University, ul. Pirogova 2, 630090 Novosibirsk, Russian Federation
E-mail: [a] zavest@sci.lebedev.ru, [b] deyev@ibch.ru, [c] S.Yu.Taskaev@inp.nsk.su, [d] d.petrunya@lebedev.ru

Received 25 May 2026
Uspekhi Fizicheskikh Nauk **196** (7) 726 – 762 (2026)
Translated by the authors

1. Introduction

Nuclear physics methods based on the effects of ionizing and nonionizing radiation have become an integral part of high-technology medicine [1–3]. At present, half of all modern medical devices employ ionizing radiation technologies for the diagnosis and treatment of a broad range of socially significant diseases, including cardiology, oncology, neurology, and others [4]. This category encompasses nuclear medicine, which utilizes radiation from radioisotopes introduced into the patient's bloodstream, as well as diagnostic radiology and radiotherapy that employ ionizing radiation from external sources.

The inception of this field was catalyzed by fundamental scientific discoveries made in the late 19th century. The discovery of X-rays by W.C. Röntgen in 1895 [5] — radiation capable of penetrating opaque media — immediately stimulated new research in physics, biology, and medicine. The first X-ray tubes were developed, and as early as the beginning of 1896, Russian scientists N.G. Egorov and co-workers pioneered the clinical application of X-ray imaging for the

* This review is based on the report presented for the Scientific Session of the Physical Sciences Division of the Russian Academy of Sciences (PSD RAS), on May 21, 2025 (see *Physics–Uspekhi* **69** (7) 663 (2026); *Uspekhi Fizicheskikh Nauk* **196** (7) 707 (2026)).

diagnosis of limb fractures [1]. Concurrently, the foundations of radiobiological science were being laid. The St. Petersburg physiologist I.R. Tarkhanov, while conducting experiments on irradiated frogs and insects, was among the first to suggest that X-rays could be used not only for imaging but also for influencing the physiological processes of living organisms [6].

In the same year, A. Becquerel discovered the phenomenon of spontaneous radioactivity in uranium salts [7]. Continuing this line of investigation, in 1898, M. Sklodowska-Curie and P. Curie isolated from pitchblende two novel radioactive chemical elements — polonium [8] and radium [9]. In 1901, A. Becquerel observed skin damage on the skin over his waistcoat pocket, where he had carried a container of radium. Upon learning of this, P. Curie performed an experiment on himself, deliberately inducing a radiation burn on his forearm. This observation was immediately interpreted as evidence of the potential for selective radiation effects on pathological tissues [10].

In 1903, A. Bell proposed the use of radium for the treatment of malignant tumors [11]. In the same year, in St. Petersburg, under the direction of E.S. London, the first successful treatment of two patients with basal-cell skin carcinoma was performed using surface radium applicators [12, 13]. In 1904, radium needles provided by the Curies were successfully employed in the treatment of patients at the Morozov Cancer Institute of the Imperial Moscow University [4]. In 1908, radium was used for the first time in the treatment of uterine cancer, and in 1909, for intracavitary treatment of prostate cancer [14].

Further research showed that penetrating radiation can damage or destroy any biological tissue [15, 16]. Radiation-induced alterations in various biochemical processes were identified, including disturbances in enzyme activity in tissues and organs, and the appearance of leukotoxins in the blood [17]. Data emerged indicating differences in the resistance of various biological objects to ionizing radiation. In 1906, the fundamental law of cellular radiosensitivity was formulated: the inhibitory effect of radiation on cells is greater the more intensively they divide and the less defined their morphology and function — i.e., the less differentiated they are [18]. From 1910 onward, a research group led by the Russian radiologist M.I. Nemenov published a series of works demonstrating the suppressive effects of radiation on the immune system, metabolism, embryogenesis, and reproductive function [19].

In 1911, the world's first monograph on the practical application of radiation in medicine, "Radium in Biology and Medicine" by E.S. London [13], was published. It provided a comprehensive description of the fundamental biochemical and physiological processes underlying radiation injury, the differences in radiosensitivity among various biological objects and systems, as well as the biomedical aspects of radiation sickness.

In 1918, in Petrograd, through the joint efforts of M.I. Nemenov and A.F. Ioffe, the world's first specialized State Institute of Radiology and Radiology (now the Academician A.M. Granov Russian Scientific Center of Radiology and Surgical Technologies of the Ministry of Health of the Russian Federation) was established, followed in 1922 by the Radium Institute, where domestic radium preparations were produced for the first time [20].

By the early 1930s, the potential of natural radioactive sources had been essentially exhausted. Further advances in

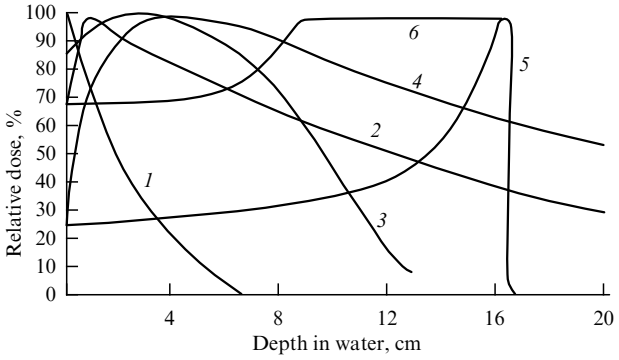


Figure 1. Depth-dose distributions for: *1* — Xrays (140 keV), *2* — ^{60}Co γ-rays (1.17 and 1.33 MeV), *3* — electron beam (25 MeV), *4* — high-energy bremsstrahlung photons (25 MeV), *5* — monoenergetic proton beam (160 MeV), and *6* — spread-out Bragg peak for irradiation of an extended target at depths from 9 to 16 cm.

fundamental and applied nuclear physics required higher energies and intensities of ionizing radiation fluxes. The response to this challenge was the development of various types of charged-particle accelerators: high-voltage direct-action accelerators (1931) [21, 22], the cyclotron (1931) [23], the betatron (1940) [24], the microtron (1945) [25], the synchrocyclotron (1947) [26], the strong-focusing synchrotron (1952) [27], and several others. The use of accelerators laid the foundation for external-beam radiotherapy and to produce diagnostic and therapeutic radionuclides for nuclear medicine.

In modern oncology, radiotherapy (RT) and nuclear medicine technologies occupy a key position among non-invasive antitumor treatment modalities, serving as an effective alternative to surgical intervention [1–4, 28–31]. Radiotherapy, either alone or in combination with other methods, is employed in approximately 70% of cancer patient treatment cases [3]. The primary goal of radiotherapy is the eradication of tumor cells through the action of ionizing radiation while minimizing damage to healthy tissues. In practice, this requires a spatial dose distribution gradient that ensures delivery of a tumoricidal radiation dose to the target while minimizing the dose received by healthy tissues and organs. The problem of achieving dose conformity — i.e., optimal matching of the absorbed dose distribution to the shape and location of the target (tumor) — is addressed for each type of ionizing radiation. This is due to differences in the depth-dose distributions, as illustrated in Fig. 1 for all radiation types currently used in radiotherapy.

The first steps toward the application of particle accelerators in radiotherapy were taken in 1934 in Berkeley, USA. The physicist E. Lawrence and his brother, physician J. Lawrence, were the first to treat a patient using a Sloan-type high-frequency X-ray generator [32]. The device was installed at the University of California Hospital and consisted of a high-voltage resonant transformer operating at radio frequencies under high vacuum conditions, which enabled the attainment of therapeutic voltages on the order of 800–1000 kV.

As early as 1936, merely four years after the discovery of the neutron by J. Chadwick [33], the American physicist G. Locher proposed a fundamentally new radiotherapy modality — neutron capture therapy (NCT) [34]. The concept involved the preliminary accumulation in the tumor of a

stable isotope possessing a high capture cross-section for low-energy neutrons, followed by irradiation with a thermal neutron flux to induce a nuclear reaction whose products are high-linear-energy-transfer particles with potent cytotoxic effects. However, NCT did not receive immediate development, since in the mid-1930s researchers were focused on investigating the biological effects of fast neutrons, which did not require the development of boron-containing agents or methods for producing intense slow-neutron fluxes [35]. At that time, neutron therapy attracted extraordinary interest both for its own potential and as an alternative to X-ray therapy.

In 1936, E. Lawrence and J. Lawrence initiated studies on the effects of fast neutrons on laboratory animals [36]: using E. Lawrence's 27-nch cyclotron, a neutron beam was accelerated to energies of several MeV and directed onto a beryllium neutron-generating target. After examining the growth dynamics of more than one hundred transplanted murine tumors, it was demonstrated that fast neutrons were several times more effective than X-rays [37].

The first clinical trials of fast-neutron therapy for the treatment of human malignant tumors were conducted in 1938 under the leadership of R. Stone, Head of the Department of Radiology at the University of California [38].

Between 1938 and 1943, R. Stone and his colleagues treated 250 patients. By the end of 1943, only 18 remained alive. Stone attributed this disappointing outcome to severe long-term effects of patient overtreatment [39]. This was due to an insufficient understanding of the radiobiological effectiveness of fast-neutron exposure [35]. The resurgence of interest in the clinical application of fast-neutron therapy occurred only in the early 1970s, when accumulated radiobiological data made it possible to calculate equivalent dose. By 1978, more than 3000 patients had been treated in eleven centers across Europe, Japan, and the United States. Fast-neutron therapy at an energy of 7.5 MeV demonstrated twice the therapeutic efficacy of X-rays in the treatment of advanced hypoxic forms of superficial tumors [35].

Concurrently with the development of neutron therapy, photon irradiation techniques were also being refined. The era of conventional photon radiotherapy began in the 1940s, when high-voltage accelerators and betatrons came into use in radiation therapy [24]. In Canada and the United States, betatrons with energies ranging from 13 to 25 MeV, as well as direct-action accelerators with energies up to 4 MeV, were employed. In 1953, the first dedicated medical traveling-wave electron linear accelerator with an energy of 8 MeV was constructed in London [40].

It is noteworthy that the construction of the first cyclotrons enabled the discovery of numerous artificial radioisotopes (^{32}P, ^{131}I, ^{99m}Tc, ^{14}C, ^{60}Co, etc.), which found extensive application in nuclear medicine [41]. In the 1950s and 1960s, electron linear accelerators began to lose ground in prevalence to cobalt units — devices utilizing natural radioactive sources based on the isotope cobalt-60, which emits gamma radiation with energies of 1.17 and 1.33 MeV [42]. At that time, cobalt units were technologically simpler and more accessible to most clinics.

Furthermore, as early as the 1940s, the concepts of stereotactic radiosurgery of the brain were being developed. The Swedish neurosurgeon L. Leksell proposed the concept of radiosurgery, which became known as the Gamma Knife [43]. The concept involves the focusing of multiple gamma rays to a single point corresponding to the location of a brain tumor. The first Gamma Knife unit incorporated 192 cobalt sources, and the first stereotactic procedure using this device was performed in 1968 [44].

In Russia, accelerator and nuclear technologies were also being actively developed in the 1930s–1940s [1]. In early 1937, at the Radium Institute, under the leadership of L.V. Mysovskii, G.A. Gamov, and I.V. Kurchatov, the first cyclotron in Europe with a pole diameter of 1 m was commissioned, and a proton beam with an energy of 3.2 MeV was obtained. In 1944, under the direction of I.V. Kurchatov, the M-1 cyclotron with a pole diameter of 73 cm was constructed at Laboratory No. 2 of the USSR Academy of Sciences (now the National Research Centre 'Kurchatov Institute'). This was the first cyclotron in the USSR and Europe in which a deuteron beam was extracted from the accelerator chamber to the outside. Using this facility, the foundations of radiochemistry were established, and the first samples of 'cyclotron-produced' plutonium in Europe were obtained. In 1946, the physical startup of the largest cyclotron was carried out at the Leningrad Physical-Technical Institute (now the Ioffe Physical-Technical Institute of the Russian Academy of Sciences). The development and commissioning of the first cyclotrons provided a powerful impetus for the further advancement of domestic accelerator technologies.

However, the capabilities of the first cyclotrons proved insufficient to produce radionuclides on the scale required for medical applications. The mass production of numerous artificial radioisotopes became possible only with the advent of nuclear reactors. In 1942, the first controlled nuclear reactor was commissioned in Chicago under the leadership of E. Fermi [45]. On December 25, 1946, as part of the Soviet atomic project under the direction of I.V. Kurchatov, the F-1 reactor — the first in the USSR and Europe — was brought into operation, followed two years later by the 'Annushka' reactor [1]. These developments formed the foundation of a unique scientific and technological reactor infrastructure, which came to be known as the 'Kurchatov tree.' From a single root — the atomic project — dozens of branches emerged, encompassing not only energy production, defense, aviation, marine engineering, and materials science, but also nuclear medicine, diagnostic radiology, and radiotherapy.

The scientific and technological infrastructure established in the postwar years enabled the development of fundamentally new modalities of nuclear radiotherapy — proton and ion beam therapy. In 1946, the American physicist R. Wilson proposed the use of proton beams in radiotherapy [46]. Unlike photons, protons have a finite range in tissue and are characterized by the Bragg peak — a sharp maximum of absorbed dose at the end of the particle track [47] — which makes it possible to significantly reduce the integral dose to healthy tissues (see Fig. 1). The first experiments on the treatment of cancer patients with proton beams were conducted in the United States and Sweden in the late 1950s and early 1960s. In the USSR, work in the field of proton beam therapy (PBT) began in 1967 at the Joint Institute for Nuclear Research (JINR, Dubna), in 1969 at the Institute of Theoretical and Experimental Physics (now NRC 'Kurchatov Institute' — ITEP, Moscow), and at the Leningrad Institute of Nuclear Physics (now NRC 'Kurchatov Institute' — PNPI, Gatchina). By 1990, a total of 2544 patients had been treated

at Russian centers, accounting for one-third of the global clinical experience in PBT [29].

At present, there are 127 clinical PBT centers operating worldwide. According to the Particle Therapy Co-Operative Group (PTCOG), by the end of 2022, more than 300,000 patients had received proton beam therapy [48]. In the Russian Federation, three specialized PBT centers are currently in operation. In addition, two large-scale projects are being implemented at the NRC 'Kurchatov Institute' — the 'OKO' proton ophthalmology facility in Gatchina and the 'Luch-Proton' proton synchrotron with a gantry in Moscow. Their commissioning, scheduled for 2027 and 2029, respectively, will significantly expand the accessibility of this modality in the Russian Federation.

The first attempts at irradiation with heavy ion beams were carried out at the cyclotron of the Lawrence National Laboratory in Berkeley in the 1950s–1960s. By 1992, a total of 2045 patients had been treated with helium ion beams at Berkeley. In 1994, clinical studies with ion beams commenced in Japan following the construction of the HIMAC accelerator at the National Institute of Radiological Sciences, designed to generate a broad spectrum of different ion species [31]. In Russia, in 1967, the U-70 carbon ion accelerator was commissioned at the Institute of High Energy Physics (now NRC 'Kurchatov Institute' — IHEP, Protvino, Moscow Region), and a project is currently underway at this facility to create a medical installation for ion therapy of tumors of various nosologies. The start of clinical use is scheduled for 2028. Worldwide, a total of 17 centers for carbon ion (^{12}C) beam therapy are currently in operation [48].

Today, photon radiotherapy remains the most widely employed modality of external-beam radiotherapy in clinical practice [49]. Photon beams exhibit high penetrating power and allow irradiation of deep-seated tumors. The principal limitation is the exponential attenuation of γ-ray intensity as it passes through body tissues. The depth-dose distribution of high-energy photons exhibits a maximum within the first few centimeters of tissue penetration and gradually decreases as the beam approaches the target, inevitably resulting in irradiation of healthy organs both along the beam path and beyond the tumor (see Fig. 1). To minimize this effect, techniques such as multifield conformal and stereotactic irradiation have been developed, including IMRT, IGRT, VMAT, RapidArc, Tomotherapy, CyberKnife, SRS, and SBRT/SABR [50–52].

However, the efficacy of radiation exposure is determined not only by the conformality of the absorbed dose distribution within the tumor volume, but also by the relative biological effectiveness (RBE) of the specific radiation type [53]. The quality of radiotherapy is governed by the energy-loss mechanisms of different types of ionizing radiation (photons, protons, carbon ions, neutrons, etc.) and the concomitantly enhanced biological efficacy. Figure 2 presents a comparison of the effectiveness of various ionizing radiation modalities employed in radiotherapy. They differ in linear energy transfer (LET), which determines the ability of radiation to deposit a greater or lesser amount of energy per unit path length in matter and, accordingly, to produce a corresponding number of ionization events over the same path length. It is evident that the most effective modalities are hadron therapy techniques — neutron, proton, and ion therapy.

In the energy range applicable to radiotherapy, the LET of so-called sparsely ionizing radiation does not exceed 3–5 keV μm^{-1}. The LET of densely ionizing radiation, depending on its energy, reaches 50–200 keV μm^{-1}. The magnitude of LET, which characterizes the density of ionization events along the track of a photon or particle, is directly related to the RBE of the radiation. RBE begins to increase at LET values of approximately 10 keV μm^{-1} and reaches a maximum at LET values between 100 and 200 keV μm^{-1}. It should be noted that RBE depends not only on LET, but also on the radiosensitivity of the irradiated tissue, the absorbed dose and dose rate, as well as the chosen criterion for assessing biological effect. High LET values make it possible to reduce the influence of the oxygen enhancement ratio (OER), which characterizes the resistance of hypoxic cells to irradiation. It is for this reason that beams of neutrons, π-mesons, and ions heavier than protons — all belonging to densely ionizing radiation — enable effective overcoming of the hypoxia-induced radioresistance of tumors.

A particularly prominent position in terms of both efficacy and targeting precision is occupied by neutron capture therapy, which ensures the selective destruction of tumor cells irrespective of their hypoxia, cell cycle phase, radiosensitivity, or other individual factors. An analogous approach in nuclear medicine is targeted radionuclide therapy, which is currently being actively developed [54–56]; in this modality, radioactive isotopes (α- or β-emitters) are conjugated to targeting molecules that selectively bind to tumor antigens — receptors on the surface of pathogenic cells [1]. However, even with a highly selective carrier, a certain fraction of the radionuclide inevitably accumulates in critical

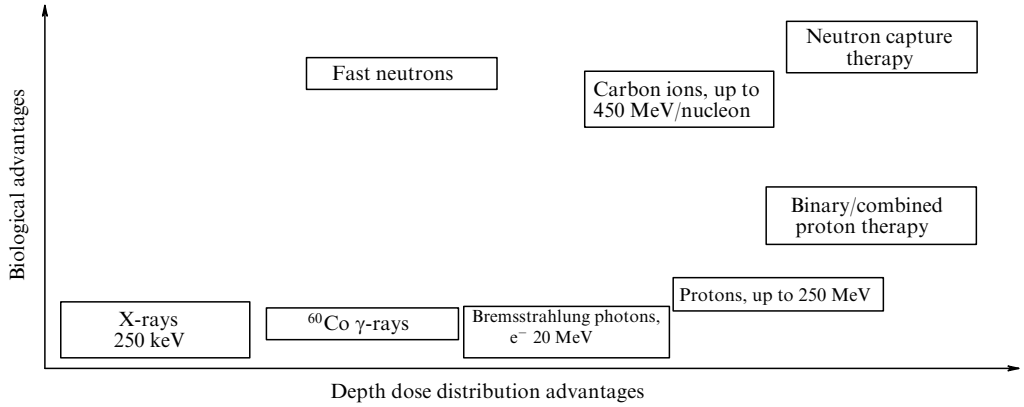


Figure 2. Comparison of the biological effectiveness of different radiation modalities.

organs (liver, kidneys, bone marrow, etc.), creating an undesirable radiation burden [57].

NCT is a binary hadron therapy modality that overcomes the limitations inherent in both conventional radiotherapy and targeted radionuclide therapy [58]. The principle of NCT is based on the action of the products of the thermal neutron capture nuclear reaction by isotopes possessing a high capture cross-section (>500 barns) for this process. Among non-radioactive isotopes, only boron-10 (^{10}B) and lithium-6 (^{6}Li) can provide localized energy deposition due to the high stopping power of the reaction products from $^{10}\mathrm{B}(\mathrm{n},\alpha)^{7}\mathrm{Li}$ or $^{6}\mathrm{Li}(\mathrm{n},\alpha)^{3}\mathrm{H}$. In essence, NCT is a method of producing a radiopharmaceutical *in situ*. Only in a slow-neutron field does the nontoxic, nonradioactive therapeutic isotope become a potent agent for tumor cell destruction through the short-range products of the neutron capture nuclear reaction.

The implementation of NCT requires a neutron source capable of providing the requisite beam parameters, as well as a boron- or lithium-containing agent that enables targeted and selective delivery and retention of the required therapeutic isotope concentrations in tumor cells. This review examines the development of neutron capture therapy technologies, with emphasis on the epithermal neutron sources employed and novel tumor-selective ^{10}B-based agents characterized by high accumulation selectivity and prolonged tumor retention, as well as the dosimetry tools and methods used at all stages of treatment.

2. Historical background and fundamental physical principles of neutron capture therapy

For a radical enhancement of the efficacy of external-beam radiotherapy modalities, the most promising approach is the development of binary technologies based on radiosensitization through the delivery to the tumor of agents that increase the physical and/or effective biological dose, thereby enhancing tumor cell killing upon irradiation. The delivery of such agents is conveniently accomplished using nanoparticles (NPs) with sizes ranging from 5 to 100-nm, composed of the primary sensitizing material, a biologically inert coating ensuring biocompatibility, and ligands (vectors) for targeted delivery to the tumor, improved cellular internalization, and retention until the therapeutic effect is achieved [3, 56, 59–61]. An important attribute of radiosensitizers is their specificity — i.e., a differential affinity for normal versus tumor tissues.

Binary radiation technologies include photon capture therapy (PCT), binary proton beam therapy (PBT) techniques, and neutron capture therapy (NCT).

In PCT, the primary radiation consists of photons from X-ray units and medical accelerators. Tumor cell destruction is achieved through the production of photoelectric absorption electrons and the associated Auger cascade on atoms with high atomic numbers ($Z > 52$): $_{53}$I, $_{64}$Gd, $_{78}$Pt, $_{79}$Au, and others. To date, several agents utilizing NPs of various heavy metals have demonstrated encouraging results in clinical trials. The agent NBTX3® [38] (Nanobiotix, France), based on hafnium oxide NPs, has received marketing authorization for the treatment of soft tissue sarcomas [62, 63]. The agent AGuIX® [39] (NH TherAguix SAS, France), based on gadolinium polysiloxane NPs, is currently in Phase II clinical trials [64]. In May 2024, AGuIX — was granted Fast Track designation by the FDA for the treatment of glioblastoma, and quantitative analysis using magnetic resonance imaging (MRI) has confirmed its selective accumulation in tumor tissue and rapid clearance from normal tissues.

In several experimental *in vitro* and *in vivo* studies of binary PBT techniques employing various NPs, a significant enhancement of proton therapy efficacy has been demonstrated, enabling a substantial reduction in the number of irradiation fractions required to achieve a therapeutic effect [65–69]. In binary proton therapy using NPs, two main mechanisms of therapeutic efficacy enhancement are distinguished: ionization and the generation of reactive oxygen species (ROS) through water radiolysis by secondary electrons. ROS act both as chemical damaging agents and as modulators of biological mechanisms leading to apoptosis. Notably, to ensure high sensitization efficiency, the NPs must be internalized within the cell. In addition, the concept of boron-proton therapy has been proposed, which is based on the nuclear reaction $\mathrm{p} + {}^{11}\mathrm{B} \rightarrow 3\alpha$ [3]. The α-particles are of particular interest, as they exhibit high ionization losses and short ranges (tens of micrometers), resulting in significant localized damage. However, it has been demonstrated both theoretically and experimentally that the yield of nuclear reactions from the interaction of a proton beam with ^{11}B NPs is negligibly small to account for the observed significant enhancement of proton therapy efficacy *in vitro* and *in vivo*, including in boron-proton therapy [70–73]. It has been established that the secondary electrons generated have short ranges, and most of their energy is deposited in the immediate vicinity of the NPs, without producing any appreciable macroscopic dose enhancement within the cell volume [71].

Thus, the purely physical stage of interaction is insufficient to explain the experimentally observed significant sensitization in binary PBT. The development of binary PBT technologies is therefore linked to the investigation of physicochemical and biological mechanisms of enhanced biological effectiveness associated with the intrinsic properties of NPs, which can be induced or amplified by proton irradiation. For example, both theoretical and experimental evidence suggests that ionizing radiation induces a positive charge shift on NPs, leading to improved cellular internalization and enhanced cytotoxicity [74].

Boron neutron capture therapy (BNCT) is also a binary hadron therapy modality based on the selective destruction of tumor cells by high-LET heavy charged particles generated via a nuclear reaction upon interaction of thermal neutrons with a therapeutic agent containing the ^{10}B isotope delivered to the tumor. Absorption of a thermal[1] neutron by a ^{10}B nucleus initiates the prompt nuclear reaction $^{10}\mathrm{B}(\mathrm{n},\alpha)^{7}\mathrm{Li}$, which has a capture cross-section of 3835 barns. The reaction releases 2.79 MeV of kinetic energy, which in 6.1% of events is partitioned exclusively between the lithium nucleus (1.01 MeV) and the α-particle (1.78 MeV), while in 93.9% of events the lithium nucleus emerges in an excited state and subsequently emits a 0.48 MeV-photon. The combined range of the lithium ion and the α-particle in biological tissue does not exceed 12 μm, which is comparable to the size of a single cell. Consequently, 84% of the energy released in the $^{10}\mathrm{B}(\mathrm{n},\alpha)^{7}\mathrm{Li}$ reaction is confined to a single cell diameter. Thus, selective accumulation of the ^{10}B isotope in tumor cells followed by thermal neutron irradiation should result in the preferential destruction of malignant cells with relatively little

[1] Here and throughout the text, 'thermal neutrons' refers to neutrons with an energy of 0.025 eV.

Table 1. Isotopes with high thermal neutron capture cross-sections.

Isotope	Natural abundance, %	Half-life	Reaction type	Cross-section, barns
^{3}He	0.000013	Stable	(n, p)	5333
^{6}Li	7.5	Stable	(n, α)	940
^{10}B	20	Stable	(n, α)	3835
^{113}Cd	12	Stable	(n, γ)	20600
^{135}Xe	—	9.14 hours	(n, γ)	2720000
^{149}Sm	14	Stable	(n, γ)	42080
^{151}Eu	48	Stable	(n, γ)	9200
^{155}Gd	15	Stable	(n, γ)	61100
^{157}Gd	15	Stable	(n, γ)	259000
^{174}Hf	0.16	2×10^{15} years	(n, γ)	561
^{199}Hg	17	Stable	(n, γ)	2150
^{235}U	0.7	7×10^{8} years	(n, f)	681
^{241}Pu	—	13.2 years	(n, f)	1380
^{242}Am	—	16 hours	(n, f)	8000

damage to surrounding healthy tissues.

The concept of BNCT was first formulated by the American radiologist G. Locher in his 1936 paper "Biological effects and therapeutic possibilities of neutrons" [34], one year after H. Taylor and M. Goldhaber described the $^{10}B(n,\alpha)^{7}Li$ nuclear reaction [75]. In the late 1940s, the concept of NCT was independently developed in the USSR by the eminent biochemist A.T. Kachugin [76].

It should be noted that there are more than a dozen other nuclides with high thermal neutron capture cross-sections (Table 1). However, neutron absorption by most of these does not provide localized energy deposition. For example, thermal neutron capture by ^{113}Cd, ^{135}Xe, ^{149}Sm, ^{151}Eu, ^{155}Gd, ^{157}Gd, ^{147}Hf, ^{199}Hg nuclei leads to (n, γ) reactions. The low stopping power of the resulting γ-photons in biological tissues deprives NCT of its main advantage — the selective destruction of only those cells that have accumulated the therapeutic isotope.

Nevertheless, a considerable body of experimental work in the field of NCT has been devoted to the use of gadolinium-157 [77–80]. This is primarily due to the large thermal neutron capture cross-section of this nuclide (248000 barns), as well as the existence of clinically approved MRI contrast agents based on gadolinium, whose pharmacokinetics and pharmacodynamics are well characterized [81]. However, the main dose-producing product of the $^{157}Gd(n,\gamma)^{158}Gd$ reaction is hard photon radiation in the unresolved part of the spectrum, concentrated mainly in the energy range from 2 to 3 MeV. The mean range of such γ-photons in biological tissue is about 40 cm. Of the total decay energy of 7.937 MeV, only 63 keV from conversion and Auger electrons is deposited within 50 μm. Thus, gadolinium neutron capture therapy (GdNCT) does not provide localized action of the $^{157}Gd(n,\gamma)^{158}Gd$ reaction products but can only ensure a relatively uniform absorbed dose distribution over a large volume.

Localized energy deposition can only be achieved through a few (n, α)- and (n, f)-reactions, owing to the high stopping power of the resulting α-particles or nuclear fission fragments. However, beyond the short range of the reaction products, important requirements for isotopes intended for NCT include the absence of radioactivity, low toxicity, and sufficient natural abundance to enable the production of agents highly enriched in the therapeutic isotope. Among the nuclides considered, only boron-10 satisfies all these criteria. It is therefore the basis for the major experimental and clinical developments in the field of NCT [82].

The only competitor to boron-10 among stable isotopes is lithium-6, whose potential for NCT was also discussed in the early publications on the subject [34, 83]. Lithium neutron capture therapy (LiNCT) is based on the reaction $^{6}Li(n,\alpha)^{3}H$, which has a capture cross-section of 940 barns and releases 4.785 MeV of energy. The reaction products — α-particles with an energy of 2.051 MeV and triton nuclei with an energy of 2.734 MeV — have LET values of 150 and 25 keV μm^{-1}, respectively. The range in biological tissue is 11 μm for the α-particle and 63 μm for the triton. The nuclear characteristics of this reaction offer the possibility of releasing 100% of the reaction energy within tumor cells.

However, LiNCT has not undergone significant development comparable to that of BNCT. Progress in this area has been hampered by concerns about lithium toxicity and the lack of efficient carriers analogous to those developed for BNCT. Although lithium salts have been used clinically for more than 60 years in the treatment of psychiatric disorders and are not toxic at the concentrations required for NCT [84], there are still no systematic preclinical *in vivo* studies demonstrating a therapeutic efficacy of LiNCT comparable to that achieved with BNCT [82]. This is due to the high chemical reactivity of lithium, which complicates the design of selective carriers capable of effectively delivering the isotope to tumor cells and retaining it there for the required time.

Thus, boron-10 — owing to its optimal combination of a high thermal neutron capture cross-section, the short range of the $^{10}B(n,\alpha)^{7}Li$ reaction products, the availability of targeted agents, and the active development of production technologies — remains the only isotope currently used in NCT.

Upon irradiation with thermal neutrons, in addition to the selective destruction of tumor cells that have accumulated boron-10, there is always a background contribution to the total absorbed dose arising from nuclear reactions on elements of healthy tissues. According to the International Commission on Radiation Units and Measurements (ICRU), the elemental composition of soft biological tissue by mass includes 76.2% oxygen, 11.1% carbon, 10.1% hydrogen, and 2.6% nitrogen [85]. Among these, the reactions on hydrogen and nitrogen nuclei are the most significant for BNCT dosimetry and require separate consideration.

A reaction of paramount importance in neutron physics and all its applications, including NCT, is elastic scattering of neutrons on hydrogen — $^{1}H(n,n')^{1}H$. This reaction governs the spatial-energy distribution of neutron fields, absorbed dose, albedo, and neutron slowing-down length in irradiated objects. Its cross-section for thermal neutrons is 30 barns.

Another important process is radiative capture of a neutron by hydrogen — $^{1}H(n,\gamma)^{2}H$ — which has a thermal neutron capture cross-section of 0.322 barns and a reaction yield of 100%. The macroscopic absorption cross-section of thermal neutrons by hydrogen far exceeds the total macro-

scopic cross-section of all other elements in normal biological tissue. The γ-photons emitted in this reaction have an energy of 2.22 MeV and a mean range in soft biological tissue of about 40 cm. The LET of electrons generated by the interaction of these γ-photons with biological tissue is 0.3 keV μm^{-1}.

The neutron capture reaction on nitrogen-14 — $^{14}N(n,p)^{14}C$ — produces a recoil proton with an energy of 585 keV and makes a substantial contribution to the neutron absorbed dose in normal biological tissue. The thermal neutron cross-section for this reaction is 1.7 barns. The LET of the emitted proton in tissue-equivalent medium is about 50 keV μm^{-1} [86]. The ^{14}C recoil nuclei have an energy of 40 keV and their contribution to the biological effect of neutrons is small. The spatial distribution of the 'nitrogen' component of the absorbed dose practically coincides with the thermal neutron field.

Negligible contributions to the absorbed dose come from radiative capture reactions on carbon and oxygen — $^{12}C(n,\gamma)^{13}C$ and $^{16}O(n,\gamma)^{17}O$. The thermal neutron cross-sections for these reactions are only 0.0032 and 0.0002 barns, respectively. The elastic scattering cross-section of neutrons on these nuclei is about 2 barns over the entire energy range of interest for NCT.

In addition to radiative capture, inelastic scattering reactions can occur when fast neutrons interact with tissue nuclei. These take place when the neutron energy exceeds the first excitation level of the target nucleus. In these reactions, the neutron is not absorbed but merely slowed down, emitting a γ-photon. Although the cross-sections of such processes reach several barns, their direct contribution to the absorbed dose is negligible. The main significance of inelastic scattering in NCT is the modification of the neutron beam energy spectrum as it passes through tissue.

Thus, the most critical requirement for successful NCT is a high concentration gradient of the therapeutic isotope between tumor cells and normal tissues. If this condition is not met, the background reactions on hydrogen and nitrogen will contribute a dose comparable to or even greater than that from the therapeutic isotope, inevitably leading to severe radiation damage to healthy organs at the expense of the therapeutic effect. This very circumstance predetermined the trajectory and outcome of the early stages of NCT development.

In the early 1940s, the first encouraging experimental evidence for the efficacy of BNCT was obtained. In 1940, P. Kruger published the results of an experiment on the survival of mouse tumor fragments that had been pre-irradiated with a slow-neutron flux in a boric acid solution. The samples were irradiated with a neutron beam generated by bombarding a beryllium target with 16 MeV deuterons from the 60-inch cyclotron at Berkeley [87]. It was found that pre-irradiation of tumor fragments in a boric acid solution at a concentration of ~ 700 μg ml^{-1} (with respect to ^{10}B) resulted in a dose-dependent reduction in their take rate when implanted into healthy mice after irradiation. The results of this experiment provided the first confirmation of BNCT efficacy.

In the same year, P. Zahl, F. Cooper, and J. Dunning conducted an *in vivo* study on mice bearing sarcoma-180 — an aggressively growing tumor that caused death in control animals within 3–4 weeks after inoculation. The authors demonstrated for the first time that intratumoral injection of a boron-containing agent based on boric acid, followed by slow-neutron irradiation, reduced tumor growth by 45% [88]. At the same time, they noted an uneven distribution of boron within the tumor and concluded that for clinical application of BNCT, it would be necessary to develop methods for selective boron delivery that would allow systemic administration of the agent.

An attempt to solve the problem of selective delivery of neutron-capture elements was made in 1941 by P. Zahl and F. Cooper, who administered lithium salts of anionic dyes (Pontamine Sky Blue, Trypan Blue) intravenously to mice bearing transplanted sarcoma-180 [89]. The selective accumulation of these dyes in tumor tissue after intravenous injection had been demonstrated in earlier studies [90, 91]. However, spectroscopic analysis performed 24 h after injection showed that lithium was no longer detectable in the tissues, while the dye remained in the tumor. This indicated that the dye-lithium complex was unstable *in vivo* and could not be used for selective delivery.

In 1950, the American neurosurgeon W. Sweet proposed the use of ^{10}B-containing agents for the treatment of brain tumors, linking the selective accumulation of ^{10}B in tumor cells to the disruption of the blood-brain barrier (BBB) in malignant tissues compared with healthy tissues [92]. Together with M. Javid, he was the first to demonstrate selective boron accumulation in brain tumors. The study was conducted on dozens of volunteer patients who received intravenous injections of borax (sodium tetraborate decahydrate, $Na_2B_4O_7{\cdot}10H_2O$) enriched to 96% in ^{10}B [93]. These results prompted the first clinical trials of BNCT.

The first BNCT procedure in history was performed on February 15, 1951, at Brookhaven National Laboratory on a patient following surgical resection of a brain tumor [94]. Irradiation was carried out at the Brookhaven Graphite Research Reactor (BGRR). Between February 1951 and January 1953, the first ten patients with malignant glioma were treated at the BGRR, eight of whom had previously received photon radiotherapy.

Irradiation was delivered in one, two, or four fractions with intervals of 5–6 weeks. Before irradiation, each patient received an intravenous injection of 100 ml of an aqueous solution containing 20 g of borax. The BNCT results showed short-term clinical improvement in nine of the ten patients; however, the median survival was 97 days, which was comparable to the results achieved with photon therapy at the time [58]. For the second series of clinical trials, involving nine patients, the BGRR reactor was modified, and sodium pentaborate (NaB_5O_8) was chosen as the ^{10}B-containing agent, as it had shown lower toxicity compared with borax. Despite these efforts, patients experienced severe side effects, including severe radiodermatitis of the scalp [95]. The median survival was 147 days [96]. In the third series of clinical trials, which included nine patients, sodium pentaborate was administered before irradiation via the internal carotid artery on the side of the affected hemisphere to avoid high ^{10}B concentrations in the scalp. This approach was successful in eliminating severe skin reactions; however, the median survival was only 96 days [58].

In 1959, specialized high-flux nuclear reactors were built for BNCT at Brookhaven National Laboratory (BMRR, 5 MW) [97] and the Massachusetts Institute of Technology (MITR, 6 MW) [58]. Between 1959 and 1961, a total of 35 patients were irradiated at these reactors. The clinical trials conducted at BGRR, BMRR, and MITR in the United States did not demonstrate the efficacy of BNCT [58, 95, 98, 99]. The reason for this failure was the low selectivity of boron accumulation, which resulted in an unfavorable depth-dose

distribution of thermal neutrons — the scalp received the major dose rather than the tumor. In addition, BNCT dosimetry was based only on boron concentrations in the tumor and surrounding healthy tissues, but not in the blood, which was paradoxical since it was already known at the time that damage to the vascular system was a critical limitation in brain radiotherapy [100]. Another important factor was the underestimation of the 'background' dose to healthy tissues from recoil protons and γ-photons arising from the $^{14}N(n,p)^{14}C$ and $^{1}H(n,\gamma)^{2}H$ reactions. These results led to the cessation of BNCT clinical trials in the United States for three decades. Thus ended the first era of BNCT development.

A pivotal event that influenced the course of BNCT occurred in Japan, where in 1968 H. Hatanaka initiated the first clinical trials of intraoperative BNCT with thermal neutrons, treating the first patient at the Hitachi Research Reactor (HTR, 100 kW) in Tokai. The treatment protocol was designed with the experience of the early US trials in mind [101]. At 10–12 h before irradiation, the agent BSH (sodium mercaptoundecahydro-closo-dodecaborate, $Na_2B_{12}H_{11}SH$), synthesized by the American chemist A. Soloway [102], was administered intra-arterially. By 1989, Hatanaka had achieved impressive results: the 5 year survival rate in patients with grade-3 and grade-4 malignant gliomas was 58% [103]. These findings stimulated new clinical trials of BNCT both in Japan and abroad.

Another BNCT pioneer worth noting is the Japanese professor Y. Mishima. In 1987, he began using boronophenylalanine (BPA) for the treatment of superficial malignant melanoma [104–106], thereby applying BNCT for the first time to tumors outside the central nervous system. Since melanoma is a superficial tumor, thermal neutrons were ideally suited for its irradiation. The selective accumulation of BPA in the tumor occurs because BPA is actively transported into tumor cells by the amino acid transport system LAT1 [107], which is overexpressed in various types of cancer.

In the USSR, research in the field of NCT began in 1964 at the Research Institute of Medical Radiology in Obninsk under the leadership of Yu.S. Ryabukhin [108]. Soviet scientists continued the search for ways to improve BNCT and to develop new approaches [109]. As early as 1966, Ryabukhin provided a theoretical justification for the optimal neutron energy for NCT, which became the basis for subsequent physical treatment planning [110]. In the late 1960s, the scope of research expanded considerably: computational [111] and experimental methods of neutron beam dosimetry were developed [112], the biodistribution of various neutron-capture nuclides, including ^{109}Cd [113] and ^{6}Li [114, 115], was studied, and the potential use of antibodies for targeted delivery to tumors was discussed [116]. The results of the first stage of research in the USSR were summarized in two review articles by Ryabukhin [117, 118].

In the 1970s and 1980s, Soviet NCT research became systematic. Work continued dosimetric support for the method [119–123]. Neutron activation autoradiography methods were developed for quantitative analysis of ^{6}Li distribution in biological specimens [124], preclinical studies of LiNCT were conducted [125], and the possibility of extrapolating the research results to clinical practice was discussed [126]. The prospects of using accelerator-based intermediate-energy neutron sources were also considered [127].

In the mid-1970s, at the horizontal experimental channel (HEC) No. 7 of the IR-8 research nuclear reactor (8 MW) at the Kurchatov Institute, G.I. Borisov and his colleagues built

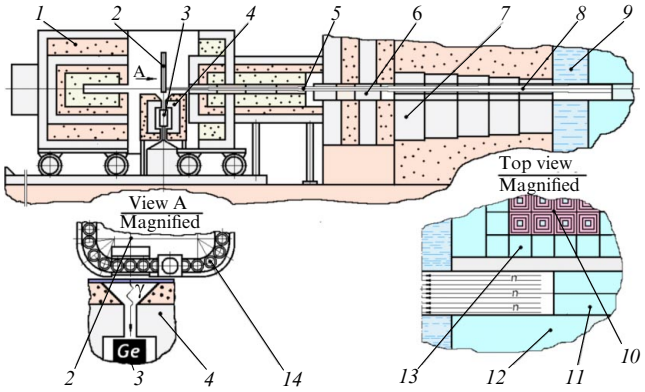


Figure 3. The first experimental facility in the USSR for testing novel ^{10}B-containing agents based on HEC No. 7 of the IR-8 research reactor [130]: *1* — neutron trap, *2* — test objects, *3* — semiconductor detector, *4* — detector shielding, *5* — exit collimator, 6 — outer shielding door, *7* — reactor shielding door, *8* — inner collimator, *9* — reactor pool, *10* — reactor core, *11* — beryllium scatterer, *12* — fixed beryllium reflector, *13* — removable beryllium reflectors, *14* — automatic sample changer.

the first experimental facility in the USSR for NCT research (Fig. 3). A set of theoretical and semi-empirical methods for rapid NCT calculations was developed, along with effective experimental techniques for research and real-time BNCT monitoring based on semiconductor spectrometry of prompt photon radiation generated by neutron interactions with irradiated objects. Unique methods and facilities for shaping therapeutic, diagnostic, and research neutron beams were also developed, including the use of capillary neutron-optical systems [128]. Between 1980 and 2004, using the experimental equipment at the HEC-7 beamline of the IR-8 reactor (see Fig. 3), the total number of *in vitro* measurements of ^{10}B concentration in the organs and tissues of experimental animals exceeded 10,000, and more than 300 experimental animals were irradiated *in vivo*. The measurements were performed virtually around the clock, owing to their full automation.

In the 1980s, Soviet scientists focused on fundamental radiobiological aspects of NCT and the development of conceptual therapeutic approaches. Principles for individual monitoring of tumor and normal tissue response during radiotherapy were developed [129]. The concept of isoeffective dose was formulated, allowing comparison of the biological effects of different radiation types [130]. The synthesis of ion-potential proteins in human cells was investigated, providing insight into the role of these proteins in human biological processes [131]. Biophysical models of radiation-induced effects were proposed to describe the nonlinear response of cells to neutron and γ-irradiation [132].

The research conducted at that time was aimed at preparing for clinical trials that would ensure sufficient safety and reliability of the results. Ryabukhin outlined the following requirements for conducting clinical NCT studies: trials on large animals, monitoring of tumor response to each irradiation fraction, generation of neutron beams with appropriate energy spectra and intensity, selection of the most effective neutron-capture nuclides and suitable carriers for them, physical and radiobiological treatment planning including preliminary determination of RBE values and fractionation regimens, selection of appropriate tumor types for NCT, and development of *in vivo* monitoring methods for neutron-capture nuclides.



Figure 4. Photographs of K.N. Zaitsev (a) and V.N. Mitin (b) in the irradiation room based on HEC No. 4 of the IRT MEPhI research reactor.

Thus ended the second era of BNCT development. The second-generation agents (BSH and BPA) demonstrated a significant improvement in boron accumulation selectivity in tumor cells compared with the first-generation agents (sodium borates, boric acid, and its derivatives).

It became clear that further progress and success in BNCT depended on the ability to treat deeper-seated tumors, which required the production of higher-energy neutron beams. This marked the beginning of the third era of BNCT development, associated with the upgrading of neutron channels at research and experimental nuclear reactors to obtain epithermal[2] neutron beams.

At the National Research Nuclear University 'MEPhI,' in the early 1990s, a facility based on the tangential HEC No. 4 of the IRT MEPhI reactor (2.5 MW) was built for preclinical NCT studies (Fig. 4) [134]. An experimental base was established for the quantitative determination of ^{10}B and Gd in biological tissues using neutron radiation analysis, track autoradiography, and instrumental neutron activation analysis, which enabled measurements of ^{10}B concentrations down to 0.2 μg g^{-1} and Gd down to 1 μg g^{-1} in biological tissue samples [135].

Under the leadership of the prominent Russian veterinary surgeon and oncologist V.N. Mitin, in the 2000s, a study on 60 dogs with spontaneous tumors demonstrated the high efficacy of BNCT in the extracorporeal treatment of osteosarcoma and other malignant neoplasms [58, 136]. Using BPA, complete tumor regression was achieved in 78% of cases. In 2006, following successful trials, a decision was made to upgrade the experimental volume of HEC No. 1 at the IRT MEPhI reactor to enable clinical studies with a convertible beam of thermal and epithermal neutrons. Unfortunately, since 2009 the IRT MEPhI reactor has been in a prolonged shutdown, and the reconstruction of the experimental volume of HEC No. 1 was never completed.

In 1994, new clinical trials began in the United States using epithermal neutron beams at the Brookhaven National Laboratory [137] and the Massachusetts Institute of Technology [138]. In Europe, clinical BNCT trials with epithermal neutrons commenced at the high-flux HFR reactor (45 MW) in the Netherlands in 1996 [139]. Soon after, clinical studies were launched in Finland [140], Sweden [141], the Czech Republic [142, 143], Japan [144], Argentina [145], and Taiwan [146]. The indications for BNCT expanded: in addition to brain tumors, the method was applied to head and neck cancer [147, 148], meningioma [149], pleural mesothelioma [150], and hepatocellular carcinoma [151]. It was clinically confirmed that BNCT is effective in cases where the tumor site had previously received a high dose from conventional radiotherapy, making retreatment with traditional methods impossible.

Despite these efforts, scientific progress, and positive clinical results, funding for BNCT research in the United States and Europe declined significantly in the early 2000s. One important reason was the low level of interest from the Western medical community in continuing BNCT clinical trials [58]. Most research reactors in use at the time were located far from university hospitals and were not readily accessible for medical applications. As a result, it was not feasible to conduct clinical trials with enough patients to obtain statistically significant results that could justify the continued use of expensive nuclear reactors. In Europe, the longest-running active clinical studies were those in Finland at the FiR-1 reactor (250 kW), but these too were discontinued in 2012 [58].

In Japan, a continuous transition from thermal to epithermal neutron beams was successfully achieved. In 1995–1996, the neutron channel of the Kyoto University Research Reactor (KURR, 5 MW) was upgraded to enable neutron spectra ranging from nearly purely thermal to epithermal. A similar facility was built in 1996 at the Japanese research reactor JRR-4 (3.5 MW). Regrettably, following the Fukushima accident in 2011, the JRR-4 reactor was damaged beyond repair [58]. Today, the only reactor in Japan still suitable for patient treatment is KURR. Outside Japan, BNCT continues to be performed at the RA-6 reactor (1 MW) at the Bariloche Atomic Centre (Argentina), the THOR reactor (2 MW) at Tsing Hua National University (Taiwan), and a dedicated compact medical reactor in Beijing (30 kW, China) for emergency treatments. The largest numbers of patients have been treated at reactors in Japan (~ 800), Finland (~ 250), and Taiwan (~ 200).

Although nuclear reactors have been used and continue to be used for a considerable number of BNCT studies, the scientific community has reached a consensus that the widespread clinical implementation of BNCT can only be achieved with accelerator-based neutron sources [58, 82]. The development of dedicated medical neutron sources based on nuclear reactors is hindered by high cost, operational complexity, licensing requirements, and the impossibility of installing them in hospital settings. For example, in Japan it proved impossible to register the KURR research reactor as a medical device [152].

The difficulties in implementing BNCT with nuclear reactors led to the fourth era of the method's development — the transition to accelerator-based epithermal neutron sources. Accelerator-based sources are safer, more compact and can produce epithermal neutron beams only through specially designed systems capable of accelerating proton or deuteron beams with currents of several milliamperes to energies ranging from a few to tens of MeV for use in neutron-generating reactions. In 1994, the first international workshop on accelerator-based neutron sources for BNCT was held in the United States, where existing projects and achieved results were discussed in detail [153]. In 2003, T. Blue and J. Yanch published the most comprehensive review of accelerators for BNCT available at that time [154].

Today, the challenge of creating integrated accelerator-based neutron sources for BNCT has been largely resolved [58, 82, 155]. It can be assumed that BNCT is now entering the fifth era of its development, associated with the design of novel targeted agents that can more selectively deliver and retain the

[2] Here and throughout the text, 'epithermal neutrons' refers to neutrons with energies in the range from 0.5 eV to 10(30) keV.

required ^{10}B concentrations in tumor cells during therapy. For decades, clinical BNCT practice has been limited to just two second-generation low-molecular-weight compounds — BPA and BSH — both of which have serious drawbacks [58].

In recent years, research on third-generation agents has been actively pursued worldwide [156–158]. The main directions are focused on the development of targeted nanosystems, boron conjugates with amino acids, and various therapeutic platforms. The primary goal in developing new agents is to increase boron concentration, accumulation selectivity, and tumor retention time. Solving this problem would open the door to broader clinical application of BNCT for various forms of cancer and would allow the full potential of this unique method to be realized.

Beyond the development of targeted ^{10}B-containing agents, the issues of metrological and dosimetric support for BNCT are no less pressing [58, 82]. The complex mixed radiation field (thermal, epithermal, and fast neutrons, primary and secondary γ-radiation, and nuclear reaction products) requires separate determination of the contribution of each component to the absorbed dose in both the tumor and critical organs and healthy tissues. The lack of standardized dosimetry methods and protocols remains a serious obstacle to the widespread implementation of BNCT in clinical practice.

Addressing these challenges requires new research-grade sources of low-energy neutrons. In the Russian Federation, only two neutron sources are currently available for NCT experiments: the VITA^{TM} research accelerator-based neutron source at the Institute of Nuclear Physics of Siberian Branch Russian Academy of Sciences (hereinafter BINP SB RAS) [159] and a biological beamline based on HEC No. 1 of the IRT-T research reactor at Tomsk Polytechnic University [160]. To address this problem, a project was launched in 2025 to build a biological beamline at HEC No. 7B of the IR-8 reactor at the National Research Centre 'Kurchatov Institute' (Moscow).

3. Modern neutron sources for boron neutron capture therapy

The history of BNCT development has convincingly demonstrated that the success of the method critically depends on the quality of the neutron beam. In BNCT, neutrons are classified by energy range as follows: thermal neutrons are those with energies below 0.5 eV, epithermal neutrons are those with energies from 0.5 eV to 10(30) keV, and fast neutrons are those with energies above 10 keV [82]. The upper boundary of the epithermal range at 30 keV is set because neutrons with this energy provide the greatest treatment depth with minimal impact on healthy tissues. An ideal source should deliver an intense epithermal neutron flux, sufficient tissue penetration depth, minimal contributions to the total absorbed dose from background γ-radiation and fast neutrons and should be suitable for installation in a hospital setting.

Charged-particle accelerators used for BNCT include mainly proton cyclotrons (5–30 MeV), electrostatic accelerators (2.0–2.8 MeV), and linear resonant (radio-frequency) accelerators (2.5–10 MeV). Figure 5 shows a schematic diagram of a typical accelerator-based BNCT source, which consists of three main components: a charged-particle accelerator, a beam transport system, and a neutron-generating system. The accelerated proton or deuteron beam is delivered via the beam transport system to the neutron-generating target. The fast neutrons generated in the target pass through a beam shaping assembly (BSA), whose primary task is to moderate the generated neutrons to the epithermal energy range as efficiently as possible without significant loss of flux intensity, while suppressing the accompanying background γ-radiation. The therapeutic beam then enters the irradiation room where the patient is positioned. The final moderation of neutrons to thermal energies occurs in the tissue of the patient on the path to the tumor site.

This chapter discusses the main nuclear reactions used for neutron generation in BNCT, the typical structure of a BSA for producing epithermal neutrons, and currently operational accelerator-based neutron sources for BNCT.

3.1 Major neutron-generating nuclear reactions

For neutron generation using charged-particle beams, nuclear reactions involving nuclei with weakly bound neutrons are typically employed. From an energy standpoint, these are divided into exothermic and endothermic reactions (Table 2).

Table 2. Main nuclear reactions for neutron generation.

Exothermic reactions	Endothermic reactions
$d + d \rightarrow {}^{3}He + n + 3.265$ MeV	$T + p \rightarrow {}^{3}He + n - 0.764$ MeV
$T + d \rightarrow {}^{4}He + n + 17.588$ MeV	$^{7}Li + p \rightarrow {}^{7}Be + n - 1.646$ MeV
$^{7}Li + d \rightarrow {}^{8}Be + n + 15.028$ MeV	$^{7}Li + p \rightarrow {}^{7}Be + \gamma + n - 1.646$ MeV
$^{7}Li + d \rightarrow 2{}^{4}He + n + 15.122$ MeV	$^{9}Be + p \rightarrow {}^{9}B + n - 1.851$ MeV
$^{9}Be + d \rightarrow {}^{10}B + n + 4.362$ MeV	$^{45}Sc + p \rightarrow {}^{45}Ti + n - 2.840$ MeV
	$^{51}V + p \rightarrow {}^{51}Cr + n - 1.536$ MeV
	$^{12}C + d \rightarrow {}^{13}N + n - 0.282$ MeV

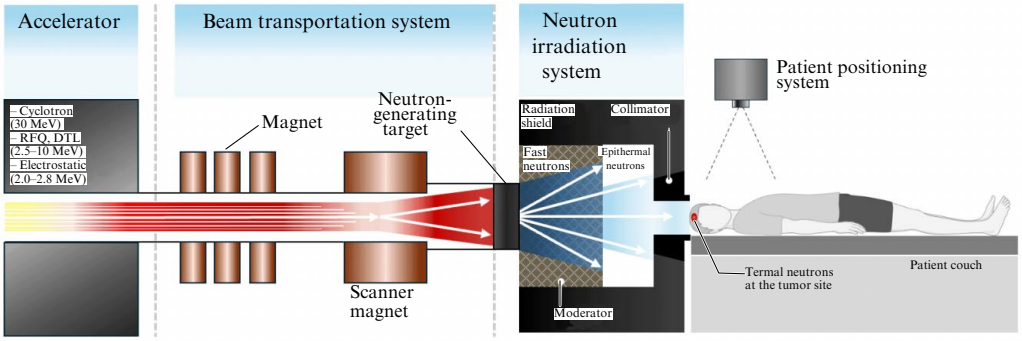


Figure 5. Schematic of an acceleratorbased neutron source for BNCT showing its main components.

Exothermic reactions do not require a minimum kinetic energy of the incident charged particle, except for that needed to overcome the Coulomb barrier. The energy yield of such reactions, written as $Q = (M_i - M_0)c^2$, where M_i is the sum of the rest masses of the initial particles and M_0 is the sum of the rest masses of the reaction products, is always positive. A typical example of an exothermic reaction is the d–d reaction, one channel of which produces helium-3 and a neutron. The energy yield of this reaction is 3.265 MeV. Neglecting the kinetic energy of the incident deuteron, the energy of the emerging neutron is 2.451 MeV.

For comparison, the energy spectrum of fission neutrons in nuclear reactors, well described by the Maxwell distribution $F(E) = 0.77\sqrt{E}\exp(-0.775E)$, covers the energy range up to 10 MeV and has a mean value of about 2 MeV. Thus, the energy of neutrons generated in the d–d reaction exceeds the average energy of fission neutrons. Therefore, from the standpoint of the energy of generated neutrons, d–d generators have no crucial advantage over reactors. Both types of sources require filtering and moderation of fast neutrons to obtain an energy spectrum suitable for BNCT. The most effective approach is to use a generation process that initially minimizes the fast-neutron flux intensity.

Endothermic reactions, in contrast, require a minimum threshold energy of the incident particles. Near the threshold, the neutron energy is very low, making endothermic reactions highly efficient for BNCT. For this reason, only three threshold reactions that produce neutrons with energies lower than those from nuclear reactors are generally considered: $^{7}\mathrm{Li}(\mathrm{p,n})^{7}\mathrm{Be}$, $^{9}\mathrm{Be}(\mathrm{p,n})^{9}\mathrm{B}$ and $^{12}\mathrm{C}(\mathrm{d,n})^{13}\mathrm{N}$. The last of these is not actually used because of its low neutron yield (Fig. 6). Of the remaining two, the most efficient is the $^{7}\mathrm{Li}(\mathrm{p,n})^{7}\mathrm{Be}$ reaction, since its cross-section is more than three times higher than that of the $^{9}\mathrm{Be}(\mathrm{p,n})^{9}\mathrm{B}$ reaction (Fig. 7). Nevertheless, the $^{9}\mathrm{Be}(\mathrm{p,n})^{9}\mathrm{B}$ reaction can also be used, but to achieve a comparable neutron flux intensity, higher proton energies are required, which inevitably leads to higher neutron energies.

Let us consider in more detail the $^{7}\mathrm{Li}(\mathrm{p,n})^{7}\mathrm{Be}$ reaction, which is considered the best solution for BNCT in terms of neutron-physical characteristics. The proton threshold energy is $E_p = 1.882$ MeV. At this incident proton energy, the neutron is emitted with zero energy in the center-of-mass system and has an energy of about 30 keV in the laboratory system, which corresponds to the upper boundary of the epithermal range. At $E_p < 1.92$ MeV, the neutrons are emitted in the forward direction due to kinematic collimation. For example, at $E_p = 1.91$ MeV, the maximum neutron energy is 105 keV, the average energy is 42 keV, and the maximum and average emission angles are 60° and 28°, respectively [161]. Kinematic collimation provides high efficiency in terms of the ratio of usable neutrons to generated neutrons. When the proton energy significantly exceeds the reaction threshold, neutrons are also emitted predominantly in the forward direction in the laboratory system, and the neutron energies for angles greater than 90° are negligible.

The fabrication of a lithium target initially appeared problematic because of the low melting point of lithium (182 °C), its low thermal conductivity (71 W m^{-1} K^{-1}), and its high chemical reactivity. To achieve the required therapeutic epithermal neutron flux of about 10^9 cm^{-2} s^{-1} at the tumor site, relatively high proton beam currents on the order of 10 mA are required. The substantial heat load on the target, about 1 kW cm^{-2}, necessitates efficient cooling.

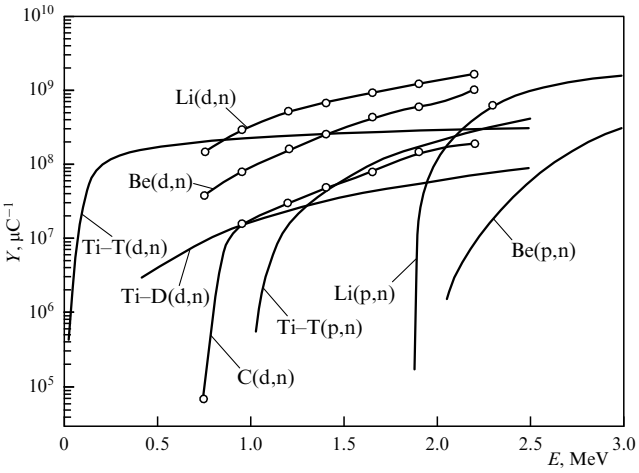


Figure 6. Neutron yield from various reactions in thick [3] targets.

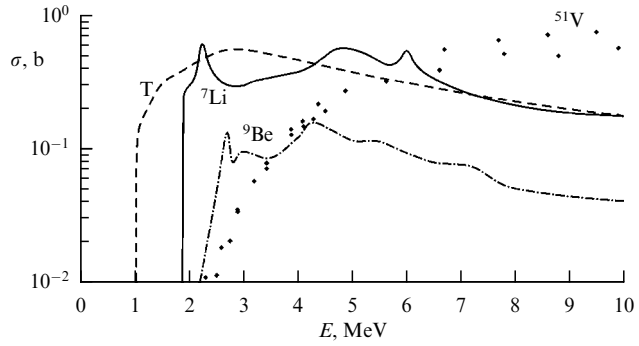


Figure 7. Neutron production cross-section — as a function of proton energy E for proton-induced reactions on tritium (T), lithium (^{7}Li), beryllium (^{9}Be), and vanadium (^{51}V) targets.

It should be noted that neutron generation via the $^{7}\mathrm{Li}(\mathrm{p,n})^{7}\mathrm{Be}$ reaction is accompanied by the production of the radioactive isotope ^{7}Be, and the interaction of the proton beam with lithium produces 478 keV γ-photons through inelastic proton scattering on lithium nuclei. In addition, the radioactive decay of ^{8}Be nuclei formed in the $^{7}\mathrm{Li}(\mathrm{p},\gamma)^{8}\mathrm{Be}$ reaction emits γ-photons with energies of 16–19 MeV, while the thermonuclear reactions $^{7}\mathrm{Li}(\mathrm{p},\alpha)\alpha$ and $^{6}\mathrm{Li}(\mathrm{p},\alpha)^{3}\mathrm{He}$ produce α-particles.

Although the development of a reliable lithium neutron-generating target initially seemed unattainable, these difficulties were successfully overcome through a combination of research and engineering solutions. At the BINP SB RAS, a technology was developed for fabricating lithium targets that ensures long-term, stable neutron generation without yield degradation. To achieve the optimal target configuration, techniques were developed for depositing a thin layer of pure lithium with controlled thickness, the most radiation-resistant and low-activation substrate materials were identified, and provisions were made for easy removal of the target substrate together with the activated lithium. It was found that blister formation on the copper substrate surface does not reduce the neutron yield, and virtually all the radioactive beryllium remains in the lithium layer. All technological solutions and research results are described in detail in the monograph [159] and review [162].

[3] A target is considered thick if the incident particle loses enough energy in it to fall below the reaction threshold.

3.2 Epithermal neutron beam shaping assembly

A key element of accelerator-based neutron sources for BNCT is the beam shaping assembly (BSA). The main functions of the BSA are to provide the neutron beam characteristics required for BNCT and to transport the neutron beam to the exit aperture and into the irradiation room where the patient is positioned. Several requirements are imposed on the neutron beam characteristics at the exit aperture.

The neutron energy spectrum should have a high fraction of neutrons in the therapeutic energy range, determined by the tumor location. As a rule, thermal neutron beams are used for treating superficial tumors (e.g., melanoma), while epithermal neutrons are used for deeper-seated tumors (head and neck or brain tumors).

The intensity of the therapeutic neutron flux delivered to the patient must be sufficiently high to complete the irradiation in about one hour. In some cases, the treatment may be split into two one-hour fractions. According to IAEA recommendations [82], with current boron-containing agents, the epithermal neutron flux intensity at the beam exit aperture should reach $\phi_{\text{epi}} \geqslant 5 \times 10^8$ cm^{-2} s^{-1} when measured *in air*. From a clinical standpoint, shorter irradiation times (e.g., 30 minutes) are preferable, which would require twice the epithermal neutron flux intensity.

Beam directionality is also important; it is defined as the ratio of the neutron current J to the neutron flux intensity ϕ. The ratio J/ϕ serves as a measure of the neutron beam parallelism. In simpler terms, it represents the average cosine of the angle between the beam axis and the direction of motion of neutrons entering the irradiated object. The directionality value indicates how much the penetration of therapeutic neutrons with the original energy spectrum into tissue is reduced. Ideally, this value should be close to unity for two reasons. First, it limits beam divergence and thus reduces irradiation of healthy tissues. Second, a forward-directed beam allows the patient to be positioned farther from the exit aperture when anatomically necessary. In addition, beam directionality is desirable for boron imaging by prompt gamma spectroscopy [163], although this method can also be implemented without meeting this requirement. According to IAEA recommendations [82], for treating deep-seated tumors, the J/ϕ_{epi} ratio should be at least 0.7; for superficial tumors, values around 0.3 are acceptable.

Any therapeutic neutron beam is contaminated with high-energy neutrons and photons. The intensity of this background radiation should be minimized by choosing the optimal configuration and material composition of the BSA elements. The fraction of fast neutrons that cause damage to healthy tissues both at the surface and deep within the irradiated volume should be reduced by a moderator and filters placed in the BSA. Photons, generated both by the interaction of the primary accelerated charged particles with the neutron-generating target and by interactions with other structural materials of the target assembly, also cause undesirable radiation damage to healthy organs and tissues and should be filtered out by dedicated BSA components. When the therapeutic neutron energies lie in the epithermal range, the thermal neutron flux intensity should be minimized to reduce the absorbed dose to the skin.

Typically, the BSA is surrounded by biological shielding, which ensures that the absorbed dose to nontarget organs and tissues of the patient is reduced to acceptable levels.

The BSA configuration, its components, their dimensions, and material composition are determined by the energy distribution of the primary neutrons generated by the source and the required therapeutic spectrum. A typical BSA structure for producing an epithermal neutron beam includes the following elements: a fast-neutron filter, a neutron moderator, a neutron reflector, thermal neutron and gamma filters, a collimator, and biological shielding. For generating a thermal neutron beam, the thermal neutron filter is omitted, and the moderator dimensions may be increased.

As a rule, in modern accelerator-based BNCT sources, materials with high cross-sections or resonance peaks in the high-energy neutron range, such as iron or lead, are used for the fast-neutron filter. These materials can reduce neutron energy to about 1 MeV through inelastic scattering, as well as through (n, 2n), (n, 3n) and (n, xn) reactions. However, it should be noted that some of these reactions produce long-lived radioactive nuclides.

As noted in Section 3.1, modern accelerator-based neutron sources mainly use two threshold neutron-generating reactions: ^{7}Li(p,n)^{7}Be and ^{9}Be(p,n)^{9}B. In accelerator-based sources with a beryllium target, the proton energies E_{p} range from 5 to 30 MeV. The maximum energy of neutrons emitted in the forward direction relative to the target is $E_{\text{p}} - E_{\text{thresh}}$, where $E = 2.057$ MeV. Therefore, unlike sources with a lithium target, where at proton energies $E_{\text{p}} \sim 2.5$ MeV the energy of the generated neutrons is on the order of several hundred keV, the use of a beryllium target requires a fast-neutron filter in the BSA, whose thickness depends on E_{p}. According to IAEA recommendations, the absorbed dose from fast neutrons per unit epithermal flux should satisfy $D_{\text{fast}}/\int \phi_{\text{epi}}(t)\,\mathrm{d}t \leqslant 7 \times 10^{-13}$ Gy cm^2, where $\int \phi_{\text{epi}}(t)\,\mathrm{d}t$ — is the epithermal neutron fluence.

Typically, the energy of neutrons that have passed through the fast neutron filter (if present) is too high for patient irradiation. The main function of the moderator in the BSA is to reduce the neutron energy to the required therapeutic range at the beam exit aperture. For the reasons mentioned above, the moderator in accelerator-based sources with a lithium target is considerably more compact. When designing the moderator, a compromise must be reached between the neutron flux intensity and the neutron energy spectrum at the beam exit aperture. In principle, the fraction of fast neutrons can be reduced arbitrarily by increasing the moderator size, but this will also reduce the therapeutic neutron flux intensity due to neutron absorption within the moderator or leakage through the reflectors.

The moderator may consist of one or several different materials. The main requirements for these materials are high radiation resistance, no moisture desorption under intense ionizing radiation, high density, and the absence of long-lived neutron activation products. It is generally believed that the moderator for the BSA should be made of a material with the highest possible fluorine concentration, since only fluorine has a significant inelastic scattering cross-section for neutrons below 1 MeV, enabling rapid moderation to energies of about 200 keV.

Table 3 presents data on the density of fluorides and their fluorine concentration. In terms of fluorine concentration and density, magnesium and aluminum fluorides are the best, making them the most effective moderator materials. The fluorine concentration in calcium fluoride and Teflon is noticeably lower, while lithium fluoride is considered only as a thin filter at the BSA exit to absorb thermal neutrons via the ^{6}Li(n, α)^{3}H reaction.

Table 3. Density and fluorine concentration of various fluorides.

Material	Density, g cm^{-3}	Fluorine nuclei concentration, 10^{22} cm^{-3}
Aluminum fluoride, AlF_3	2.88	6.19
Magnesium fluoride, MgF_2	3.177	6.14
Lithium fluoride, LiF	2.639	6.13
Teflon, C_2F_4	2.2	5.29
Calcium fluoride, CaF_2	3.18	4.90

Let us now consider the elastic scattering of neutrons on magnesium and aluminum. Since the mass numbers of magnesium and aluminum nuclei are close, the average logarithmic energy decrements ξ are also close: 0.08 for magnesium and 0.072 for aluminum. The inelastic scattering cross-sections are such that neutron moderation on magnesium is more efficient than on aluminum over almost the entire energy range, except in the regions around 25 and 150 keV. For this reason, it is optimal to use a composite moderator: magnesium fluoride near the target and aluminum fluoride at the exit, since neutrons with energies below 20 keV scatter weakly on aluminum.

To prevent leakage of neutrons scattered by the filter and moderator materials from the BSA, it is surrounded by reflectors, typically made of materials with high cross-sections or resonance peaks in the high-energy neutron range. Lead or graphite are often used as BSA reflectors for epithermal neutron production. The choice of lead as a reflector only changes the neutron direction without energy loss ($\xi = 0.01$), unlike graphite ($\xi = 0.158$). When the neutrons generated in the forward direction have significantly higher energies than those emitted at angles greater than 90°, a graphite reflector should be used in the forward hemisphere and a lead reflector in the rear hemisphere to obtain a neutron beam as close to monochromatic as possible.

After the moderator, or in the collimator before the exit aperture of the epithermal neutron beam, a thermal neutron filter made of cadmium or ^{6}Li is installed. Cadmium has a higher thermal neutron capture cross-section compared with ^{6}Li (see Table 1), but the advantage of ^{6}Li is that the ^{6}Li(n,α)^{3}H reaction is not accompanied by γ-ray emission. According to IAEA recommendations [82], the ratio of thermal neutron flux (ϕ_{th}) to epithermal neutron flux (ϕ_{epi}) should satisfy $\phi_{th}/\phi_{epi} \leqslant 0.05$. However, the allowable thermal neutron fraction in the beam depends on the tumor location and size. For example, in the case of large head-and-neck tumors extending to the skin surface, the thermal component may be beneficial.

As neutrons pass through the BSA, they can activate its structural materials, leading to the emission of a significant number of photons that contribute to the background absorbed dose in healthy tissues. Some photons arise from prompt (n,γ)-reactions, but the γ-background also builds up gradually from the activation of long-lived radionuclides. Therefore, a γ-ray filter is installed in the exit part of the BSA, typically made of lead or bismuth — materials with high atomic number Z that effectively attenuate γ-radiation. Bismuth has the advantage of being more transparent to neutrons than lead. However, neutron irradiation of bismuth can produce the radioactive isotope ^{210}Po, an alpha-emitter with a half-life of 138 days, which requires additional safety measures. According to IAEA recommendations [82], the absorbed dose from γ-radiation per unit epithermal flux should satisfy $D_{fast}/\int\phi_{epi}(t)\,dt \leqslant 2 \times 10^{-13}$ Gy cm^2, where $\int\phi_{epi}(t)\,dt$ — is the epithermal neutron fluence.

The neutrons, now having the energy spectrum required for BNCT, then enter the collimator, whose main role is to efficiently transport the neutron beam to the exit aperture. The central part of the collimator along the beam direction is usually an air cavity surrounded by materials that effectively reflect neutrons. The collimator is typically cone-shaped, focusing the neutrons onto the beam aperture. The space near the collimator exit is surrounded by neutron-absorbing materials to prevent neutron leakage beyond the beam aperture. The collimator is usually made of polyethylene or lead; to reduce neutron leakage, lithium fluoride (LiF) or boron carbide (B_4C) is added to the polyethylene.

The optimal collimator length is determined by a compromise between neutron flux intensity and beam directionality J/ϕ at the beam aperture, as well as by the biological shielding configuration. On the one hand, a longer collimator improves beam directionality, but this comes at the cost of reduced neutron flux intensity at the beam aperture. On the other hand, a collimator that is too short requires a reduction in the thickness of the biological shielding between the BSA and the irradiation room where the patient is positioned, which may lead to neutron leakage.

It should be noted that, unlike conventional radiotherapy techniques, where multileaf collimators are typically used to shape the radiation beam, the use of such devices in BNCT is essentially meaningless. Unlike photons, protons, or carbon nuclei, the exact location of a neutron within the patient's body cannot be predicted due to the inevitable diffusion of thermal neutrons inside the body. One can only say that from the point of entry into the body, a neutron may be somewhere within a volume of about one liter, with the highest probability at a depth of 2–3 cm [164]. In BNCT, the dose gradient between the tumor and healthy tissues is determined by the required boron concentrations in the tumor cells and their retention during irradiation.

The exit aperture of the therapeutic neutron beam is typically circular in shape, made of materials that effectively absorb neutrons and photons, and its diameter is adjusted according to the size and shape of the irradiation field using special applicators. For irradiating head-and-neck tumors, brain tumors, and malignant melanomas, beam apertures with diameters of 10–15 cm are typically used. For irradiating the chest area in cases of mesothelioma or lung cancer, larger-diameter apertures are employed.

Currently, efforts are underway to develop collimation and beam aperture systems that allow more flexible patient positioning while reducing over-irradiation of healthy tissues. For example, in [165], a collimation system was developed that, by extending the collimator by 5–10 cm, reduces irradiation time by 60%, decreases the dose to the mucosa by 25%, and provides more comfortable patient positioning while maintaining the therapeutic neutron flux intensity.

IAEA recommendations [82] for the characteristics of an epithermal therapeutic neutron beam are presented in Table 4. It should be noted that the beam quality parameters listed in the table apply to the use of epithermal neutron beams from accelerator-based sources for BNCT of deep-seated tumors when BPA is used as the boron-containing agent. For other clinical cases and boron compounds, a different set of values may be considered optimal.

Table 4. Reference beam quality parameters for epithermal neutron beams.

Beam quality component	Value
Therapeutic epithermal flux	$\geqslant 5 \times 10^8$ cm^{-2} s^{-1}
Thermal to epithermal flux ration	$\leqslant 0.05$
Beam directionality	$\geqslant 0.7$
Fast neutron dose per unit epithermal fluence	$\leqslant 7 \times 10^{-13}$ Gy cm^2
Gamma dose per unit epithermal fluence	$\leqslant 2 \times 10^{-13}$ Gy cm^2

3.3 Operational accelerator-based neutron sources for boron neutron capture therapy

According to the International Society for Neutron Capture Therapy (ISNCT), there are 29 accelerator-based neutron source projects for BNCT worldwide [155]. Of these, 11 centers are already treating patients or conducting clinical trials, while the remainder are used for scientific research or are in the commissioning stage. The largest number of projects are concentrated in Japan and China; other accelerator-based neutron sources are in Italy, Russia, South Korea, Finland, Israel, Spain, and the United Kingdom.

An invaluable contribution to the development of BNCT methodology has been made by Sumitomo Heavy Industries, Ltd. (SHI), which developed an accelerator-based neutron source based on the HM-30 proton cyclotron (30 MeV, 1 mA) with a beryllium target [166]. A distinctive feature of the SHI neutron source is the use of neutrons with maximum energies up to 28 MeV, which requires an extended moderator to achieve an epithermal spectrum while keeping the fast-neutron contribution to the absorbed dose within acceptable limits. The therapeutic beam is obtained using a reflector made of lead and iron, and a moderator made of aluminum and calcium fluoride. The resulting epithermal neutron flux intensity at the beam aperture is 1.2×10^9 cm^{-2} s^{-1}.

The first facility based on the HM-30 cyclotron, named C-BENS (Cyclotron-based Epithermal Neutron Source), was installed at the Institute for Integrated Radiation and Nuclear Science (formerly the Kyoto University Research Reactor Institute, KURRI) in Kumatori Prefecture, adjacent to the KURR reactor. During clinical trials conducted from February 2016 to June 2018, 27 patients with glioblastoma were treated, with positive results [167].

The second system based on the HM-30 cyclotron (Fig. 8) was installed at the Southern Tohoku Hospital in Koriyama, where from June 2016 to February 2018, 21 patients with locally advanced head-and-neck tumors were treated, also with encouraging results [168]. Unlike the facility at KURRI, this system consists of two treatment rooms; the patient is positioned lying on a specialized procedure table in a separate preparation room located outside the irradiation room. After positioning, the procedure table is transported into the irradiation room via a rail system remotely controlled by the operator. After irradiation, the patient is transported back in the same manner. This approach effectively addresses the acute problem of personnel radiation safety, since the high yield (up to 10^{15} s^{-1}) of fast neutrons (up to 28 MeV) causes significant activation of the facility and structural materials.

In 2020, SHI received approval for the manufacture, sale, and clinical use of its system, and Stella Pharma received approval for the use of Steboronine® (Borofalan, a BPA analogue) for BNCT. Currently, treatment is being conducted at the Osaka Medical University BNCT Center, equipped with the third SHI system, and at the Southern Tohoku Hospital. Each center treats about 100 patients with locally advanced head-and-neck tumors annually. The fourth Sumitomo system is located at the BNCT Center of Pengbo Hospital (Bao, Hainan, China), where the first patient was treated in 2026 [169].

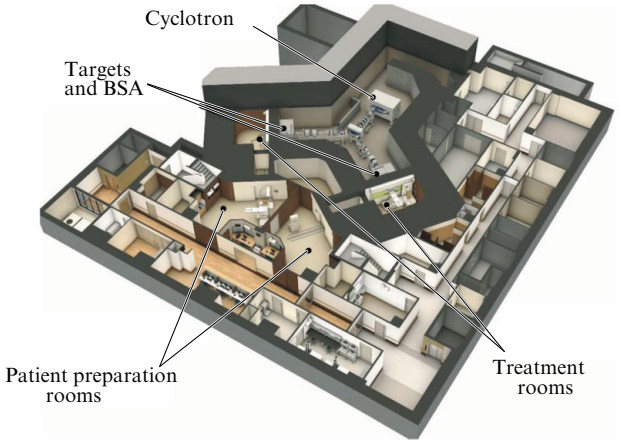


Figure 8. Layout of the BNCT center based on the HM-30 cyclotron at Southern Tohoku Hospital.

According to the protocol developed by the head of the Osaka center, Professor K. Ono, two hours before irradiation, the patient begins an intravenous infusion of Steboronine® at a rate of 200 mg per kg of body weight per hour. During irradiation, the infusion continues but at half the rate. For treatment planning, the boron concentration in the tumor is assumed to be three times that in the blood. A blood sample is taken immediately before irradiation, the boron concentration is measured, and the irradiation time is adjusted accordingly. A second blood sample is taken immediately after irradiation, and the boron concentration data are used to correct the absorbed dose.

The second major Japanese project, iBNCT, was launched in 2011. The project uses a radio-frequency drift-tube proton linear accelerator (8 MeV, 4 mA) manufactured by Mitsubishi, with a beryllium target. Notably, this accelerator was previously part of a larger JAERI facility and was later moved to a newly constructed BNCT center in Tokai. The BSA includes a fast-neutron filter made of iron, a magnesium fluoride moderator, a cadmium thermal neutron filter, a bismuth gamma-ray filter, and a polyethylene collimator with lithium fluoride. The epithermal neutron flux intensity at the beam aperture is about 7×10^8 cm^{-2} s^{-1}.

Clinical trials at the iBNCT accelerator-based neutron source are being conducted by the University of Tsukuba in collaboration with Stella Pharma [170]. The treatment protocol involves replacing the first week of the standard course of photon radiotherapy (40 Gy, 20 fractions over 5 weeks) in combination with temozolomide with a single BNCT session. As of early 2026, four patients have been treated in this manner over three years, with the clinical trial target being 8–12 patients.

The third project, based on a radio-frequency proton linear accelerator (2.5 MeV, 12 mA) with a lithium target, has been implemented since 2011 by Cancer Intelligence Care Systems (CICS) [171]. The accelerator was manufactured by

the American company AccSys Technology, Inc. For neutron generation, a lithium target developed by Linac System LLC is used [172]. A 10 μm-thick palladium layer is deposited on a copper body with eight spiral cooling channels, topped with a 50 μm-thick lithium layer enriched in ^{7}Li to 99.88%. The BSA includes a 24-cm-thick magnesium fluoride moderator, a lead reflector and radiation shielding, a lead gamma-ray filter, and a lithium fluoride thermal neutron filter.

The first CICS system was installed at the National Cancer Center (Tokyo), where clinical trials of BNCT for skin melanoma and angiosarcoma have been conducted since November 2019, and since 2024, for chest tumors. To date, 21 patients with skin melanoma/angiosarcoma and 4 patients with chest tumors have been treated. This project also uses Professor K. Ono's protocol, but the tumor-to-blood boron concentration ratio is assumed to be 3.5. A second similar system is located at Edogawa Hospital (Tokyo), where the first BNCT for breast cancer was performed on July 9, 2025.

The facility at Nagoya University (Japan), built by the Belgian company IBA, is intended for scientific research. The accelerator delivers a proton beam with an energy of 2.8 MeV and a current of 12 mA.

The second country after Japan to introduce BNCT into clinical practice is China, thanks to the VITA^{TM} accelerator-based neutron source proposed and developed at the BINP SB RAS [159]. An agreement to build the system was reached on March 1, 2016. On September 15, 2020, the manufactured and tested VITA-IIα system [162], comprising an accelerator — a vacuum-insulated tandem (2.35 MeV, 10 mA) — and a lithium target, was shipped to China. The system was commissioned at the BNCT center of Xiamen Hospital by Neuboron Medtech Ltd. (Nanjing, China). A general view of the system with beamlines to two treatment rooms is shown in Fig. 9.

On October 9, 2022, the center began clinical trials of BNCT for locally advanced head-and-neck tumors. The first successful case is described in detail in [173], which includes photographs of the patient before and after BNCT, clearly demonstrating the therapeutic effect. To date, more than 70 patients have been treated at the center. Physicians plan to complete the clinical trials and obtain a license for routine treatment already in 2026.

The VITA-IIα system demonstrates high operational reliability. Reaching operating mode (2.35 MeV, 10 mA proton beam) takes tens of seconds. The control system stably maintains the parameters during irradiation (typically about 40 minutes) and automatically shuts down the system when a preset dose level is reached on one of three dosimeters located inside the BSA.

Chinese physicians, like their Japanese counterparts, use the K. Ono protocol with irradiation time and absorbed dose correction based on blood boron concentration. However, unlike Japanese practice, they do not use a fixed tumor-to-blood conversion factor; instead, they determine BPA accumulation by performing positron emission tomography (PET) with ^{18}F-labeled BPA (^{18}F-FBPA) beforehand [174]. The BNCT center at Xiamen Hospital has established its own production of a BPA analogue, NBB-001, and has developed its own treatment planning system, NeuMANTA, which uses PET data to assign boron concentrations in the tumor and healthy tissues.

Since 2024, clinical trials have been conducted in Taiwan at the Bennu accelerator-based neutron source at China Medical University Hospital (Hsinchu). The proton cyclotron was designed and manufactured by Heron Neutron Medical Corp. and was approved by Taiwanese regulatory authorities in June 2024. Treatment is provided both within clinical trials and on a compassionate-use basis. To date, a total of 43 patients have been treated.

It should be noted that China is currently experiencing a rapid growth in the number of accelerators-based BNCT projects. In addition to the centers in Xiamen, Boao, and Hsinchu, more than 10 other projects are in various stages of implementation [155, 175], most of which are not listed in the IAEA book [82]. The Institute of High Energy Physics of the Chinese Academy of Sciences (Beijing) has commissioned a research facility, BNCT-01, in Dongguan (Guangdong Province), which is a radio-frequency proton linear accelerator (3.5 MeV, 4.5 mA) with a lithium target. Manufacturing is nearing completion for a similar medical system, BNCT-02, with a slightly lower proton energy but a significantly higher beam current (2.78 MeV, 20 mA) and a lithium target, intended for the Dongguan People's Hospital. Clinical trials are scheduled to begin in 2027.

Lanzhou University has developed a radio-frequency proton linear accelerator (2.5 MeV, 30 mA), installed at the Fujian Medical University Union Hospital. The equipment has already been commissioned, and animal experiments are currently underway. The China Institute of Atomic Energy (CIAE) has manufactured a proton cyclotron (14 MeV, 1 mA) with a beryllium target for the Tai'an Central Hospital (Shandong Province), where a dedicated building for a BNCT center has been constructed.

Xi'an Jiaotong University (XJTU) has reported the development of the X-TANS device for BNCT, based on a radio-frequency proton linear accelerator (2.5 MeV, 10 mA). The China National Nuclear Corporation and New Journey Medical Group Co., Ltd. (Langfang, China) have also begun

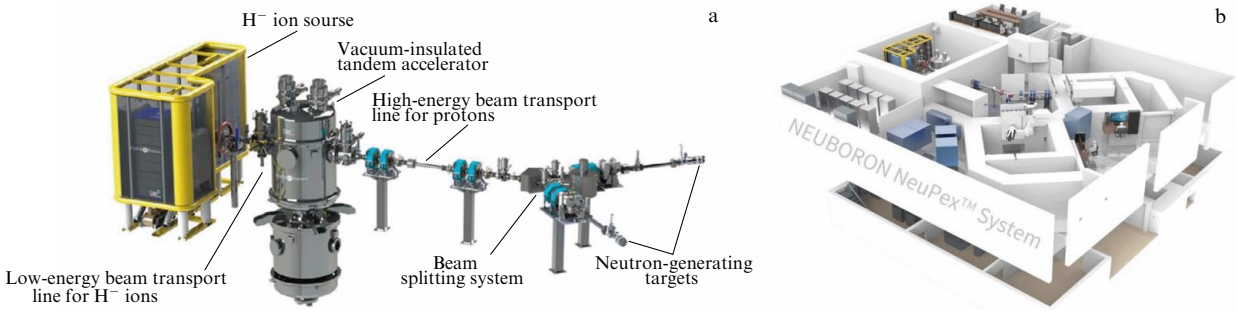


Figure 9. Schematics of the VITA-IIα system (a) and the BNCT center in Xiamen (b).

manufacturing radio-frequency linacs with lithium targets. Several other companies and institutes are known to be developing neutron sources, but reliable detailed information about them is not yet available.

The third country to initiate BNCT clinical trials is South Korea [176]. The research is led by the BNCT center in Songdo (Incheon). DAWONMEDAX has built a radio-frequency proton linac (10 MeV, 8 mA) with a beryllium target and has developed a treatment planning system and technology for producing a BPA analogue. An epithermal neutron flux intensity of 1.03×10^9 cm^{-2} s^{-1} has been achieved. Clinical trials began in 2022, and to date, 35 patients with recurrent glioblastoma and recurrent head-and-neck cancer have been treated. The drug administration protocol differs from the Japanese one: BPA infusion continues for 3 hours at a rate of 500 mg kg^{-1} h^{-1}, and irradiation begins one hour after the infusion ends. The Korea Institute of Radiological and Medical Sciences (KIRAMS, Seoul) is conducting its own development work. In 2019, the institute acquired an Argentine direct-action electrostatic deuteron accelerator (1.45 MeV, 30 mA) with a beryllium target but did not commission it, instead focusing on the development of a tandem electrostatic proton accelerator (2.5 MeV, 10 mA) with a lithium target [177].

The fourth country to begin clinical trials is Finland. The project to establish a BNCT center at the Helsinki University Hospital was implemented under a European Union program. The center is equipped with a Hyperion^{TM} direct-action high-voltage electrostatic proton accelerator (2.6 MeV, 30 mA) from Neutron Therapeutics (USA) with a rotating lithium target. The epithermal neutron flux intensity is about 1×10^9 cm^{-2} s^{-1}. The system is called nuBeam^{TM}. The treatment planning system was developed by RayStation, and a robotic patient positioning and visual monitoring system was created by the German company BEC GmbH. The system reached its design specifications in 2019 [178], and on May 16, 2025, the first patient was treated there.

It should be noted that Neutron Therapeutics accelerators are in high demand. To date, the company has delivered four systems: to the University of Birmingham (UK) and the University of Granada (Spain) for research purposes, and to Shonan Kamakura Hospital (Japan) and Brussels University Hospital (Belgium) for clinical trials and subsequent patient treatment.

The fifth country planning to begin BNCT clinical trials is the Russian Federation [179, 180]. On March 5, 2021, the Government of the Russian Federation decided to introduce BNCT into clinical practice in Russia [181]. In 2021–2024, the BINP SB RAS manufactured the VITA-IIβ accelerator-based neutron source, tested it at its site in Novosibirsk in 2024, and in the winter of 2025, delivered and installed it at the N.N. Blokhin National Medical Research Centre of Oncology (Ministry of Health of the Russian Federation, Moscow). The system is currently being commissioned. Clinical trials on the first 70 patients are scheduled to begin in April 2027.

The system includes an accelerator — a vacuum–insulated tandem that produces a stationary monoenergetic proton beam with an energy of 2.3 MeV and a current of 7 mA — a lithium target for neutron generation via the threshold reaction ^{7}Li(p,n)^{7}Be, and a BSA with a magnesium fluoride crystal moderator and a composite reflector (graphite in the forward hemisphere, lead in the rear). The VITA-IIβ accelerator-based neutron source produces a therapeutic epithermal neutron beam that meets IAEA recommendations [82] (see Table 4 in Section 3.2). A schematic of the system is shown in Fig. 10. The system is equipped with the VITA^{TM} treatment planning system, which is registered in the State Register of Computer Programs.

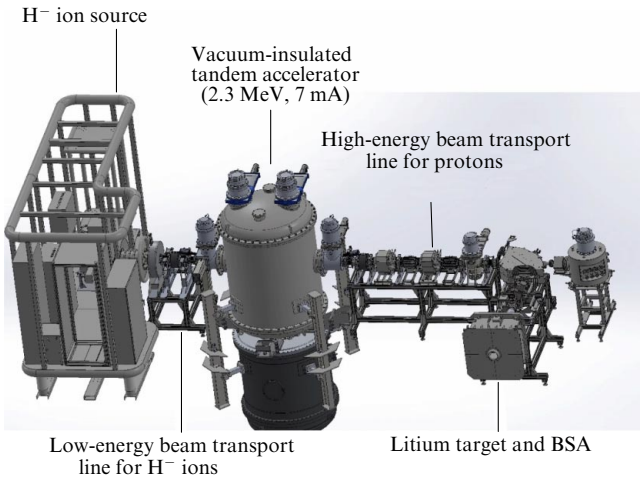


Figure 10. Schematic of the VITA-IIβ accelerator-based epithermal neutron source.

4. Development of boron delivery agents for targeted transport to tumor cells

Successful BNCT requires delivering a sufficient thermal neutron fluence ($\sim 10^{12}$ cm^{-2}) to the tumor cells, in which therapeutic concentrations of the ^{10}B isotope must be selectively accumulated and retained during irradiation [82].

An ideal boron-containing agent should provide a high ^{10}B concentration ratio between tumor and surrounding tissues $(T/N) > 3:1$, accumulate ~ 20 μg g^{-1} of ^{10}B per gram of tumor tissue (corresponding to $\sim 10^9$ ^{10}B atoms per cell), and retain ^{10}B in tumor cells throughout the irradiation period (> 1 h). The agent should have no systemic toxicity. It should also be highly water-soluble, be cleared relatively quickly from normal tissues and the bloodstream and ensure intracellular localization of ^{10}B with preferential accumulation close to DNA, which is critical for maximizing the impact of the ^{10}B(n,α)^{7}Li reaction products on tumor cells. In addition, when developing new agents, the possibility of ^{10}B imaging by PET or MRI should be considered to study pharmacokinetics and biodistribution for personalized treatment planning. Finally, the manufacturability, reproducibility, and scalability of the synthesis are also important considerations.

The first-generation agents (sodium borates, boric acid, and its derivatives), used in the early BNCT clinical trials of the 1950s and early 1960s, did not meet the above criteria. They lacked sufficient tumor selectivity, failed to achieve therapeutic ^{10}B concentrations in tumor cells without systemic toxicity, and consequently yielded no positive results.

In the 1960s, synthetic technologies for stable polyhedral boron hydrides were developed, giving new impetus to BNCT research. The ability to modify polyhedral boron hydrides by substituting hydrogen atoms with various functional groups enabled the synthesis of compounds capable of selective accumulation in tumor cells, while the presence of ten or

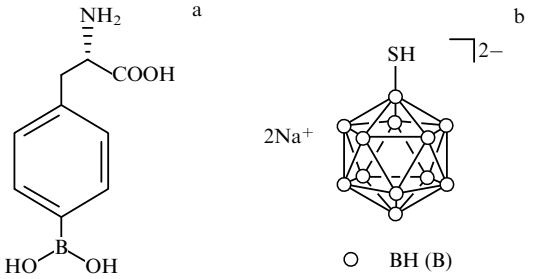


Figure 11. Chemical structures of 4-L-^{10}BPA (a) and BSH (b).

more boron atoms per molecule facilitated achieving the required boron concentration in the tumor.

Two ^{10}B delivery agents have been used in clinical practice — sodium borocaptate (BSH) and boronophenylalanine (4-L-^{10}BPA) — both belonging to the second generation of boron-containing agents for BNCT (Fig. 11). Both compounds were synthesized more than half a century ago. Despite their shortcomings, they remain the only agents that have been tested in patients [182]. For the clinical trials of BNCT at the N.N. Blokhin National Medical Research Centre of Oncology, BPA was purchased from Neuboron Medtech Ltd. The State Corporation Rosatom has been tasked with resuming ^{10}B production in the Russian Federation to organize domestic BPA production for subsequent BNCT treatments.

Sodium borocaptate belongs to the class of polyhedral boron hydrides and contains twelve ^{10}B atoms per molecule, which in principle allows the required therapeutic ^{10}B concentration in tumor cells to be achieved. In 1968, H. Hatanaka and his colleagues first demonstrated the efficacy of BNCT with BSH in mice bearing primary methylcholanthrene-induced sarcoma [183]. Since then, BSH has been used in clinical practice. Transport of BSH from the blood into tumor cells occurs via passive diffusion through the disrupted blood-brain barrier (BBB) in brain tumors or through fenestrated vessels characteristic of many malignant neoplasms (EPR effect) [184]. However, BSH has no active delivery mechanism, often does not cross the cell membrane, and localizes predominantly in the extracellular space, which significantly reduces its therapeutic efficacy [185]. No reports of BSH use in clinical BNCT practice have appeared in the last 16 years.

Boronophenylalanine has been used in clinical BNCT practice since 1987 [104–106]. It was initially thought to act in melanoma cells as a tyrosinase substrate, promoting the formation of macromolecular inclusions through the melanin metabolic pathway, but this hypothesis was later disproved. Delivery of 4-L-^{10}BPA to tumor cells occurs via active transport through L-type amino acid transporters, primarily LAT-1 [186, 187], and is independent of pH and Na^+ concentration. The heterodimeric membrane transport protein LAT-1 mediates the transport of neutral amino acids with branched side chains (valine, leucine, isoleucine) as well as aromatic amino acids (tryptophan, tyrosine) [188–190]. Overexpression of this transporter is characteristic of many tumor types [191] and can be considered a target for targeted delivery of boronophenylalanine.

Today, 4-L-^{10}BPA is the only ^{10}B-containing compound used in clinical BNCT practice for the treatment of glioblastoma, head-and-neck tumors, and melanoma. The problem of its retention in tumor cells arises from the fact that L-amino acid transporters operate via an antiport mechanism: when the extracellular concentration of 4-L-^{10}BPA decreases, intracellular 4-L-^{10}BPA is exchanged for another extracellular substrate, such as tyrosine [192]. In addition, the presence of only one ^{10}B atom per 4-L-^{10}BPA molecule is a significant obstacle to achieving the required therapeutic ^{10}B concentration in the tumor and necessitates systemic administration of large doses of the agent (500 mg kg^{-1}).

Clinical use of 4-L-^{10}BPA is also severely complicated by its low solubility (0.6 g l^{-1}) and high serum binding affinity (10^{-6} M). To increase solubility, 4-L-^{10}BPA is complexed with monosaccharides [193]. Currently, the standard clinical method for administering 4-L-^{10}BPA for BNCT is intravenous infusion of the 4-L-^{10}BPA-fructose or 4-L-^{10}BPA-D-sorbitol complex [82]. However, this approach is far from ideal: a 60 kg patient receives a systemic infusion of 1 l of solution containing 30 g of 4-L-^{10}BPA and 31.5 g of D-sorbitol. Such a high load leads to side effects including hypoglycemia, development of hepatic and renal failure in individuals with hereditary fructose intolerance (because of sorbitol metabolism), and hematuria resulting from crystallization of 4-L-^{10}BPA in the urine [194–196].

Thus, BPA and BSH have played an important role in the historical development of BNCT, initiating its clinical application. However, these agents do not meet the high standards now required for targeted therapy. The fact that they are still used in clinical practice is explained not by their pharmacological properties, but by the accumulated clinical experience, their well-established safety profile, and regulatory considerations. The development of new targeted ^{10}B-containing agents that improve the efficiency of ^{10}B accumulation and retention in tumors while reducing side effects is a priority direction in BNCT research.

In recent decades, new strategies for ^{10}B delivery to tumor cells have been actively developed. They can be classified into several main carrier types: (1) low-molecular-weight compounds: amino acid derivatives, carbohydrates, nucleic acids, porphyrins, and natural metabolites; (2) molecularly targeted conjugates: peptides, antibodies, enzyme inhibitors targeting tumor antigens; (3) nanoscaled systems: liposomes, polymeric micelles, dendrimers, inorganic NPs, and exosomes; and (4) theranostic platforms that combine boron delivery with imaging capabilities (MRI, PET, fluorescence). Figure 12 presents a classification of boron carriers by molecular weight.

4.1 Low-molecular-weight boron-containing compounds

Small boron-containing molecules consist of a boron-bearing moiety and a transport (vector) module. Ideally, the boron moiety should contain the maximum possible number of ^{10}B atoms, while the vector subunit should ensure selective tumor accumulation. A wide variety of biologically active molecules can be used as the transport component for drug synthesis; however, their modification by boron incorporation can significantly affect their original biological properties. In this regard, it is necessary to consider the different types of boron substituents used in the design of low-molecular-weight compounds.

A single boron atom represents the simplest structural moiety. It can be present in the compound as a bioisostere of carboxyl ($-B(OH)_2$), carbonyl ($-BOH$), or amide ($-B(OH)NR_2$) groups, or as trialkyl- and triarylborane fragments ($-BR_3$). Such groups may be located at the periphery of biomolecules as side substituents or be incorpo-

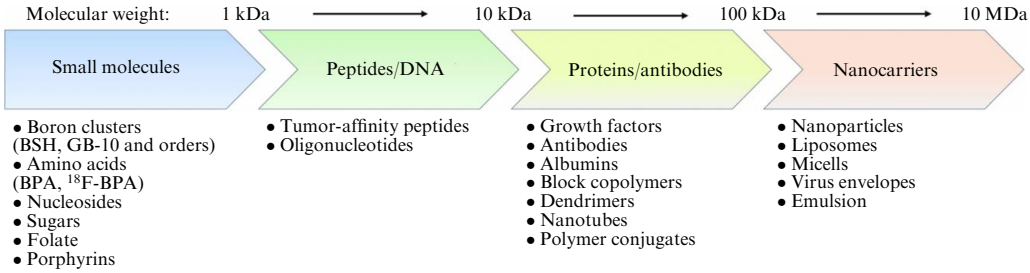


Figure 12. Classification of boron agents by molecular weight.

rated into nitrogen-containing heterocyclic systems that determine their activity. As a rule, one of the main disadvantages of compounds with a single boron atom is their low water solubility (as exemplified by 4-L-^{10}BPA described above). This limitation does not apply to derivatives of four-coordinate boron, such as aminoboranes RBH_2–NR_3. Nevertheless, the common drawback of all compounds with a single boron atom remains the low ^{10}B content per molecule.

Polyhedral boron hydrides contain ten or more boron atoms per molecule. From a chemical standpoint, the most widely used boron clusters for the synthesis of boron-containing biomolecules are icosahedral carboranes $C_2B_{10}H_{12}$, particularly *ortho*-carborane (*o*-$C_2B_{10}H_{12}$) [197]. However, the design of agents based on these compounds is greatly complicated by the extremely high hydrophobicity of carboranes, which often leads to water insolubility of the target compounds and necessitates the introduction of hydrophilic substituents into the carborane framework. In this context, particular interest lies in the synthesis of agents based on anionic polyhedral boron hydrides such as $[B_{12}H_{12}]^{2-}$, $[B_{10}H_{10}]^{2-}$, $[CB_{11}H_{12}]^{-}$, $[1-CB_9H_{10}]^{-}$ and $[7,8-C_2B_9H_{12}]^{-}$.

The negative charge, which provides water solubility in the form of sodium salts, impairs their ability to cross intracellular and membrane barriers. An effective solution to this problem is the covalent conjugation of anionic boron clusters with synthetic polymers, short peptide sequences, or lipids [198].

To overcome biological barriers in brain tumors, methods for temporary opening of the BBB are being actively developed to improve boron delivery. Among pharmacological approaches, osmotic BBB opening using mannitol [199] and the use of Cereport (a bradykinin analogue) [200] are being studied. Physical methods include focused ultrasound combined with microbubbles [201] and electroporation [202]. An alternative approach — direct intratumoral administration of agents via convection-enhanced delivery — is also being considered [203].

Let us now consider the different types of molecular vectors that provide selective accumulation of ^{10}B in tumor cells. A fundamental difference of malignant cells is their high proliferative activity, which requires increased consumption of nutrients and metabolic precursors. Consequently, endogenous biomolecules and their structural analogues are preferentially taken up by tumor tissue, offering opportunities for selective ^{10}B delivery.

Such compounds include amino acid analogues: L-3-^{10}BPA [204], 3-borono-L-tyrosine [205, 206], ^{18}F-fluoroborono tyrosine [207], carborane conjugates with cysteine [208] and levodopa [209], as well as conjugates of the closo/dodecaborate anion with diamino acids [210]. Derivatives of nucleic acids (conjugates of uridine and deoxyuridine [211], aptamers and antisense oligonucleotides [212, 213] with *closo*-dodecaborate or *ortho*-carborane clusters), porphyrins and their analogues [214–217], carbohydrate boron conjugates (glucose and mannose derivatives [218–220], hyaluronic acid [221]), as well as other biomimetics are being studied. Among the latter, boron-containing curcumin analogues [222], kojic acid conjugates [223], carbonic anhydrase IX inhibitors [224], phenylboronic acid [225], and sinomenine derivatives [226] should be noted.

Thus, low-molecular-weight boron-containing compounds that mimic natural metabolic substrates represent a flexible platform for BNCT. However, their therapeutic potential is often limited by insufficient selectivity toward healthy proliferating tissues and rapid clearance. To overcome these limitations and achieve targeted action on specific tumor antigens, the concept of covalent conjugation of boron clusters with targeting biomolecules is being actively developed and is discussed in detail in the following subsections.

4.2 Targeted boron-containing bioconjugates

In addition to low-molecular-weight compounds, bioconjugates in which boron clusters are covalently linked to peptides, antibodies, proteins, or viral vectors are being actively developed. This approach is of key importance for targeted boron delivery to various tumor cell subpopulations and intracellular structures that differ in their biochemical, physiological, and pharmacological characteristics.

Technologies have been developed for the synthesis of targeted compounds, including tyrosine kinase inhibitor derivatives [227, 228], agents targeting GLUT1 [229], TSPO [230], and integrin $\alpha_v\beta_3$ [231], as well as *closo*- and *nido*-carborane-containing conjugates of biotin [232] and matrix metalloproteinase inhibitors [233]. High efficacy has been demonstrated by the multifunctional conjugate PBC-IP, which combines a folate vector, a dodecaborate cluster, and an albumin-binding domain [234]. For delivery via the oligopeptide transporter PEPT1, BPA-tyrosine dipeptides that selectively accumulate in cells expressing this transporter have been developed [235]. For targeting GPCRs, neuropeptide Y analogues and GRPR agonists with high carborane content have been created, retaining high receptor activity [236, 237].

In [238], conjugates of PSMA ligands with boronic acid or carborane were obtained that retain nanomolar affinity and provide boron accumulation in prostate tumors at levels of 4–7 $\mu g\,g^{-1}$. For targeting tumor vasculature, the peptide IF7 (binding annexin A1) has been developed. Its conjugates with BPA or BSH provide rapid boron delivery and enhance the antitumor immune response [239]. In [240], a conjugate of the

angiopep-2 peptide with dodecaborate (ANG-B) was obtained, which effectively crosses the BBB and significantly outperforms BPA in tumor accumulation and antitumor efficacy in an intracranial glioma mouse model.

The peptide cRGD, targeting integrin $\alpha_v\beta_3$, has been used to functionalize gold NPs as carriers for BSH [241]. Intratumoral administration of the resulting nanoformulations to mice with subcutaneous glioma led to a significant increase in ^{10}B accumulation in the tumor and improved tumor-to-blood (T/B) and tumor-to-normal (T/N) ratios compared with free BSH. In [242], a KRGD tetrapeptide with two carborane groups, also targeting integrin $\alpha_v\beta_3$, was synthesized and demonstrated high water solubility and low cytotoxicity.

Work is also underway on boron-containing compounds for targeted delivery of ^{10}B directly to intracellular compartments. Conjugates of dodecaborate with peptides that selectively accumulate in mitochondria, cause ATP depletion, and induce apoptosis have been synthesized [243]. For nuclear delivery, a boronated derivative of temozolomide (TMZB) that retains the DNA-alkylating activity of the parent compound has been proposed [244]. In a glioblastoma model, BNCT with TMZB resulted in significantly greater tumor growth suppression in mice than with BPA. In [245], an acridone derivative with a carboranyl substituent (CMBA) was obtained that selectively accumulates in the cytoskeletal fraction of glioblastoma cells.

In addition to peptide conjugates, antibodies and their fragments are being investigated as targeting agents for boron delivery. Such constructs retain high affinity for tumor antigens. In [246], the peptide Z33, which binds the Fc fragment of antibodies, was modified with a dodecaborate cluster. It was shown that the resulting conjugate binds to therapeutic antibodies (e.g., against EGFR) and induces macropinocytosis, providing efficient intracellular boron accumulation. In parallel with experimental studies, computational approaches are also being developed. For example, in [247], molecular modeling demonstrated the feasibility of directly replacing amino acid residues of cetuximab with their boron-containing analogues without loss of affinity for EGFR.

Among protein carriers, conjugates with serum albumin are the most studied. MID-albumin conjugates enable administration of high boron doses (up to 15 mg kg^{-1} in terms of ^{10}B), as well as prolonged circulation and sustained retention in tumor tissue [248]. This allows the interval between infusion and irradiation to be increased without loss of therapeutic efficacy. Albumin also serves as a promising platform for combining BNCT with chemotherapy [249].

Thus, the use of targeted bioconjugates enables high selectivity of boron accumulation in tumor cells and intracellular compartments. Nevertheless, the limited boron content per individual molecule necessitates a transition to larger-scale platforms — nanoscaled delivery systems.

4.3 Nanoscaled boron-containing delivery systems

A key advantage of nanoscaled boron-containing systems is the dramatic increase in the number of ^{10}B atoms delivered to the cell [56]. In a single endocytosis event, such systems deliver several orders of magnitude more ^{10}B atoms than any low-molecular-weight compound. In addition, NPs typically localize in the perinuclear region of the cell. Through endocytosis, they are resistant to multidrug resistance mechanisms operating at the molecular level (such as efflux pumps) and can retain therapeutic ^{10}B concentrations inside the cell for longer periods.

However, some limitations of using nanosystems as delivery vectors should be noted. One is the rapid clearance of circulating NPs by cells of the mononuclear phagocyte system (mainly Kupffer cells in the liver and macrophages in the spleen). The enhanced phagocytosis is caused by opsonization — the formation of a protein corona on the NP surface, which leads to their recognition by the immune system as foreign objects and subsequent uptake by tissue macrophages.

Several strategies exist to overcome these limitations. The most direct is local intratumoral administration of nanoformulations, but even in this case, premature clearance into the systemic circulation often occurs. Another approach is the so-called blockade of the mononuclear phagocyte system [250]. This method involves the pre-administration of a saturating dose of inert NPs containing no therapeutic agent. These particles are taken up by cells of the reticuloendothelial system, temporarily reducing their phagocytic activity. As a result, the subsequent therapeutic nanocarrier circulates longer in the bloodstream and accumulates more efficiently in tumor tissue.

A significant increase in the circulation time of nanosystems in the bloodstream can currently be achieved by modifying them with long-chain hydrophilic polymers such as polyethylene glycol (PEG), polyvinyl alcohol, chitosan, or dextran [251–254]. Among these, PEG is considered the most effective, owing to its high biocompatibility, lack of toxicity, and low immunogenicity. The physicochemical properties of PEG molecules ensure their efficient hydration, creating a steric barrier around the nanostructure. This coating prevents opsonization and subsequent macrophage uptake, prolonging the circulation time of the drug in the bloodstream [255]. PEG-coated nanosystems are referred to as PEGylated, sterically stabilized, or ‘stealth’ systems.

However, increased circulation time alone does not ensure targeted transport of nanosystems to tumor cells. The most effective approach for selective localization is active targeted delivery, achieved by conjugating targeting molecules to the surface of nanosystems that can selectively bind to receptors on target cells. Various targeting agents are used for this purpose: antibodies and their fragments, transferrin, epidermal growth factor, lectins, oligonucleotides (aptamers, peptide nucleic acids), as well as small molecules (folic acid, carbohydrates). It should be noted that the mononuclear phagocyte system blockade strategy is particularly effective when combined with targeted NPs capable of actively interacting with target tumor cells [250].

Critical parameters of nanosystems are their size and surface charge. The optimal size for nondeformable spherical NPs is about 30–50 nm [3]. Ultrasmall sizes (below 10 nm) lead to rapid renal clearance of the nanodrug, while larger objects (above 200 nm) are actively taken up by macrophages. For liposomes, the optimal size range is 60–150 nm, with the lower limit constrained by the physicochemical stability of the lipid bilayer. The surface charge of nanosystems affects both their colloidal stability and electrostatic interactions with the plasma membrane and cellular organelles. In particular, the negative charge of DNA molecules, due to phosphate groups, results in highly efficient accumulation of cationic nanosystems in the perinuclear region, which is a critical factor for achieving therapeutic efficacy in BNCT [256]. However, a

high positive charge plays a dual role: while facilitating intracellular delivery, it simultaneously increases nonspecific cytotoxicity of nanosystems through membrane damage to healthy cells, necessitating careful parameter optimization in their design [257, 258].

In recent years, numerous types of nanocarriers for BNCT have been developed [158, 259, 260], including polymeric NPs, micelles, liposomes and other vesicular systems, dendrimers, nanotubes, quantum dots, and a variety of inorganic NPs.

Among polymeric boron-containing nanosystems, PEGylated polymeric micelles [261] and covalent organic polymers loaded with carborane [262] should be noted, as well as micelles based on PEG-*block*-(poly(4-vinylphenyl boronate ester)) [263]. Combining the latter with PD-L1 immune checkpoint inhibitors enhances the antitumor immune response [264]. In [265], carborane-modified exosomes were obtained that provide efficient penetration into tumor spheroids and high accumulation selectivity.

Liposomes represent a promising platform for targeted ^{10}B delivery. A wide variety of boron-containing liposomal formulations have been developed, varying in size, surface charge, and type of encapsulated agents. Hydrophilic boron compounds are localized in the aqueous inner core of liposomes, while hydrophobic ones are incorporated into the lipid membrane. The most effective approach is considered the design of liposomal systems containing boron moieties simultaneously in both the aqueous core and the lipid bilayer [153].

High efficacy has been demonstrated by polyborane liposomes [266], thermosensitive liposomal formulations for BPA delivery [267], and transferrin-targeted liposomes loaded with BSH [268]. Nanostructures with carborane-phosphatidylcholine covalently incorporated into the lipid bilayer have been developed, applicable for PET-imaging and for combining BNCT with chemotherapy [269], as well as immunoliposomes containing carborane and monoclonal antibodies against the HER2 receptor [270].

It should be noted that the use of full-length antibodies as targeting agents for nanosystems has several drawbacks. The large size of IgG immunoglobulins often hinders efficient surface modification of nanostructures and limits their diffusion into tumor tissue [271]. In addition, Fc fragments (constant domains of heavy chains) possess effector functions that can induce nonspecific phagocytosis, leading to inflammatory processes and undesirable immunomodulation *in vivo* without contributing to selective target recognition.

A more promising approach is targeting nanostructures using alternative nonimmunoglobulin scaffold proteins selected by phage display, cell display, or ribosome display. The most prominent representatives of this group of targeting agents are Affibodies and DARPins [271].

In [272], we obtained targeted nanoliposomes loaded with the 4-L-^{10}BPA-D-fructose complex (Fig. 13). The outer surface of the nanoliposomes was functionalized with an alternative scaffold protein based on ankyrin repeats, DARPin_9-29, which is highly specific for the HER2 receptor. The resulting nanodrug was given the working name DARP-Lip(BPA). The hydrodynamic diameter of the nanoliposomes, measured by dynamic light scattering (DLS), was 151.8 ± 52.8 nm, and their zeta-potential was -50.0 ± 6.7 mV. According to spectrophotometry and inductively coupled plasma mass spectrometry (ICP-MS), the encapsulation efficiency of 4-L-^{10}BPA was approximately 120000 molecules per liposome.

The specificity of DARP-Lip(BPA) binding to the HER2 receptor on the surface of SKOV-3 ovarian carcinoma cells was confirmed by flow cytometry and confocal microscopy. It was found that incubation of SKOV-3 cells with the nanoliposomes for 20 minutes led to their accumulation on the plasma membrane, while extending incubation to 120 minutes resulted in their efficient internalization into the cytoplasm (see Fig. 13).

Thus, the developed DARP-Lip(BPA) nanoliposomes demonstrate high stability, optimal physicochemical characteristics, and the ability to carry therapeutically significant amounts of ^{10}B atoms. The confirmed rapid internalization of the liposomes into SKOV-3 cells supports the potential of this targeted system for efficient selective boron delivery to HER2-positive tumors.

Among other nanoscaled systems, boron-containing nanotubes and nanorods should be noted. In [273], self-assembling A6K peptide nanotubes loaded with BSH were obtained, demonstrating high biocompatibility, a tenfold increase in boron concentration in glioma cells *in vitro* compared with free BSH, and selective tumor accumulation in human glioma xenograft models. Protein nanotubes (RHCC-NT) containing *ortho*-carborane have also been developed [274]. *In vitro* experiments showed their preferential perinuclear accumulation in breast cancer cells. In [275], multifunctional gold nanorods stabilized by PEG and modified with the cobalt bis(dicarbollide) anion (COSAN) were obtained for combining BNCT with photothermal therapy (PTT). Interesting results were presented in [276], where a study of dynamic boron-containing polymer-based nanosystems showed that nanorods exhibited the most efficient internalization into glioblastoma and cervical carcinoma cells compared with analogous spherical and worm-like nanostructures.

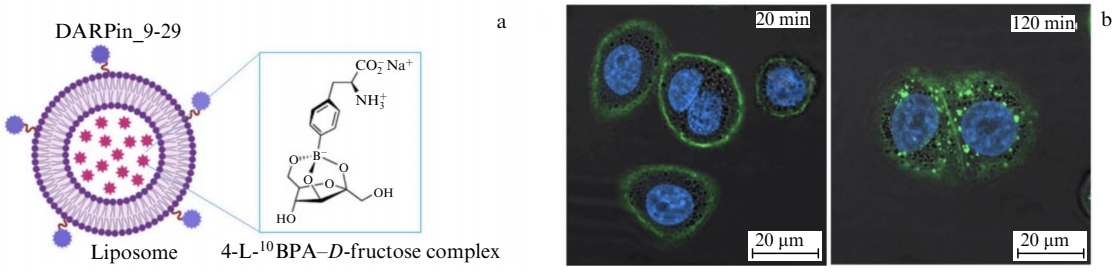


Figure 13. Schematic representation of targeted DARP-Lip(BPA) nanoliposomes (a); confocal microscopy images demonstrating binding and internalization of the nanoliposomes in SKOV-3 cells (b). Green signal corresponds to AF-488-labeled nanoliposomes; blue signal corresponds to stained cell nuclei [262].

The synthesis of boron-containing quantum dots with sizes of 2–10 nm, characterized by tunable fluorescence and functionalizable surfaces, is being actively developed. In [277], biocompatible boron carbide (B_4C) quantum dots of about 7 nm in size were obtained, exhibiting bright fluorescence due to defects in the crystal structure. In [278], hybrid exosomal nanosystems loaded with boron-doped carbon dots were synthesized; these effectively cross the BBB and selectively accumulate in orthotopic glioma tissues ($T/N > 5$), providing a ^{10}B concentration in the tumor of over 100 μg g^{-1} at 4 hours after intravenous injection.

The development of boron-containing nanosystems based on silica NPs should be noted separately; these are characterized by high structural stability, tunable porosity, and versatile surface chemistry. Dendritic mesoporous silica NPs loaded with carborane and doxorubicin, functionalized with polyethyleneimine and the cyclic peptide Arg-Gly-Asp (PEI-cRGD), have been developed for targeted delivery to pancreatic tumors [279]. These NPs demonstrated high boron loading capacity (up to 141.5 mg g^{-1}) and achieved a ^{10}B concentration of 24.4 μg g^{-1} in tumor tissue with a T/B ratio 27.1. In another study [280], multifunctional fluorescent mesoporous silica NPs modified with an activatable cell-penetrating peptide and a gadolinium complex as an MRI contrast agent were obtained. The feasibility of producing stable composite mesoporous silica NPs loaded with carborane and functionalized with chitosan, lactobionic acid, and thioctic acid for targeted delivery to hepatocellular carcinoma cells has also been demonstrated [281]. In the tumor microenvironment, this nanocomposite provided pH- and redox-sensitive carborane release while exerting antioxidant and anti-inflammatory effects.

Another promising approach is the use of magnetic boron-containing nanosystems that combine targeted boron delivery with imaging or magnetic hyperthermia. For example, biocompatible nanocomposites based on magnetite (Fe_3O_4) NPs functionalized with organosilane linkers have been developed as stable transport platforms for carborane immobilization and targeted delivery [282]. In [283], bimetallic iron–boron (Fe–B) NPs were obtained by nanosecond laser ablation of a solid target in liquid; these NPs exhibit low toxicity, MRI contrast properties, and physicochemical characteristics optimal for BNCT combined with magnetic hyperthermia.

In addition to the nanosystems listed above, hybrid nanoplatforms combining BNCT with other therapeutic modalities have been actively developed in recent years. These include pullulan-based nanogels containing boron oxide (B_2O_3) [284], Zr-TCPP metal-organic frameworks loaded with boric acid [285], redox-sensitive boron–iron (B–Fe) nanochains that generate boron quantum dots *in situ* [286], and biomimetic structures: apoferritin nanocontainers with COSAN complexes [287] and HVJ-E virus-like particles [288].

A fundamentally different approach involves the use of elemental boron NPs synthesized from material highly enriched in the ^{10}B isotope. In this case, a single NP with a diameter of 50 nm contains no fewer than 200000 ^{10}B atoms, which significantly exceeds the target isotope content of any other nanosystem. Moreover, such NPs can be obtained by physical methods without complex multistep chemical synthesis.

We have demonstrated the feasibility of synthesizing boron-containing nanomaterials by nanosecond and femtosecond pulsed laser ablation of a solid target (LA) and laser fragmentation of micropowder (LF) in liquid [289–291], yielding corresponding NPs (LA-NPs and LF-NPs). In [292], colloidal solutions of polycrystalline and amorphous elemental boron NPs were obtained by LA and LF, respectively. The synthesis was performed in two steps: the large particle fraction formed after laser exposure to the target or micropowder was removed in the second step by centrifugation.

The size and morphology of the obtained nanostructures were characterized by transmission electron microscopy (TEM). The average diameter of LF-NPs was 25 nm, and that of LA-NPs was 50 nm (Fig. 14). The surface of both NP types was modified with PEG to enhance their colloidal stability and biocompatibility. The average hydrodynamic diameter of PEGylated LF-NPs and LA-NPs in phosphate-buffered saline (PBS), simulating physiological conditions, was 96 and 121 nm, respectively. The average zeta-potential of PEGylated LF-NPs and LA-NPs was −25 and −34 mV, respectively.

Both NP types demonstrated low cytotoxicity in the concentration range of 50–400 mg l^{-1} on U87 glioblastoma and SW-620 colorectal cancer cell lines. Prior to BNCT, cells were incubated with the NPs for 24 hours at a concentration of 40 μg ml^{-1} in terms of ^{10}B. Irradiation with a thermal neutron flux was performed at the VITA™ research accelerator-based neutron source. Cryoampoules with the cell suspension were placed in a polymethyl methacrylate (PMMA) phantom, and the exposure time was 30 minutes. The proton beam energy and current on the lithium neutron-

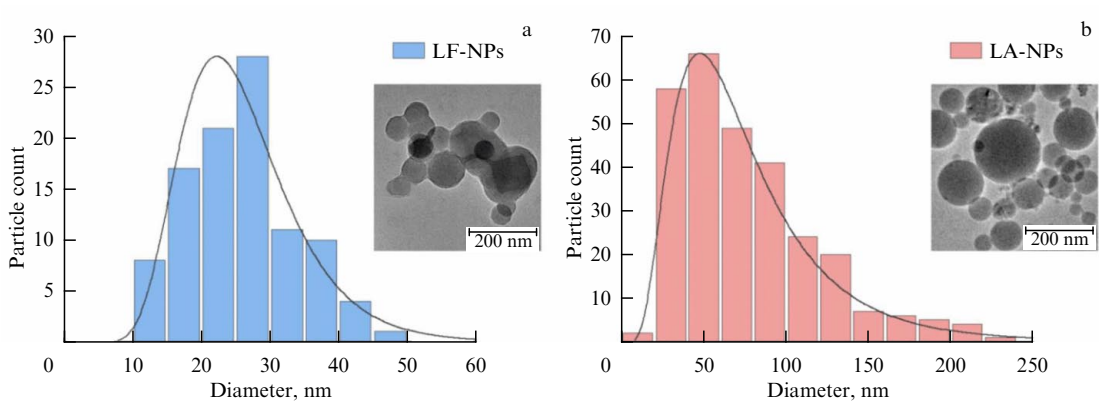


Figure 14. TEM images and corresponding particle size distribution histograms for (a) LF-NPs and (b) LA-NPs [282].

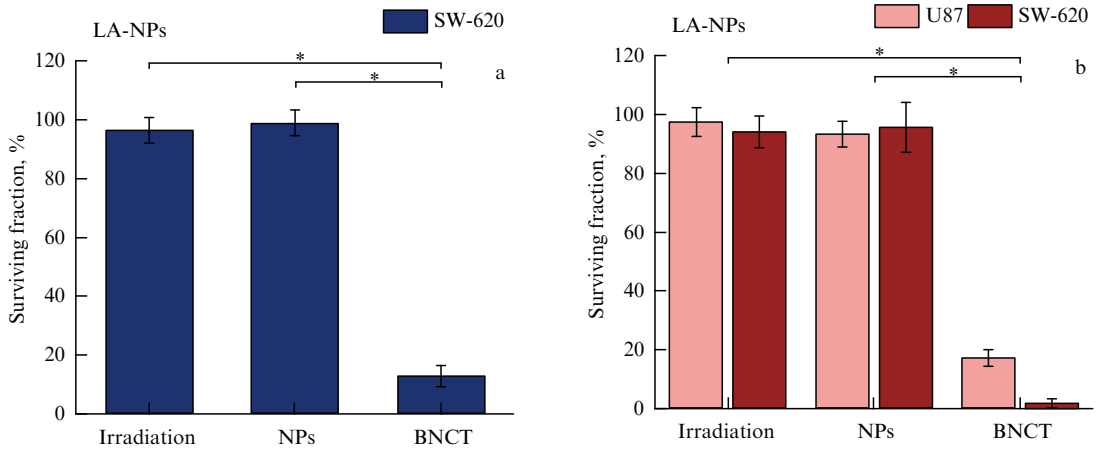


Figure 15. Results of the clonogenic assay after BNCT with PEGylated LF-NPs (a) and LA-NPs (b). Data are presented as mean ± standard deviation. * – $p < 0.05$, significance of differences compared with the control group, Mann–Whitney U test ($n = 6$) [282].

generating target were 2.0 MeV and 1 mA, respectively. The equivalent dose in the samples with NPs, calculated by the Monte Carlo method, was 8 Gy-eq. The *in vitro* experimental results demonstrated nearly complete inhibition of clonogenic cell activity after BNCT (Fig. 15).

The biodistribution of LA-NPs following intratumoral administration to immunodeficient SCID mice bearing U87 glioblastoma xenografts was studied by inductively coupled plasma atomic emission spectrometry (ICP-AES) (Fig. 16). Boron accumulation in the tumor was 56 and 82 μg g^{-1} at 30 and 90 minutes, respectively; however, the concentration differences between these time points were not statistically significant. The boron concentration in the blood was substantially lower, at 0.37 and 0.34 μg g^{-1} at 30 and 90 minutes, respectively. Boron accumulation in surrounding normal tissues (skin and muscle) was at background levels at 30 minutes but increased to 1 μg g^{-1} in skin and 0.2 μg g^{-1} in muscle by 90 minutes. A similar trend was observed for the liver: the boron concentration increased from 2.7 to 4.4 μg g^{-1} over the observation period. In the spleen and brain, background levels were recorded at both time points.

It is important to note that in the presented study the NPs contained natural boron, in which the concentration of the therapeutic ^{10}B isotope was only 20%. Our subsequent work focused on the development of laser synthesis technologies and biological studies of nanoformulations based on elemental boron NPs enriched to 85.1% in the ^{10}B isotope (hereinafter, ^{10}B-NPs) [293–297].

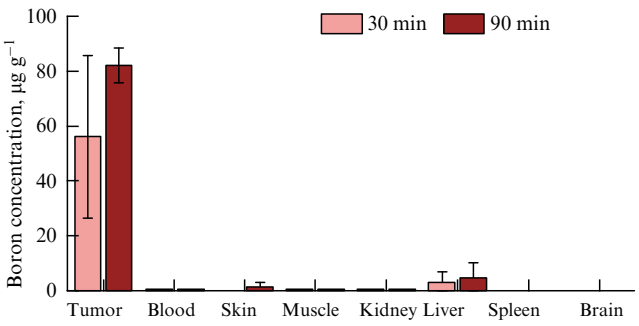


Figure 16. Biodistribution of PEGylated LA-NPs at 30 and 90 minutes after intratumoral administration to SCID mice bearing U87 glioblastoma xenografts. Data are presented as mean ± standard deviation ($n = 3$) [282].

The development of these methods was associated with solving several technological challenges. For LA synthesis of ^{10}B-NPs, optimal regimes for fabricating solid targets from enriched boron powder by free sintering were found [293]. To increase the synthesis yield of NPs by LF in isopropanol, methods for pre-milling the initial powder in planetary ball mills to sizes below 500 nm were developed [294].

Two types of laser-synthesized ^{10}B-NPs were obtained for the first time. According to scanning electron microscopy (SEM), the average diameter of LA-^{10}B-NPs was 37 nm, while that of LF-^{10}B-NPs was 53 nm (Fig. 17). TEM analysis revealed a polycrystalline structure for LA-^{10}B-NPs and an amorphous structure for LF-^{10}B-NPs. For biological studies, the surface of both NP types was modified with PEG. The average hydrodynamic diameter of PEGylated LA-^{10}B-NPs was 104 nm, and that of PEGylated LF-^{10}B-NPs was 141 nm. Colloidal solutions of both NP types remained stable in cell culture medium supplemented with 10% serum for at least 24 hours. Both types of PEGylated NPs exhibited low cytotoxicity in the concentration range of 10–320 μg g^{-1} (in terms of ^{10}B) on U87 glioblastoma, BT-474 breast carcinoma, and immortalized BJ-5TA dermal fibroblasts (Fig. 18) [295].

In [295], the biological efficacy of BNCT using PEGylated LF-^{10}B-NPs was studied. Prior to irradiation, cells were incubated with the NPs for 24 hours at a concentration of 40 μg ml^{-1} in terms of ^{10}B. Cryoampoules with the cell suspension were then placed in a PMMA phantom and irradiated with a thermal neutron flux at the VITA^{TM} facility at the BINP SB RAS. Irradiation was performed for 30 minutes with a proton beam energy of 2.0 MeV and a current of 2 mA on the lithium target. Colony formation assay results showed that the greatest biological effect of BNCT was observed for the BT-474 breast carcinoma cell line, with a surviving fraction of less than 1% (Fig. 19). This result is explained by the fact that PEGylated LF-^{10}B-NPs exhibit the best intracellular accumulation and retention specifically in BT-474 cells (Fig. 20) [296].

In [297], the effects of intravenous and subcutaneous administration of PEGylated LA-^{10}B-NPs and LF-^{10}B-NPs at doses of 10, 30, and 100 mg kg^{-1} on the health status of immunodeficient SCID mice were studied. It was found that both NP types, over the investigated dose range, showed no significant adverse effects on disease development, indicating their high biocompatibility *in vivo*.

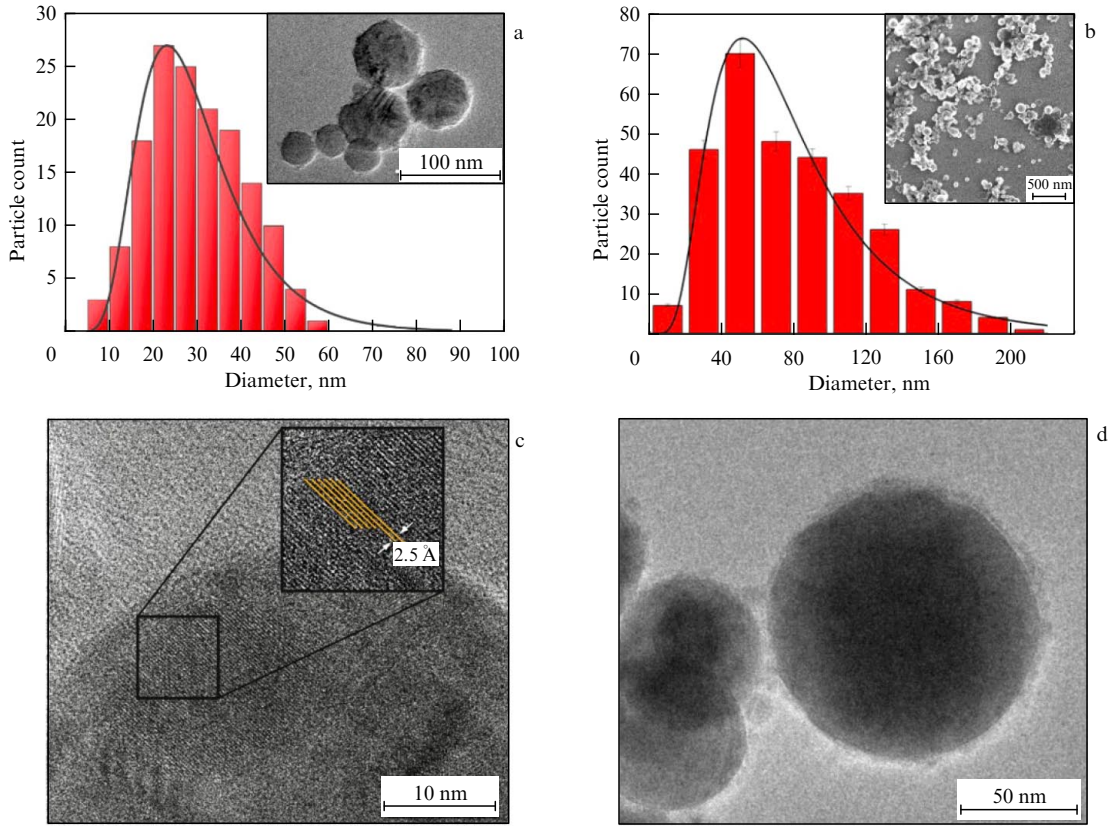


Figure 17. SEM images and corresponding particle size distribution histograms for LA-^{10}B-NPs (a) and LF-^{10}B-NPs (b), and TEM images showing the polycrystalline structure of LA-^{10}B-NPs (c) and the amorphous structure of LF-^{10}B-NPs (d).

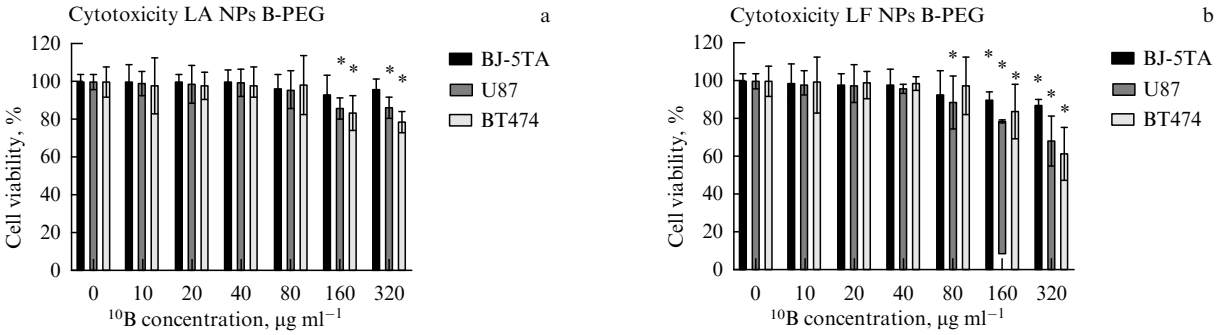


Figure 18. Cytotoxicity of LA-^{10}B-NPs (a) and LF-^{10}B-NPs (b) at different ^{10}B concentration [285].

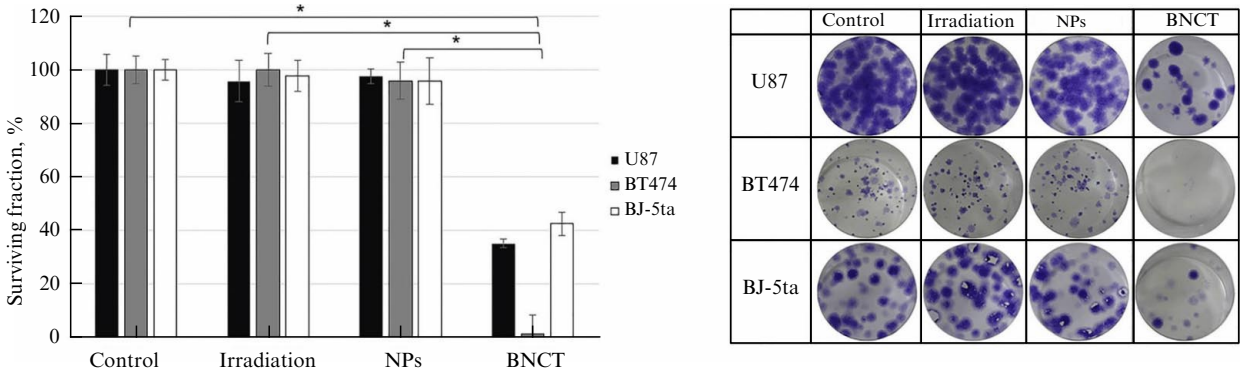


Figure 19. Clonogenic assay results after BNCT with PEGylated LF-^{10}B-NPs. * – $p < 0.001$, significance of differences compared with the control group, Mann–Whitney U test ($n = 4$) [285].

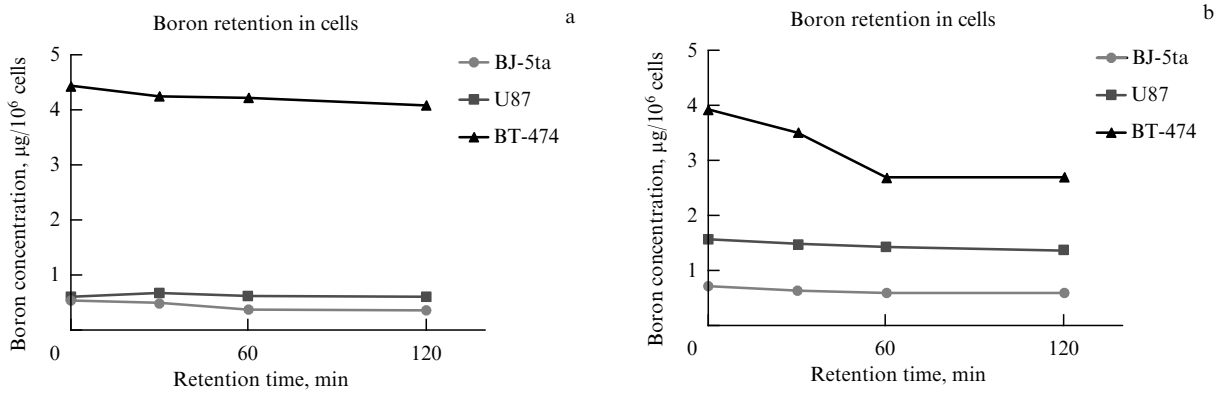


Figure 20. Accumulation and retention of ^{10}B in normal and tumor cell lines after 24 h incubation with PEGylated LA-^{10}B-NPs (a) and LF-^{10}B-NPs (b) [286].

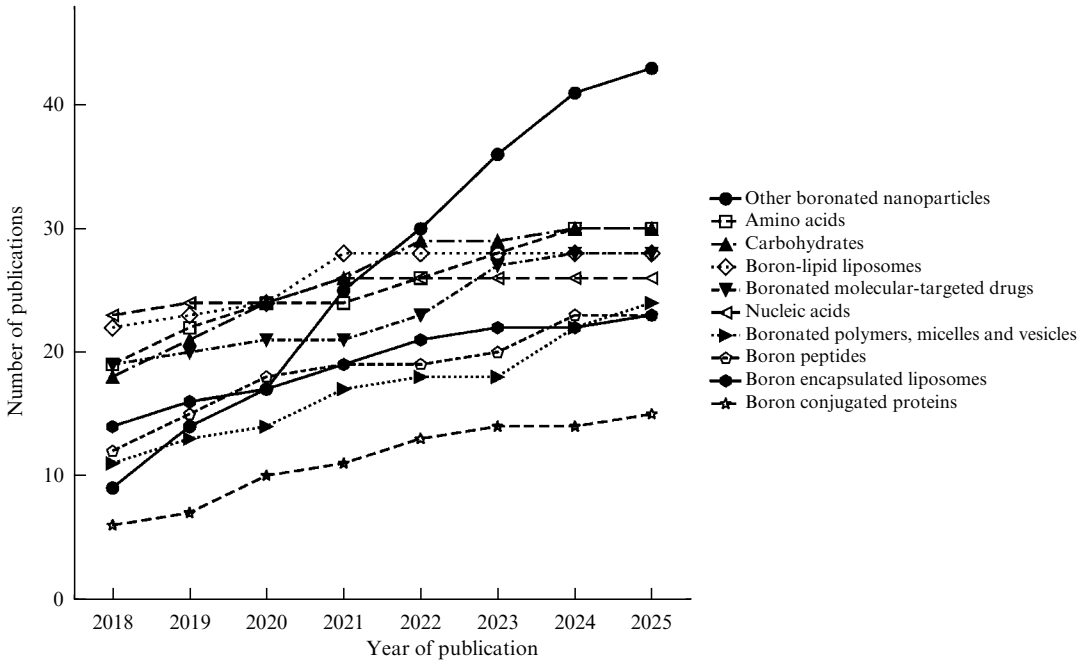


Figure 21. Bar chart showing the growth in the total number of publications in the field of various third-generation boron-containing agents over the period from 2018 to 2025.

In further development of these studies, we obtained targeted nanoformulations based on LF-^{10}B-NPs and LA-^{10}B-NPs functionalized with the scaffold protein Affibody $Z_{HER2:342}$, which is specific to the HER2 receptor. Biological testing of the developed nanostructures demonstrated a significant increase in boron accumulation at the cellular level, as well as sustained inhibition of BT-474 breast carcinoma xenograft growth in immunodeficient SCID mice following BNCT. In addition, studies are currently underway on the combined use of these nanoformulations with the recombinant immunotoxin DARP-loPE, which selectively blocks protein synthesis in HER2-positive tumor cells, to investigate synergistic effects of combination therapy.

To conclude this chapter, it is useful to analyze the global publication statistics in the field of new-generation boron-containing agents for BNCT (Fig. 21). The presented distribution shows a steady increase in the number of studies devoted to nanoscaled carriers over the past 8 years.

5. Absorbed dose monitoring techniques

BNCT differs fundamentally from conventional radiotherapy in its mixed radiation field. As the neutron field passes through the patient's body, it undergoes complex changes due to elastic and inelastic scattering on H, C, N, and O nuclei, as well as neutron absorption accompanied by the emission of secondary charged particles and γ-photons. Moreover, the therapeutic dose in BNCT is determined not so much by the radiation parameters as by the concentration and spatial distribution of the ^{10}B isotope in the patient's body. All this requires fundamentally different methods of dosimetric planning.

The total absorbed dose in BNCT is the sum of four components: the boron dose D_B, resulting from the dose-producing nuclear reaction $^{10}B(n,\alpha)^7Li$; the nitrogen dose D_N, from proton emission in the $^{14}N(n,p)^{14}C$ reaction; the fast-neutron dose D_H, due primarily to elastic scattering of neutrons on hydrogen nuclei; and the γ-ray dose D_γ. The latter component D_γ includes γ-radiation emitted directly in

body tissues through (n,γ)-reactions, mainly the $^{1}H(n,\gamma)^{2}H$ reaction, as well as the γ-background from the target assembly and structural materials of the facility.

Thus, the total absorbed dose in BNCT can be written as $D = D_B + D_N + D_H + D_\gamma$, where D_B is the boron dose, D_N is the nitrogen dose, D_H is the fast-neutron dose, and D_γ is the gamma dose. To calculate the equivalent dose, the D_N, D_H and D_γ components are multiplied by their respective RBE factors: $RBE_N = 2.9$, $RBE_H = 2.4$, $RBE_\gamma = 1$ [82]. For the boron dose, a compound biological effectiveness (CBE) factor is used, which depends on the properties of the ^{10}B-containing agent and the irradiated tissue. For clinical BNCT practice with 4-L-^{10}BPA, the following CBE factors are used: for tumor tissue $CBE_{tumour} = 3.8$, for skin $CBE_{skin} = 2.5$, for brain tissue $CBE_{brain} = 1.34$ and for soft tissue $CBE_{soft\ tissue} = 1.34$ [82].

The set of dosimetric studies in BNCT can be divided into three main areas. The first involves characterization of the neutron field *in air* to determine its energy and spatial distribution. The second area includes dosimetric studies using phantoms, in which depth dose distributions of the dose components are measured or the dose burden to critical organs outside the therapeutic beam is assessed [298–300]. The third area concerns the measurement of the $^{10}B(n,\gamma)^{7}Li$ reaction intensity for real-time monitoring of the boron dose during irradiation.

Treatment planning systems are used to calculate and visualize dose distributions. Based on patient CT or MRI data, together with experimentally verified parameters of the neutron and γ-radiation at the BSA exit, treatment planning systems allow the contribution of each of the four components to the total absorbed dose to be calculated.

5.1 Neutron energy spectrum measurement

The neutron energy spectrum at the BSA exit is a key characteristic that determines the penetration depth, the dose component ratios, and ultimately the therapeutic efficacy of BNCT. The most widely used methods for neutron spectrum measurement are the activation method and Bonner sphere spectrometry.

The activation method is based on the dependence of the neutron interaction cross-section with various isotopes on neutron energy [301]. Some nuclides have high thermal neutron capture cross-sections, while others exhibit pronounced resonances in the epithermal region or energy thresholds for fast-neutron reactions. If the resulting product is radioactive, the induced activity of the sample is proportional to the neutron flux in those energy ranges where the cross-section of the given reaction is large. Irradiating several materials with different energy-dependent cross-sections in the same beam allows the neutron spectrum to be reconstructed from the measured induced activities [302].

A classic material for activation foils is gold (^{197}Au). It has a high thermal neutron capture cross-section, producing the isotope ^{198}Au, which emits γ-photons with an energy of 0.411 MeV, as well as a pronounced capture resonance in the epithermal region at a neutron energy of about 4.9 eV. The use of cadmium shields, which completely absorb neutrons with energies below the 'cadmium cut-off' (about 0.5 eV), allows the thermal and epithermal flux components to be evaluated separately. Manganese (^{55}Mn) is also of interest; it is activated via the $^{55}Mn(n,\gamma)^{56}Mn$ reaction. The resulting isotope ^{56}Mn has a half-life of about 2.6 hours and emits characteristic γ-lines at 0.847 and 1.810 MeV [301].

Indium-115 (^{115}In) offers unique capabilities for the activation method. This nuclide has a pronounced resonance in the epithermal neutron capture cross-section at an energy of about 1.46 eV, producing the radioactive isotope ^{116}In. In addition to capture reactions, for fast neutrons above a threshold energy of about 400 keV, the inelastic scattering reaction $^{115}In(n,n')^{115m}In$ becomes possible. The resulting metastable isomer ^{115m}In (half-life 4.48 hours) subsequently decays to the ground state with the emission of a 0.336 MeV γ-photon [301]. Thus, measuring the induced activity of ^{115}In from different γ-lines allows simultaneous information on three energy ranges of the neutron spectrum to be obtained: thermal, epithermal, and fast.

Another method is Bonner sphere spectrometry [302]. Each sphere consists of a polyethylene moderator with a thermal neutron detector at its center. A set of spheres of different diameters allows measurements over a wide energy range — from thermal energies to tens of MeV — since the sensitivity maximum of a sphere depends on its diameter. Thermal neutron detectors used include $^{6}LiI(Eu)$ scintillators, $^{10}BF_3$ or ^{3}He proportional counters, and activation foils. Advantages of the method include high neutron detection efficiency with low sensitivity to γ-photons, as well as simplicity of measurement. The spherical shape of the moderator provides an isotropic response. The main limitation is the relatively low energy resolution due to the broad and strongly overlapping response functions of spheres of different diameters.

Another method is time-of-flight (TOF) spectrometry, which provides direct neutron energy measurement with high resolution [302]. For its application, the neutron source must operate in pulsed mode with a short pulse duration (typically less than 1 ns), which is often incompatible with the continuous operation mode of accelerator-based BNCT sources [82]. For this reason, this method is not used for routine beam monitoring in the clinic. Nevertheless, it can be used to verify the spectral characteristics of the beam during the development and commissioning of new accelerator-based neutron sources.

A promising direction in neutron spectroscopy is the detection of three-dimensional recoil nuclear tracks produced when neutrons interact with the active medium of the detector. This approach is implemented in time-projection chambers based on microstructured gas amplification systems (particularly the MICROMEGAS geometry) [303]. Such devices allow reconstruction not only of the kinetic energy but also of the momentum vector direction in the laboratory coordinate system. The most developed technological platform of this type is the MIMAC (Micro-TPC MATrix Chamber) family of detectors [304–308].

For correct dosimetric planning, it is necessary to know not only the neutron energy spectrum but also their spatial distribution at the BSA exit. The most common method involves irradiating a matrix of activation foils placed at equal spacing in a plane perpendicular to the beam axis. After irradiation, the induced activity of each foil is measured on a semiconductor γ-spectrometer [58, 82]. To obtain a two-dimensional distribution with high spatial resolution, the irradiated foil can also be exposed on an imaging plate, which provides a continuous image of the induced activity distribution [309, 310].

An alternative method is the use of radiochromic films (e.g., EBT2/EBT3), which directly record the spatial dose distribution. However, in a mixed neutron-gamma field, the

film response arises from the combined effects of γ-radiation and recoil protons generated by elastic scattering of fast neutrons on hydrogen nuclei in the organic film matrix [311, 312]. Therefore, the dose profile measured with radiochromic film represents a superposition of gamma and neutron contributions, requiring correction to separate the individual absorbed dose components [82].

5.2 Measurement of individual absorbed dose components

One method for separating the neutron and gamma contributions in BNCT mixed fields is the use of paired ionization chambers [82, 313, 314]. This approach is based on the simultaneous use of two chambers with identical sensitive volume geometry but substantially different relative sensitivities to neutrons and gamma radiation, achieved through the choice of wall material and gas filling.

The first chamber is made of A-150 plastic, which is close in elemental composition to soft biological tissue, and is filled with a tissue-equivalent gas mixture. This chamber has high sensitivity to both gamma rays and neutrons. The second chamber has magnesium walls and is filled with argon. Its sensitivity to fast neutrons is less than 5% of that of the first chamber. Both chambers operate to record the mixed radiation response, and the separation of dose components is achieved by solving a system of two linear equations relating the chamber readings to the neutron and gamma doses.

An alternative method for separating the neutron and gamma components of the absorbed dose is thermoluminescent dosimetry (TLD). This approach is based on the ability of certain crystalline materials to accumulate ionizing radiation energy in metastable states (traps). Upon subsequent controlled heating of the detectors, charge carrier recombination occurs, accompanied by the emission of light quanta — thermoluminescence — whose integrated yield is proportional to the absorbed dose.

Separate determination of the thermal neutron and gamma contributions to the absorbed dose is achieved using pairs of detectors based on lithium fluoride (LiF:Mg,Ti or LiF:Mg,Cu,P) with different ^{6}Li enrichment [315, 316]. The neutron absorbed dose is determined from the difference in readings of the paired detectors, with calibration factors and corrections for thermal neutron self-shielding in the detector [166, 317, 318]. For gamma dosimetry, radiophotoluminescent (RPL) detectors based on phosphate glasses are also used [319, 320].

The small size of TLD and RPL detectors allows simultaneous measurement of the gamma absorbed dose at multiple points both inside phantoms and directly during *in vitro* and *in vivo* studies. Disadvantages of TLD include the need for strict adherence to thermal annealing protocols and individual calibration of each crystal, as well as the irreversible destruction of dosimetric information during readout. RPL detectors, in contrast, allow repeated nondestructive readout, exhibit negligible fading, and have high long-term stability of the accumulated dose; however, they require specialized readout equipment. In addition, RPL detectors are inferior to TLD in tissue equivalence and require energy compensation filters when working with low-energy photons [320].

A promising approach for assessing the quality and biological effectiveness of the therapeutic beam is the microdosimetric method using miniaturized tissue-equivalent proportional counters (TEPCs) operating at reduced pressure [321–323]. The various components of the mixed radiation field, including gamma radiation, fast neutrons, and the products of the $^{10}B(n,\alpha)^{7}Li$ nuclear reaction, generate characteristic microdosimetric spectra, allowing their contributions to the total absorbed dose to be separated.

Compact scintillation detectors are used to measure the spatial distribution of thermal neutrons and gamma radiation [82, 159, 299, 300]. Their operating principle is based on detecting the charged products of the $^{10}B(n,\alpha)^{7}Li$ and $^{6}Li(n,\alpha)^{3}H$ nuclear reactions. The scintillation signal is transmitted via an optical fiber to a remote optoelectronic system. This allows measurements with high spatial resolution to be performed with minimal exposure of the recording electronics to ionizing radiation. Unlike integral methods operating in cumulative mode, this approach enables online monitoring of the spatial distribution of dose components with millimeter resolution directly during irradiation.

At the BINP SB RAS, a measurement system based on a compact three-channel detector has been developed, consisting of two polystyrene scintillators, one of which is doped with the ^{10}B isotope [159, 324]. The scintillators are cylindrical, with a diameter and length of 1 mm. The third channel is a light guide without a scintillator. Light collection from all channels is performed via flexible optical fibers to silicon photomultipliers (SiPM) [325]. The difference between the readings of the boronated and nonboronated scintillators gives the neutron component, while subtracting the signal from the 'empty' fiber from the nonboronated scintillator readings eliminates the background signal generated in the optical fiber and allows the gamma component to be estimated.

This measurement system is used routinely at the VITA^{TM} research accelerator-based neutron source for verifying the neutron beam and monitoring it during irradiation of cell cultures and laboratory animals, as well as in the treatment of domestic animals with spontaneous tumors [326]. It is also integrated into the medical system based on the VITA-IIβ accelerator-based neutron source at the N.N. Blokhin National Medical Research Centre of Oncology.

A measurement system with a similar detector configuration but based on the ^{6}Li isotope is described in [300]. The authors successfully performed online monitoring of the thermal neutron flux during BNCT in 16 patients. In that study, three separate detectors were placed at three positions: on the skin at the center of the tumor location, at the periphery of the tumor, and directly in front of the collimator. The first served to monitor the neutron flux in the tumor, the second to detect patient movement during irradiation, and the third to monitor the stability of the neutron beam.

A separate class of dosimetric monitoring systems in BNCT is represented by chemical methods [327]. Their action is based on quantitative analysis of radiation-induced transformations initiated by free radicals — products of water radiolysis. The most widely used chemical dosimeter is the Fricke ferrous sulfate dosimeter.

In its classic form, the system consists of an air-saturated aqueous solution containing ferrous sulfate (or ferrous ammonium sulfate) in sulfuric acid (H_2SO_4). Under the action of ionizing radiation, primary radiolysis of H_2O molecules occurs, producing highly reactive radicals ($OH^{\bullet}$, $H^{\bullet}$) and hydrogen peroxide (H_2O_2). The reaction of $H^{\bullet}$ radicals with dissolved oxygen generates hydroperoxyl

radicals ($HO_2^{\bullet}$). These intermediates successively oxidize Fe^{2+} ions to Fe^{3+} ions, which are stable in acidic medium.

A gel modification of the Fricke dosimeter enables three-dimensional dosimetry in BNCT. To fix the spatial dose distribution, the liquid phase is immobilized in macromolecular matrices based on gelatin, agarose, or polyvinyl alcohol, forming gel phantoms. To assess the contribution of the boron dose component D_B, boron-containing compounds (e.g., boric acid or borax) are additionally introduced into the hydrogel during synthesis. The local concentration of Fe^{3+} ions can be visualized by MRI [328].

For quantitative optical analysis of the absorbed dose, a modification of the Fricke dosimeter with the addition of the metal-chromic indicator xylenol orange is used [329, 330]. Xylenol orange forms a stable chelate complex with Fe^{3+} ions, which has an intense absorption maximum in the visible spectral region at about 585 nm. The change in optical density of the dosimetric gel, recorded by spectrophotometry, correlates linearly with the absorbed dose up to the radiation saturation stage of the system. The Fricke dosimeter provides measurement stability in the range up to 10–400 Gy at dose rates up to 1.5×10^4 Gy h^{-1} [331].

To estimate the combined contribution of the D_N and D_H components, a method called the 'cellular dosimeter' has been proposed at the BINP SB RAS [332, 333]. Cell cultures are irradiated for the same time in two modes: with gamma radiation only, and with mixed neutron and gamma radiation. By adjusting the proton beam current, the same cell survival is achieved in both modes. Since cell survival and irradiation time are the same, the equivalent doses are also the same. The gamma dose in both modes is measured with a gamma dosimeter. The difference between the measured doses corresponds to the combined contribution of the nitrogen component and the fast-neutron dose.

The method is based on the threshold behavior of the $^7Li(p,n)^7Be$ reaction: below the threshold (1.882 MeV), only photons from the $^7Li(p,p'\gamma)^7Li$ channel are emitted from the lithium target, while above it, neutron radiation is also produced. The same cell survival over the same irradiation time is achieved by reducing the proton beam current in the mixed-radiation mode compared with the photon-only mode. Experiments on U251 glioblastoma cells showed that the combined contribution of the D_N and D_H components is 1.23 Gy-eq (31% of the gamma dose).

5.3 Real-time *in vivo* dosimetry methods

The efficacy of BNCT is largely determined by the spatial distribution of the ^{10}B isotope in the tumor and surrounding healthy tissues [58]. Traditional approaches — biopsy followed by ICP analysis or PET imaging with ^{18}F-FBPA — provide data only *ex vivo* or before the irradiation session, which does not allow monitoring of boron pharmacokinetics directly during irradiation [82].

To overcome this limitation, real-time *in vivo* dosimetry methods are being developed. These methods are based on detecting the 478 keV γ-photons emitted in 93.9% of the $^{10}B(n,\alpha)^7Li$ nuclear reactions. Detection of such γ-photons provides direct information on the intensity of the nuclear reactions, i.e., on the boron dose D_B in the region of interest. This approach has been known for a long time but has not yet been implemented in clinical BNCT practice.

The difficulty of implementation lies in the fact that the γ-spectrometer must be resistant to the neutron field and have good energy resolution. In addition, when a lithium target is used, inelastic proton scattering on lithium nuclei also produces photons with the same energy — 478 keV. If a γ-spectrometer relatively insensitive to neutrons is used, its energy resolution does not allow the 478 keV line to be separated from the more intense 511 keV annihilation line. A high-purity germanium (HPGe) semiconductor γ-spectrometer can resolve these lines, but it is sensitive to neutrons. It is therefore placed away from the target, and collimators are used to extract the useful signal, which reduces efficiency but preserves spectral resolution.

The first attempts at *in vivo* ^{10}B concentration determination were made as early as the 1980s–1990s [334–337]. One of the first successful implementations of prompt gamma spectroscopy was a system installed at the HFR reactor in Petten [337–339]. Tests on anthropomorphic phantoms showed that at a ^{10}B concentration of 5 μg g^{-1}, the 478 keV photopeak area could be determined with a relative standard deviation of 3% in a 2 minute exposure, with a spatial resolution of about 1.6 cm FWHM.

At the BINP SB RAS, this direct method of boron dose measurement has been implemented for the treatment of domestic animals with spontaneous tumors [159, 333]. A schematic of the experimental setup is shown in Fig. 22. The lithium neutron-generating target with a Plexiglas moderator is placed in the first bunker. The HPGe γ-spectrometer is in an adjacent bunker behind a 1.5-m-thick concrete wall. A 100 mm-diameter hole is made in the wall for radiation detection. A 50-mm-thick lead collimator with a 25×50 mm or 50×50 mm aperture is placed in front of the animal.

To suppress neutron penetration into the second bunker, a 12-mm-thick Plexiglas plate is installed in front of the hole in the wall of the first bunker to scatter neutrons. An identical plate is installed in the second bunker in front of the spectrometer. The spectrometer detector is wrapped in 0.1 mm-thick cadmium foil to absorb thermal neutrons and protect the spectrometer. The detector is placed inside a lead collimator to reduce the background signal and reduce detector loading.

Figure 23 shows a typical spectrum of the detected radiation. The 478 keV photon line is broadened but clearly detectable. After successful testing, the method was used to treat another ten domestic animals; the results are presented in [340].

The development of prompt gamma spectroscopy has led to the concept of PG-SPECT (Prompt Gamma Single Photon Emission Computed Tomography), which involves the use of multi-detector systems with radiation collimation for three-dimensional reconstruction of the absorbed dose distribution in real time. HPGe detectors, which have high energy resolution but require cryogenic cooling, as well as compact CdTe detectors capable of operating at room temperature but with lower detection efficiency, were initially considered as detectors [341–344].

In subsequent modifications, multi-element arrays based on $LaCl_3(Ce)$ [345] and $LaBr_3(Ce)$ [346, 347] scintillation crystals with lead or tungsten collimators were proposed to achieve high detection efficiency. The main factor limiting the performance of these scintillators is the intense background from the 2.22 MeV line and the 511 keV annihilation peak, which form a continuous background in the energy spectrum in the region of the 478 keV analytical peak. To reduce this contribution, shielding and active suppression systems based on BGO ($Bi_4Ge_3O_{12}$) crystals operating in anti-coincidence mode are used [348].

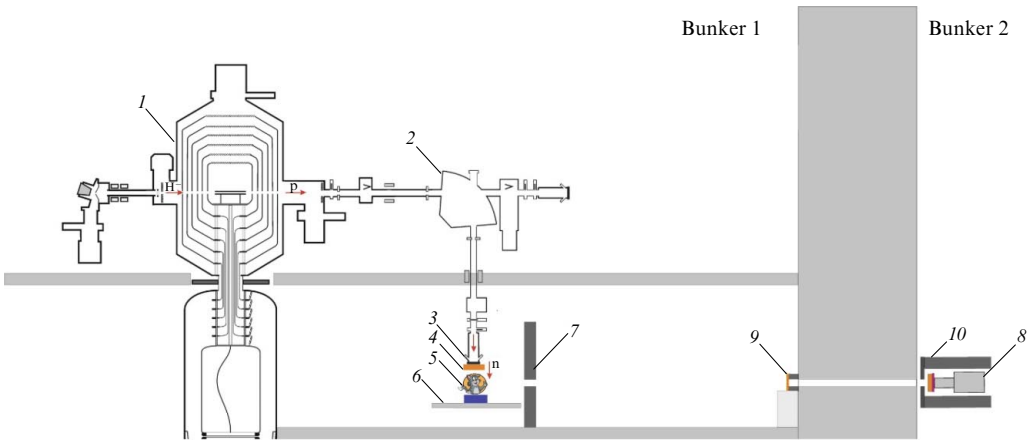


Figure 22. Schematic of the experimental setup: *1* — vacuum-insulated tandem accelerator, *2* — bending magnet, *3* — lithium neutron-generating target, *4* — moderator, *5* — irradiated object, *6* — irradiation table, *7* — lead collimator, *8* — HPGe spectrometer, *9* — neutron scatterer, *10* — lead collimator of the HPGe spectrometer.

Detectors based on CdZnTe (CZT) have also been investigated; they offer energy resolution close to that of CdTe while providing more stable performance [349–353]. However, the use of collimators significantly reduces the geometric efficiency of any multi-element system by cutting off a substantial portion of the useful photon flux. An alternative solution free from this drawback is the transition to Compton cameras.

The principal difference between Compton cameras and PG-SPECT systems is that the trajectory of the primary γ-photon is reconstructed kinematically from the Compton scattering angle. This eliminates the need for massive collimators, which not only reduce the fraction of detected photons but are also susceptible to neutron activation in mixed radiation fields. The spatial resolution of the method in this case is determined by the accuracy of the energy deposition and interaction position measurements in the absorber and scatterer detectors.

The first experimental confirmation of the method's feasibility for BNCT applications was obtained in [354]. The researchers used a Si/CdTe Compton camera, ASTROCAM 7000HS. An ^{241}AmBe isotopic neutron source with a graphite moderator was used, and a boron carbide (B_4C) powder served as the target. The experiments successfully resolved the 478 keV and 511 keV γ-peaks, reconstructed a two-dimensional image of the irradiated target, and visualized it when placed in water simulating biological tissue. The main limitations of the method remain the high detector count rate in an intense clinical neutron beam and the background from neutron capture on cadmium nuclei in the detector matrix (558 keV peak).

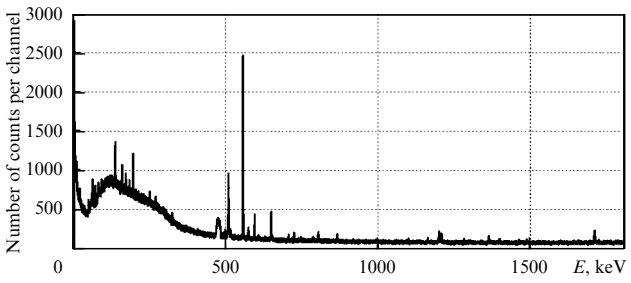


Figure 23. Typical spectrum measured with the HPGe γ-spectrometer.

A significant step forward was made in [355], where the i-TED Compton camera was presented. This system consists of four modules based on monolithic $LaCl_3$(Ce) crystals coupled to silicon photomultiplier arrays. According to the authors, the energy resolution allows reliable separation of the 478 keV peak from the 511 keV annihilation background. The spatial resolution of the system is 49–54 mm. The instrument is resistant to neutron background and remains operational at count rates up to 500 kHz, with sensitivity sufficient to detect ^{10}B masses below 1 μg. In experiments at the ILL reactor (Grenoble, France), the i-TED camera successfully reconstructed the two-dimensional ^{10}B concentration distribution in phantoms with melanoma, glioblastoma, and squamous cell carcinoma of the tongue cell lines. The results showed good agreement with reference HPGe spectrometry data.

5.4 Treatment planning systems

The goal of dosimetric planning is to determine the optimal irradiation conditions for the patient before the start of the therapeutic course through computer modeling. For this purpose, specialized software packages — treatment planning systems (TPS) — are used. Since the radiation field in BNCT is mixed and the ratio of the four dose components critically depends on the elemental composition of tissues and the spatial distribution of boron in the patient's body, standard analytical dose calculation algorithms are not applicable here. In clinical BNCT planning, the main tool is numerical simulation of neutron and photon transport using the Monte Carlo method, which provides the highest calculation accuracy [58, 82].

The main planning steps include creating a three-dimensional anatomical model of the patient based on CT or MRI data, as well as contouring the target volumes and critical organs. For correct neutron transport modeling, the elemental composition of tissues is specified, considering the concentrations of hydrogen, nitrogen, and other key elements. In addition, experimentally verified beam characteristics — the energy-angular spectrum and spatial distribution — are defined. Based on these input data, Monte Carlo codes (MCNP, PHITS, Geant4, etc.) are used to calculate three-dimensional distributions of all four absorbed dose components.

A key parameter for the boron dose calculation is the ^{10}B concentration in the tumor and healthy tissues. In clinical practice, it is usually estimated indirectly from the blood boron concentration using fixed pharmacokinetic ratios. For example, for 4-L-^{10}BPA, a tumor-to-blood ratio of 3:1 or 3.5:1 is used depending on the protocol, while for brain tissue the ratio is 1:1 [58]. Blood boron concentration is measured by ICP-AES, ICP-MS, or neutron activation analysis. A more accurate, though not yet routine, approach is PET imaging with ^{18}F-FBPA [174, 356], which allows a patient-specific three-dimensional boron concentration distribution to be obtained and used for more precise dosimetric planning.

The practical implementation of Monte Carlo calculations in a clinical setting requires optimization of computational resources. Direct particle tracking from the primary source through the entire BSA to the patient is extremely resource-intensive. To speed up the calculations, a two-stage simulation scheme is used. In the first stage, a detailed calculation is performed accounting for the entire facility geometry, simulating radiation transport from the source to the beam exit aperture. The physical characteristics of all escaping particles are recorded and stored at this boundary. The virtual source obtained in this way must undergo experimental verification by comparing the simulation results with experimental dosimetric measurements. In the second stage, based on the verified beam characteristics, the dose distribution in the patient's anatomical structures is calculated. This approach eliminates the need to re-simulate the processes in the BSA, significantly reducing the dosimetric planning time while maintaining high calculation accuracy.

Several TPSs have been developed for clinical BNCT applications. Noncommercial software packages used at reactor facilities include NCTPlan (MIT, USA) [357, 358], SERA (USA) [359–361], JCDS (JAEA, Japan) [362, 363], and THORplan (Taiwan) [364]. With the development of accelerator-based sources, commercial TPSs have been created: Tsukuba-Plan (University of Tsukuba, Japan) [365–367] and NeuCure Dose Engine (Sumitomo Heavy Industries, Japan) integrated with the RayStation platform (RaySearch Laboratories, Sweden) [58]. Commercial TPSs are also being actively developed by Neutron Therapeutics (USA/Finland) and TAE Life Sciences (USA) [58].

A significant limitation of current preclinical BNCT research should be noted separately: the lack of specialized treatment planning systems for experimental radiobiology. This problem becomes particularly important in the context of the pressing task of developing and screening promising third-generation targeted boron-containing agents. Without knowing the magnitude and spatial distribution of the absorbed dose in the biological sample, it is impossible to properly evaluate the therapeutic index of new compounds or interpret the experimental results.

To address this problem, we have developed a computational dosimetric model designed for planning and optimizing protocols for preclinical *in vitro* and *in vivo* studies, as well as for the treatment of domestic animals with spontaneous tumors at the VITA™ accelerator-based neutron source [368, 369]. The computational dosimetric model was developed using the Geant4 toolkit and includes a validated computational model of the neutron-generating system of the VITA™ facility (Fig. 24) and a library of software phantoms for various biological objects (Fig. 25). The

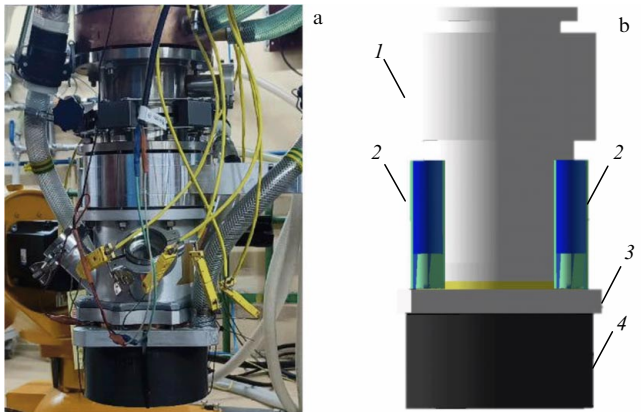


Figure 24. Photograph (a) and computational model (b) of the neutron-generating system of the VITA™ research accelerator-based neutron source: *1* — high-energy proton beam transport line, *2* — pipes of the target assembly cooling system, *3* — target assembly, 4 — neutron moderator.



Figure 25. Software phantoms of biological objects in the Geant4 simulation environment: vials with cell cultures (a), laboratory mice (b), rats (c), and a cat head phantom (d).

developed software package allows the calculation of each of the four absorbed dose components and the generation of spatial dose maps in the irradiated volume.

Thus, the analysis of current dosimetric monitoring methods in BNCT shows that the main problem determining the direction of technological development in the coming years is the absence of clinically implemented methods for measuring the intensity of $^{10}B(n,\alpha)^7Li$ nuclear reactions directly during irradiation. In addition, the therapeutic effect of BNCT critically depends on the subcellular distribution of boron, which is determined by the type of boron-containing

compound used, the histological structure of the tumor, and individual patient characteristics. Therefore, the second priority research direction is microdosimetric approaches that, based on experimental data on the heterogeneity of cellular ^{10}B distribution, allow more accurate calculation of the biological effectiveness of treatment.

6. Conclusion. Prospects for the development of boron neutron capture therapy

Boron neutron capture therapy represents one of the most effective methods of binary hadron therapy.

In the last decade, the problem of creating compact accelerator-based neutron sources suitable for installation in oncology clinics for BNCT — a challenge that had long hindered the development of the method — has been successfully resolved. A rapid growth is observed in the number of projects under development, employing different types of charged-particle accelerators and different neutron-generating targets: to date, 11 centers worldwide are already treating patients or conducting clinical trials, while 13 centers are commissioning systems or completing their manufacture.

The expanding clinical application of BNCT is driving rapid progress in the development of targeted agents that can more selectively deliver and retain the required ^{10}B concentrations in tumor cells during therapy. Solving this problem will pave the way for broader clinical application of BNCT in various forms of cancer and will allow the full potential of this unique method to be realized.

Equally pressing is the issue of metrological and dosimetric support for BNCT. The complex nature of the mixed radiation field requires precise separation of the contributions of each component to the total absorbed dose — both in the tumor and in adjacent healthy tissues and organs at risk. The lack of standardized methods and dosimetric protocols continues to hinder the widespread implementation of BNCT in clinical practice. Among the dosimetry methods being actively developed in recent years, the most promising appears to be prompt gamma spectrometry, which provides direct measurement of the number of neutron capture reactions on boron in the observed volume and, consequently, allows boron pharmacokinetics to be monitored directly during irradiation. The feasibility of this approach has recently been demonstrated experimentally, and the authors strongly recommend its implementation in clinical practice, integrated into the treatment planning system for irradiation time correction.

Turning to the conceptual aspects of BNCT, in our view, the most promising directions that could enhance its therapeutic efficacy include combination therapy strategies in which BNCT is combined with (1) conventional chemotherapy, (2) targeted biological toxins (immunotoxins), and (3) immunotherapy using immune checkpoint inhibition (PD1/PD-L1). For BNCT itself, the most promising approach appears to be the design of ^{10}B NPs with biocompatibility and colloidal stability (hydrophilic polymer coating), as well as functionalization with targeting molecules for highly specific binding to target cells (antibody mimetics — alternative scaffold proteins). Additional potential can be realized using peptides that mediate intracellular internalization (cell-penetrating peptides) and deliver ^{10}B NPs to the cell nucleus (nuclear localization signals). The synergistic effects of such combination therapy are expected to bring substantial progress in BNCT in the coming years.

Acknowledgments. This study was supported by the Russian Science Foundation, grant No. 24-62-00018 (https://rscf.ru/project/24-62-00018/).

References

1. Kovalchuk M V, Deyev S M, Sergunova K A *Nanobiotechnol. Rep.* **18** 524 (2023); *Ross. Nanotekhnol.* **18** 436 (2023)
2. Kaprin A D, Smirnov V P "Yadernaya meditsina," in *Akademiya Nauk i Atomnaya Otrasl'. Nauchnye Sessii Obshchego Sobraniya Chlenov RAN i Obshchikh Sobranii Otdelenii RAN. Dekabr' 2020 g.* (The Academy of Sciences and the Nuclear Industry. Scientific Sessions of the General Meeting of the Members of the RAS and the General Meetings of the Divisions of the RAS. December 2020) (Eds V G Bondura, G N Rykovanova, A A Makosko) (Moscow: Rossiiskaya Akademiya Nauk, 2021) p. 307
3. Zavestovskaya I N, Kolobov A V, Ryabov V A *Phys. Usp.* **67** 866 (2024); *Usp. Fiz. Nauk* **194** 917 (2024)
4. Chernyaev A P *Phys. Usp.* **68** 923 (2025); *Usp. Fiz. Nauk* **195** 982 (2025)
5. Röntgen W C *Science* **3** 227 (1896)
6. Tarkhanov I R *Izv. St. Petersburg. Biol. Lab.* **1** (3) 47 (1896)
7. Becquerel H *C. R. Hebdomadaires Seances Acad. Sci.* **122** 420 (1896)
8. Curie P, Sklodowcka-Curie M *C. R. Acad. Sci. Paris* **127** 175 (1898)
9. Curie P, Sklodowcka-Curie M *C. R. Acad. Sci. Paris* **127** 1215 (1898)
10. Becquerel H, Curie P *C. R. Acad. Sci. Paris* **132** 1289 (1901)
11. Bell A G, Sowers Z T *Nature* **68** 320 (1903)
12. Baltas D, Sakelliou L, Zamboglou N *The Physics of Modern Brachytherapy for Oncology* (Boca Raton, FL: Taylor and Francis, 2007)
13. London E S *Das Radium in der Biologie und Medizin* (Leipzig: Akademische Verlagsgesellschaft, 1911)
14. Pasteau O, Degrais P *J. Urologie Med. Chirurgicale* **4** 341 (1913)
15. Heineke H *Münchener medizinische Wochenschrift* **50** 2090 (1903)
16. Heineke H *Mitteilungen Grenzgebieten Med. Chirurgie* **14** 21 (1904)
17. Kudryashov Yu B *Radiatsionnaya Biofizika* (*Ioniziruyushchie Izlucheniya*) (Radiation Biophysics (Ionizing Radiations)) (Moscow: Fizmatlit, 2004)
18. Bergonie J, Tribondeau L *C. R. Acad. Sci. Paris* **143** 983 (1906)
19. Nemenov M I *Rentgenoterapiya* (X-ray Therapy) (Petrograd: Gos. Izd., 1920)
20. Khlopin V *Usp. Fiz. Nauk* **3** 99 (1922)
21. Van de Graaff R J *Phys. Rev.* **38** 1919 (1931)
22. Cockroft J D, Walton E T S *Proc. R. Soc. London A* **136** 619 (1932)
23. Lawrence E O, Livingston M S *Phys. Rev.* **40** 19 (1932)
24. Kerst D W *Phys. Rev.* **58** 841 (1940)
25. Veksler V I *Dokl. Akad. Nauk SSSR* **43** 346 (1944)
26. Brobeck W M et al. *Phys. Rev.* **71** 449 (1947)
27. Courant E D, Livingston M S, Snyder H S *Phys. Rev.* **88** 1190 (1952)
28. Akulinichev S V *Phys. Usp.* **57** 1239 (2014); *Usp. Fiz. Nauk* **184** 1363 (2014)
29. Klenov G I, Khoroshkov V S *Phys. Usp.* **59** 807 (2016); *Usp. Fiz. Nauk* **186** 891 (2016)
30. Krasavin E A *Phys. Usp.* **59** 411 (2016); *Usp. Fiz. Nauk* **186** 435 (2016)
31. Zhuikov B L, Ermolaev S V *Phys. Usp.* **64** 1311 (2021); *Usp. Fiz. Nauk* **191** 1387 (2021)
32. Stone R S *Radiology* **72** 109 (1959)
33. Chadwick J *Proc. R. Soc. London A* **136** 692 (1932)
34. Locher G L *Am. J. Roentgenol.* **36** 1 (1936)
35. Field S B *Curr. Top. Radiat. Res. Quarterly* **11** (1) 1 (1976)
36. Lawrence J H, Lawrence E O *Proc. Natl. Acad. Sci. USA* **22** 124 (1936)
37. Lawrence J H, Aebersold P C, Lawrence E O *Proc. Natl. Acad. Sci. USA* **22** 543 (1936)
38. Stone R S, Lawrence J H, Aebersold P C *Radiology* **35** 322 (1940)
39. Stone R S *Am. J. Roentgenol. Radium Ther.* **59** 771 (1948)
40. Bewley D K *Br. J. Radiol.* **58** 213 (1985)
41. Lawrence E O *Science* **90** 407 (1939)
42. Johns H E, Bates L M, Watson T A *Br. J. Radiol.* **25** 296 (1952)
43. Leksell L *Acta Chir. Scand.* **102** 316 (1951)
44. Leksell L *Acta Chir. Scand.* **134** 585 (1968)
45. Fermi E *Proc. Am. Philos. Soc.* **90** 20 (1946)

46. Wilson R R *Radiology* **47** 487 (1946)
47. Bragg W H, Kleeman R *Philos. Mag.* **8** 726 (1904)
48. The Particle Therapy Co-Operative Group, PTCOG, https://ptcog.online
49. Podgorsak E B *External Photon Beams: Physical Aspects* (Vienna: IAEA, 2005)
50. Zamani H et al. *Phys. Med.* **140** 105682 (2025)
51. Balasubramanian S et al. *Radiat. Environ. Biophys.* **63** 47 (2024)
52. Jung H et al. *Radiat. Oncol.* **19** 19 (2024)
53. Sminia P et al. "Clinical radiobiology for radiation oncology," in *Radiobiology Textbook* (Ed. S Baatout) (Cham: Springer, 2023) p. 237
54. Wenker S T M et al. *Nucl. Med. Biol.* **140** 108971 (2025)
55. Primac I et al. *Nature Rev. Clin. Oncol.* **22** 869 (2025)
56. Roy I et al. *ACS Nano* **16** 5036 (2022)
57. Mititelu M R et al. *Clin. Oncol.* **43** 103857 (2025)
58. Sauerwein W A G et al. (Eds) *Neutron Capture Therapy. Principles and Applications* (Cham: Springer, 2025)
59. Lipengolts A et al. *J. Phys. Conf. Ser.* **2058** 012039 (2021)
60. Sheino I N et al. *Byull. Sibirsk. Med.* **16** (3) 192 (2017)
61. Kulakov V N et al. *Pharm. Chem. J.* **50** 388 (2016); *Khim.-Farm. Zh.* **50** (6) 19 (2016) DOI:10.30906/0023-1134-2016-50-6-19-25
62. Bonvalot S et al. *Lancet Oncol.* **20** 1148 (2019)
63. Le Tourneau C et al. *JAMA Otolaryngol. Head Neck Surg.* **152** 284 (2026)
64. Boux F et al. *J. Neurooncol.* **177** 91 (2026)
65. Zavestovskaya I N et al. *Nanomaterials* **13** 2167 (2023)
66. Zavestovskaya I N et al. *Mater. Today Nano* **27** 100508 (2024)
67. Filimonova M V et al. *Bull. Exp. Biol. Med.* **176** 626 (2024); *Byull. Eksp. Biol. Med.* **176** (11) 647 (2023)
68. Filimonova M V et al. *Dokl. Biochem. Biophys.* **516** 111 (2024)
69. Ryabtseva M S et al. *Pharmaceutics* **17** 515 (2025)
70. Azarkin M, Kirakosyan M, Ryabov V *Int. J. Mol. Sci.* **24** 13400 (2023)
71. Azarkin M, Kirakosyan M, Ryabov V *Int. J. Mol. Sci.* **25** 9525 (2024)
72. Zavestovskaya I N et al. *Bull. Lebedev Phys. Inst.* **50** 279 (2023); *Kratk. Soobshch. FIAN* (7) 22 (2023)
73. Rusetskii A S et al. *Nucl. Instrum. Meth. Phys. Res. B* **563** 165651 (2025)
74. Zygmanski P, Sajo E, Brivio D *Z. Med. Phys.* **33** 119 (2023)
75. Taylor H J, Goldhaber M *Nature* **135** 341 (1935)
76. "Neitrony vmesto skal'pelya." Atomnaya Energiya 2.0 ("Neutrons instead of a scalpel." Atomic Energy 2.0), https://www.atomic-energy.ru/articles/2015/05/06/15795
77. Deagostino A et al. *Future Med. Chem.* **8** 899 (2016)
78. Ho S L et al. *ACS Omega* **7** 2533 (2022)
79. Lipengolts A A et al. *Onkolog. Zh. Luchevaya Diagnostika Luchevaya Terapiya* **3** (2) 63 (2020) DOI:10.37174/2587-7593-2020-3-2-63-70
80. Kanygin V et al. *Veterinary Sci.* **10** (4) 274 (2023)
81. Karpovich N I et al. *Sibirsk. Med. Zh.* **32** (3) 77 (2017)
82. Ahmed M et al. *Advances in Boron Neutron Capture Therapy* (Vienna: Intern. Atomic Energy Agency, 2023)
83. Zahl P A, Cooper F S *Science* **93** 64 (1941)
84. Taskaeva I et al. *Life* **13** 518 (2023)
85. "Photon, electron, proton and neutron interaction data for body tissues," ICRU Report 46 (Bethesda, MD: ICRU, 1992)
86. Berger M J et al., PSTAR: Stopping-Power and Range Tables for Protons (Gaithersburg, MD: NIST, 2005)
87. Kruger P G *Proc. Natl. Acad. Sci. USA* **26** 181 (1940)
88. Zahl P A, Cooper F S, Dunning J R *Proc. Natl. Acad. Sci. USA* **26** 589 (1940)
89. Zahl P A, Cooper F S *Radiology* **37** 673 (1941)
90. Ludford R J *Proc. R. Soc. London B* **104** 493 (1929)
91. Duran-Reynals F *Am. J. Cancer* **35** 98 (1939)
92. Sweet W H *New England J. Med.* **245** 875 (1951)
93. Sweet W H, Javid M *Trans. Am. Neurol. Assoc.* **76** 60 (1951)
94. Slatkin D N et al. *J. Neurol. Neurobiol.* **3** 1 (2017)
95. Archambeau J O *Radiology* **94** 178 (1970)
96. Slatkin D N *Brain* **114** 1609 (1991)
97. Farr L E *Science* **130** 1067 (1959)
98. Asbury A K et al. *J. Neuropathol. Exp. Neurol.* **31** 278 (1972)
99. Farr L E et al. *Arch. Neurol.* **4** 246 (1961)
100. Russell D S, Wilson C W, Tansley K *J. Neurol. Neurosurg. Psychiatry* **12** (3) 187 (1949)
101. Hatanaka H, in *Boron-Neutron Capture Therapy for Tumors* (Ed. H Hatanaka) (Niigata: Nishimura, 1986) p. 1
102. Soloway A H, Hatanaka H, Davis M A *J. Med. Chem.* **10** 714 (1967)
103. Hatanaka H *Basic Life Sci.* **54** 15 (1990)
104. Mishima Y et al. *Basic Life Sci.* **50** 251 (1989)
105. Mishima Y et al. *Lancet* **2** 388 (1989)
106. Mishima Y et al. *Strahlenther. Onkol.* **165** 251 (1989)
107. Wittig A, Sauerwein W A, Coderre J A *Radiat. Res.* **153** 173 (2000)
108. Ryabukhin Yu S, in *Summary Reports of the First Conf. of Institute for Medical Radiology, Obninsk, 1965*
109. Ryabukhin Yu S *Basic Life Sci.* **50** 27 (1989)
110. Ryabukhin Yu S *Med. Radiologiya* **11** 9 (1966)
111. Ivanov V N et al. *Med. Radiologiya* **14** 47 (1969)
112. Ryabukhin Yu S et al. *Med. Radiologiya* **14** 66 (1969)
113. Krasnoshchekov G P, Ryabukhin Yu S, Vasileva N A *Med. Radiologiya* **15** 46 (1970)
114. Letov V N et al. *Med. Radiologiya* **15** 12 (1970)
115. Letov V N et al. *Med. Radiologiya* **15** 50 (1970)
116. Skoropad Yu D, Ryabukhin Yu S *Med. Radiologiya* **12** 53 (1967)
117. Ryabukhin Yu S *Med. Radiologiya* **15** 74 (1970)
118. Ryabukhin Yu S *Med. Radiologiya* **15** 81 (1970)
119. Ryabukhin Yu S, Ivanov V N *Med. Radiologiya* **18** 51 (1973)
120. Ivanov V N, Parfenov E N, Ryabukhin Yu S *Med. Radiologiya* **18** 54 (1973)
121. Ivanov V N et al. *Med. Radiologiya* **19** 50 (1974)
122. Ivanov V N et al. *Atom. Energy* **39** 1006 (1975); *Atom. Energiya* **39** (5) 360 (1975)
123. Zaichik V E, Ivanov V N, Ryabukhin Yu S *Med. Radiologiya* **16** 63 (1971)
124. Zaichik V E et al. *Med. Radiologiya* **16** 47 (1971)
125. Levin Yu M, Nikitina P G, Ryabukhin Yu S *Med. Radiologiya* **17** 29 (1972)
126. Ryabukhin Yu S, Letov V N, Ivanov V N *Med. Radiologiya* **18** 41 (1973)
127. Stepanenko V F et al., in *Summary Reports at the All-Union Seminar on Problems in the Development of Radiotherapeutic Facilities, Moscow, 1975*
128. Borisov G I *Phys. Part. Nucl.* **42** 713 (2011); *Fiz. Elem. Chast. Atom. Yadra* **42** 1372 (2011)
129. Ryabukhin Yu S *Strahlentherapie* **160** 678 (1984)
130. Ryabukhin Yu S, Chekhonadsky V N, Sushikhina M A *Med. Radiologiya* **32** 3 (1987)
131. Shabalkin I P, Spryshkova R A, Serebryakov N G *Med. Radiologiya* **30** 32 (1985)
132. Obaturov G M *Med. Radiologiya* **32** 20 (1987)
133. Ryabukhin Yu S, in *Proc. of the 8th Intern. Congress of Radiation Research* Vol. 2 (Eds E M Fielden et al.) (London: Taylor and Francis, 1987) p. 27
134. Khokhlov V F et al. *Acad. Radiol.* **2** 392 (1995)
135. Khokhlov V F et al. *Appl. Radiat. Isotop.* **67** S251 (2009)
136. Zaitsev K N et al. *Atom. Energy* **91** 850 (2001)
137. Chanana A D et al. *Neurosurgery* **44** 1182 (1999)
138. Busse P M et al. *J. Neuro-Oncol.* **62** 111 (2003)
139. Sauerwein W, Zurlo A *Eur. J. Cancer* **38** S31 (2002)
140. Joensuu H et al. *J. Neuro-Oncol.* **62** 123 (2003)
141. Capala J et al. *J. Neuro-Oncol.* **62** 135 (2003)
142. Marek M et al. *Radiat. Prot. Dosimetry* **70** 567 (1997)
143. Dbaly V et al. *Čes. slov. Neurol. Neurochir.* **66** 60 (2002)
144. Nakagawa Y et al. *J. Neuro-Oncol.* **62** 87 (2003)
145. González S et al. *Appl. Radiat. Isotop.* **61** 1101 (2004)
146. Liu Y W et al. *Appl. Radiat. Isotop.* **61** 1039 (2004)
147. Kato I et al. *Appl. Radiat. Isotop.* **61** 1069 (2004)
148. Kankaanranta L et al. *Int. J. Radiat. Oncol. Biol. Phys.* **69** 475 (2007)
149. Tamura Y et al. *J. Neurosurg.* **105** 898 (2006)
150. Suzuki M et al. *Radiother. Oncol.* **88** 192 (2008)
151. Suzuki M et al. *Jpn. J. Clin. Oncol.* **37** 376 (2007)
152. Ono K *Ther. Radiol. Oncol.* **2** 40 (2018)
153. Taskaev S Yu, Kanygin V V *Bor-neitronozakhvatnaya Terapiya* (Boron Neutron Capture Therapy) (Novosibirsk: Izd. SO RAN, 2016)
154. Blue T E, Yanch J C *J. Neuro-Oncol.* **62** 19 (2003)

155. International Society for Neutron Capture Therapy, ISNCT, https://isnct.net/
156. Hu K et al. *Coord. Chem. Rev.* **405** 213139 (2020)
157. Seneviratne D S et al. *Cells* **12** 1398 (2023)
158. Monti Hughes A, Hu N *Cancers* **15** 4091 (2023)
159. Taskaev S Yu *Uskoritel'nyi Istochnik Neitronov VITA* (VITA Accelerator-Based Neutron Source) (Moscow: Fizmatlit, 2024)
160. Ovsenev A E et al. *Izv. Vyssh. Ucheb. Zaved. Fizika* **67** (3) 74 (2024) DOI:10.17223/00213411/67/3/8
161. Kreiner A J et al. *Rep. Pract. Oncol. Radiother.* **21** 95 (2016)
162. Ivanov A A et al. *Phys. Usp.* **65** 834 (2022); *Usp. Fiz. Nauk* **192** 893 (2022)
163. Kobayashi T, Kanda K *Nucl. Instrum. Meth. Phys. Res.* **204** 525 (1983)
164. Green S et al. *Appl. Radiat. Isotop.* **217** 111656 (2025)
165. Hu N et al. *Sci. Rep.* **12** 13778 (2022)
166. Tanaka H et al. *Appl. Radiat. Isotop.* **69** 1642 (2011)
167. Kawabata S et al. *Neuro-Oncol. Adv.* **3** 1 (2021)
168. Hirose K et al. *Radiother. Oncol.* **155** 182 (2021)
169. A Major Milestone: Panboron Hainan BNCT Hospital Successfully Delivers Its First BNCT Treatment, Opening a New Chapter in High-Precision Cancer Care, http://www.cbshhk.com/detail/2054.htm
170. Nakai K et al. *Appl. Radiat. Isotop.* **226** 182 (2025)
171. Nakamura S et al. *PLoS ONE* **11** e0225587 (2019)
172. Nakamura S et al. *Sci. Rep.* **11** 8090 (2021)
173. Hong Y H et al. *Adv. Rad. Oncol.* **10** 101897 (2025)
174. Teng C et al. *Sci. Rep.* **13** 15741 (2023)
175. Zhang Z et al. *Cancers* **15** 4060 (2023)
176. Bae Y S et al. *AAPPS Bull.* **32** 34 (2022)
177. Park C et al. *Appl. Radiat. Isotop.* **221** 111831 (2025)
178. Porra L et al. *Acta Oncol.* **61** 269 (2022)
179. Vyzhigina B B, Dolgushin B I, Kropotov M A *Onkolog. Zh. Luchevaya Diagnostika Luchevaya Terapiya* **8** (3) 18 (2025)
180. Tulin P E et al. *Onkolog. Zh. Luchevaya Diagnostika Luchevaya Terapiya* **8** (4) 50 (2025)
181. Pravitel'stvo Rossii (Government of the Russian Federation), http://government.ru/orders/selection/401/41771/
182. Finogenova Yu A et al. *Onkolog. Zh. Luchevaya Diagnostika Luchevaya Terapiya* **7** (4) 28 (2024)
183. Soloway A H et al. *Chem. Rev.* **98** 1515 (1998)
184. Haselsberger K et al. *J. Neurosurg.* **81** 741 (1994)
185. Michiue H et al. *Biomaterials* **35** 3396 (2014)
186. Wongthai P et al. *Cancer Sci.* **106** 279 (2015)
187. Detta A, Cruickshank G S *Cancer Res.* **69** 2126 (2009)
188. Mastroberardino L et al. *Nature* **395** 288 (1998)
189. Prasad P D et al. *Biochem. Biophys. Res. Commun.* **255** 283 (1999)
190. Kanai Y et al. *J. Biol. Chem.* **273** 23629 (1998)
191. Yanagida O et al. *Biochim. Biophys. Acta Biomembr.* **1514** 291 (2001)
192. Nomoto T et al. *Sci. Adv.* **6** eaaz1722 (2020)
193. Mori Y et al. *Pigment Cell Res.* **2** 273 (1989)
194. Kanno H et al. *Oncologist* **26** e1250 (2021)
195. Laakso J et al. *Radiat. Res.* **160** 606 (2003)
196. Henriksson R et al. *Radiother. Oncol.* **88** 183 (2008)
197. Sivaev I B, Bregadze V I *Ross. Khim. Zh.* **48** 109 (2004)
198. Barba-Bon A et al. *Nature* **603** 637 (2022)
199. Conq J et al. *Biomedicines* **11** 1957 (2023)
200. Barth R F et al. *Neurosurgery* **44** 351 (1999)
201. Yura Y, Fujita Y, Hamada M *Cancers* **16** 2770 (2024)
202. Partridge B R et al. *Front. Vet. Sci.* **9** 1039745 (2022)
203. Tsujino K et al. *Neuro-Oncol. Adv.* **6** vdae062 (2024)
204. Kondo N et al. *Pharmaceutics* **14** 1106 (2022)
205. Raitano A et al. *J. Med. Chem.* **66** 13809 (2023)
206. Raitano A et al. *Int. J. Radiat. Oncol. Biol. Phys.* **123** 1395 (2025)
207. Li J et al. *Bioconjugate Chem.* **30** 2870 (2019)
208. He T, Musah R A *ACS Omega* **4** 3820 (2019)
209. Zhu Y et al. *Bioorg. Chem.* **90** 103090 (2019)
210. Ryabchikova M N et al. *Int. J. Mol. Sci.* **26** 68 (2024)
211. Bialek-Pietras M et al. *J. Organomet. Chem.* **865** 166 (2018)
212. Vorobyeva M A et al. *Int. J. Mol. Sci.* **22** 7326 (2021)
213. Kaniowski D et al. *Int. J. Mol. Sci.* **22** 4863 (2021)
214. Shi Y et al. *ACS Appl. Mater. Interfaces* **10** 43387 (2018)
215. Viola E et al. *Inorg. Chem.* **58** 1120 (2019)
216. Nar I et al. *Chempluschem.* **84** 345 (2019)
217. Conway-Kenny R et al. *Biomater. Sci.* **9** 5691 (2021)
218. Matović J et al. *Mol. Pharm.* **17** 3885 (2020)
219. Matović J et al. *Mol. Pharm.* **18** 285 (2021)
220. Matović J et al. *Molecules* **29** 4263 (2024)
221. Yamana K et al. *Biochem. Biophys. Res. Commun.* **559** 210 (2021)
222. Azzi E et al. *Bioorg. Chem.* **93** 103324 (2019)
223. Takeuchi K et al. *Cells* **9** 1551 (2020)
224. Alberti D et al. *Sci. Rep.* **10** 19274 (2020)
225. Chen J et al. *Med. Oncol.* **41** 104 (2024)
226. Cai J et al. *Molecules* **25** 4697 (2020)
227. Couto M et al. *Chem. Eur. J.* **26** 14335 (2020)
228. Wang S et al. *Front. Oncol.* **13** 1105472 (2023)
229. Matović J et al. *ACS Omega* **7** 30376 (2022)
230. Hattori Y et al. *ACS Med. Chem. Lett.* **13** 50 (2022)
231. Tsujino K et al. *Biology* **12** 377 (2023)
232. Gruzdev D A et al. *Russ. Chem. Bull.* **72** 1861 (2023)
233. Flieger S et al. *Int. J. Mol. Sci.* **24** 6973 (2023)
234. Nishimura K et al. *J. Control. Release* **360** 249 (2023)
235. Miyabe J et al. *J. Pharmacol. Sci.* **139** 215 (2019)
236. Worm D J et al. *J. Med. Chem.* **63** 2358 (2020)
237. Hoppenz P et al. *J. Org. Chem.* **85** 1446 (2020)
238. Wang S et al. *Mol. Pharm.* **16** 3831 (2019)
239. Yoneyama T et al. *BMC Cancer* **21** 72 (2021)
240. Xiang J et al. *Front. Med.* **10** 1199881 (2023)
241. Zhang Z et al. *Pharm. Dev. Technol.* **29** 862 (2024)
242. Gruzdev D A et al. *J. Organomet. Chem.* **1008** 123052 (2024)
243. Nakase I et al. *Chem. Commun.* **55** 13955 (2019)
244. Xiang J et al. *Cells* **11** 1173 (2022)
245. Belchior A et al. *Int. J. Mol. Sci.* **23** 14929 (2022)
246. Nakase I et al. *ACS Omega* **5** 22731 (2020)
247. Rondina A et al. *Cells* **10** 3225 (2021)
248. Kashiwagi H et al. *Invest. New Drugs* **40** 255 (2022)
249. Raskolupova V I et al. *Molecules* **28** 2672 (2023)
250. Zelepukin I V, Shevchenko K G, Deyev S M *Nature Commun.* **15** 4366 (2024)
251. Immordino M, Dosio F, Cattel L *Int. J. Nanomed.* **1** 297 (2006)
252. Woodle M, Lasic D *Biochim. Biophys. Acta* **1113** 171(1992)
253. Milla P, Dosio F, Cattel L *Curr. Drug Metab.* **13** 105 (2012)
254. Mu X, Zhong Z *Int. J. Pharm.* **318** 55 (2006)
255. Mehta S, Lai J, Lu D *J. Microencapsul.* **13** 269 (1996)
256. Altieri S et al. *J. Med. Chem.* **52** 7829 (2009)
257. Fröhlich E *Int. J. Nanomed.* **7** 5577 (2012)
258. Zhang W et al. *Cell Res.* **25** 147 (2015)
259. Ailuno G et al. *Cells* **11** 4029 (2022)
260. Selg C, Hey-Hawkins E *Chem. Eur. J.* **32** e03533 (2026)
261. Zhang T et al. *Colloids Surf. B* **182** 110397 (2019)
262. Shi Y et al. *ACS Appl. Mater. Interfaces* **12** 55564 (2020)
263. Fu W Y et al. *Biomacromolecules* **25** 4215 (2024)
264. Chiu Y L et al. *Biomater. Res.* **28** 40 (2024)
265. Kawasaki R et al. *ACS Appl. Mater. Interfaces* **16** 47137 (2024)
266. Takeuchi I et al. *J. Oleo Sci.* **68** 1261 (2019)
267. Luderer M J et al. *Pharm. Res.* **36** 144 (2019)
268. Yanagie H et al. *In Vivo Athens, Greece* **35** 3125 (2021)
269. Li J et al. *Nature Commun.* **13** 2143 (2022)
270. Kawasaki R et al. *Chem. Eur. J.* **29** e202302486 (2023)
271. Shipunova V O, Deyev S M *Acta Naturae* **14** 54 (2022)
272. Proshkina G M et al. *Acta Naturae* **17** 88 (2025)
273. Michiue H et al. *J. Control. Release* **330** 788 (2021)
274. Heide F et al. *Sci. Rep.* **11** 15520 (2021)
275. Pulagam K R et al. *ACS Appl. Mater. Interfaces* **42** 49589 (2021)
276. Li J et al. *Chem. Eur. J.* **63** 14283 (2020)
277. Singh P et al. *Physica E* **132** 114766 (2021)
278. Li J et al. *Adv. Funct. Mater.* **31** 2100969 (2021)
279. Wang Y et al. *Mater. Chem. Front.* **5** 2771 (2021)
280. Vares G et al. *Nanomedicine NBM* **27** 102195 (2020)
281. Zhang T et al. *Mater. Des.* **223** 111196 (2022)
282. Korolkov I V et al. *Mater. Today Commun.* **24** 101247 (2020)
283. Torresan V et al. *Adv. Healthc. Mater.* **10** e2001632 (2021)
284. Kawasaki R et al. *Nanomedicine NBM* **49** 102659 (2023)
285. Wang Z et al. *Nano Today* **45** 101558 (2022)
286. Wang M et al. *Adv. Funct. Mater.* **34** 2407468 (2024)

287. Alberti D et al. *Nanoscale* **17** 11624 (2025)
288. Yoneoka S et al. *STAM* **20** 291 (2019)
289. Aiyyzhy K O et al. *Laser Phys. Lett.* **19** 066002 (2022)
290. Pastukhov A I et al. *Sci. Rep.* **12** 9129 (2022)
291. Aiyyzhy K O et al. *Bull. Lebedev Phys. Inst.* **51** 962 (2025); Translated from Russian: *Kvantovaya Elektron.* **54** 626 (2024)
292. Zavestovskaya I N et al. *Int. J. Mol. Sci.* **24** 17088 (2023)
293. Karpov N V et al. *Inorg. Mater.* **61** 643 (2025)
294. Fronya A A et al. *Nanobiotechnol. Rep.* **20** 733 (2026)
295. Kasatova A I et al. *Bull. Lebedev Phys. Inst.* **52** 95 (2025); *Kratk. Soobshch. Fizike FIAN* (2) 81 (2025)
296. Kasatova A I et al. *Dokl. Ross. Akad. Nauk. Nauki Zhizni* **527** 152 (2026)
297. Kichakova O I et al. *Byull. Eksp. Biol. Med.* **180** 690 (2025)
298. Koivunoro H et al. *Phys. Med. Biol.* **55** 3515 (2010)
299. Binns P J et al. *Med. Phys.* **32** 3729 (2005)
300. Ishikawa M et al. *Rad. Oncol.* **11** 105 (2016)
301. Knoll G F *Radiation Detection and Measurement* (New York: Wiley, 2000)
302. Yurevich V I *Phys. Part. Nucl.* **43** 367 (2012); *Fiz. Elem. Chast. Atom. Yadra* **43** 711 (2012)
303. Shafranov M D *Phys. Part. Nucl.* **33** 612 (2002); *Fiz. Elem. Chast. Atom. Yadra* **33** 1204 (2002)
304. Santos D et al. *Nucl. Instrum. Meth. Phys. Res. A* **977** 164458 (2020)
305. Capoulat M E et al. *Nucl. Instrum. Meth. Phys. Res. B* **445** 57 (2019)
306. Maire D et al. *IEEE Trans. Nucl. Sci.* **61** 2090 (2014)
307. Maire D et al. *IEEE Trans. Nucl. Sci.* **63** 1934 (2016)
308. Ourahou I et al. "3D-Deuteron Track Recoils Produced by Neutron Capture in Hydrogen Measured by MIMAC-35 cm," arXiv:2602.17880
309. Wang X et al. *Rad. Meas.* **174** 107133 (2024)
310. Tsai P E et al. *Appl. Radiat. Isotop.* **67** S190 (2009)
311. Hsiao M C et al. *Appl. Radiat. Isotop.* **69** 1915 (2011)
312. Hsiao M C et al. *Phys. Med. Biol.* **58** 1391 (2013)
313. Järvinen H, Voorbraak W (Eds) *Recommendations for the Dosimetry of Boron Neutron Capture Therapy* (Petten: NRG, 2003)
314. Jeon S-J et al. *Physical Dosimetry of Dawonmedax BNCT* (Vienna: IAEA, 2022)
315. Bilski P et al. *Rad. Prot. Dosimetry* **110** 623 (2004)
316. Kakino R et al. *Med. Phys.* **51** 1351 (2024)
317. Kumada H et al. *Appl. Radiat. Isotop.* **165** 109246 (2020)
318. Sakurai Y, Kobayashi T *Nucl. Instrum. Meth. Phys. Res. A* **453** 569 (2000)
319. Kim D W et al. *PLoS One* **15** e0234829 (2020)
320. Hiramatsu K et al. *EPJ Web Conf.* **153** 04009 (2017)
321. Selva A et al. *Appl. Radiat. Isotop.* **182** 110144 (2022)
322. Conte V, Bianchi A, Selva A *Appl. Sci.* **14** 216 (2024)
323. Yamazaki R et al. *Biomed. Phys. Eng. Express* **12** 025014 (2026)
324. Rykalin V et al. *J. Phys. Sci. Appl.* **5** 6 (2015)
325. Bykov T A et al. *JINST* **14** P12002 (2019)
326. Bykov T A et al. *JINST* **16** P10016 (2021)
327. Pikaev A K *Dozimetriya v Radiatsionnoi Khimii* (Dosimetry in Radiation Chemistry) (Moscow: Nauka, 1975)
328. Gambarini G et al. *Appl. Radiat. Isotop.* **48** 1477 (1997)
329. Gambarini G et al. *Rad. Prot. Dosim.* **101** 419 (2002)
330. Gambarini G et al. *Appl. Radiat. Isotop.* **61** 759 (2004)
331. Sokolova I K *Khimicheskie Metody Dozimetrii v Radiobiologii* (Chemical Dosimetry Methods in Radiobiology) (Moscow: Atomizdat, 1972)
332. Dymova M et al. *Rad. Res.* **196** 192 (2021)
333. Bikchurina M et al. *Front. Nucl. Eng.* **2** 1266562 (2023)
334. Aoki K, Kobayashi T, Kanda K *J. Nucl. Sci. Technol.* **21** 647 (1984)
335. Honda C et al. *J. Dermatol. Sci.* **1** 23 (1990)
336. Matsumoto T et al. *Phys. Med. Biol.* **36** 329 (1991)
337. Verbakel W F A R, Stecher-Rasmussen F *Nucl. Instrum. Meth. Phys. Res. A* **394** 163 (1997)
338. Verbakel W F, Stecher-Rasmussen F *Phys. Med. Biol.* **46** 687 (2001)
339. Verbakel W F A R et al. *Phys. Med. Biol.* **47** 1059 (2002)
340. Maltseva V D et al. *Appl. Radiat. Isotop.* **234** 112648 (2026)
341. Kobayashi T, Sakurai Y, Ishikfawa M *Med. Phys.* **27** 2124 (2000)
342. Murata et al. *Prog. Nucl. Sci. Technol.* **1** 267 (2011)
343. Murata I *Appl. Radiat. Isotop.* **88** 129 (2014)
344. Manabe M, Nakamura S, Murata I *Rep. Pract. Oncol. Radiother.* **21** 102 (2016)
345. Valda A et al. *Braz. J. Phys.* **35** 785 (2005)
346. Minsky D M et al. *Appl. Radiat. Isotop.* **67** S179 (2009)
347. Minsky D M et al. *Appl. Radiat. Isotop.* **69** 1858 (2011)
348. Hales B et al. *Appl. Radiat. Isotop.* **88** 167 (2014)
349. Del Sordo S et al. *Sensors* **9** 3491 (2009)
350. Kuvvetli I et al. *Nucl. Instrum. Meth. Phys. Res. A* **624** 486 (2010)
351. Fatemi S et al. *Nucl. Instrum. Meth. Phys. Res. A* **903** 134 (2018)
352. Fatemi S et al. *Nucl. Instrum. Meth. Phys. Res. A* **936** 50 (2019)
353. Abbene L et al. *J. Synchrotron Rad.* **27** 1564 (2020)
354. Sakai M et al. *Sci. Rep.* **13** 22883 (2023)
355. Torres-Sánchez P et al. *Appl. Rad. Isot.* **217** 111649 (2025)
356. Hu C R et al. *Sci. Rep.* **15** 31285 (2025)
357. Zamenhof R et al. *Int. J. Rad. Oncol. Biol. Phys.* **35** 383 (1996)
358. Provenzano L et al. *Appl. Radiat. Isotop.* **88** 171 (2014)
359. Nigg D W *Int. J. Rad. Oncol. Biol. Phys.* **28** 1121 (1994)
360. Koivunoro H et al. *Phys. Med. Biol.* **55** 15 (2010)
361. Capala J et al. *Neurooncology* **62** 135 (2003)
362. Kumada H et al. *Phys. Med. Biol.* **49** 3353 (2004)
363. Kumada H et al. *Appl. Rad. Isot.* **61** 1045 (2004)
364. Lin T, Liu Y H *Appl. Radiat. Isotop.* **69** 1878 (2011)
365. Kumada H et al. *Appl. Radiat. Isotop.* **106** 111 (2015)
366. Kumada H et al. *Rad. Prot. Dosim.* **180** 286 (2018)
367. Kumada H et al. *Appl. Radiat. Isotop.* **166** 1 (2020)
368. Azarkin M Yu et al. *Bull. Lebedev Phys. Inst.* **52** 72 (2025); *Kratk. Soobshch. Fizike FIAN* **52** (2) 48 (2025)
369. Petrunya D S et al. *Tech. Phys. Lett.* **52** 60 (2026); *Pis'ma Zh. Tekh. Fiz.* **52** (4) 16 (2026)